Mucoadhesive Nanocomposite Derived from Cellulose Nanocrystal and Chitosan for the Delivery of Hydrophobic Compounds

by

Dae Sung Kim

A thesis

presented to the University of Waterloo

in fulfillment of the

thesis requirement for the degree of

Master of Applied Science

in

Chemical Engineering

Waterloo, Ontario, Canada, 2020

AUTHOR'S DECLARATION

I hereby declare that I am the sole author of this thesis. This is a true copy of the thesis, including any required final revisions, as accepted by my examiners.

I understand that my thesis may be made electronically available to the public.

Abstract

The sea lice are a major ectoparasite of salmon aquaculture that anchor to host fish's mucus membrane, epidermis, and vascular system, thereby compromising the fish immunity. The surging amount of sea lice has caused enormous financial damage to the global salmon farming industries. Current sea lice treatment has relied on conventional drug delivery system that reduces drug efficacy that poses an environmental risk due to the excessive use of toxic chemical compounds. Nanomedicine and nano delivery system are rapidly developing to serve as therapeutic agents for targeting specific sites in a controlled manner, thereby enhancing the therapeutic effects at lower drug dosages. The objective of this research is to develop novel mucoadhesive nano drug delivery platforms that can encapsulate hydrophobic compounds, thereby enhancing the pharmaceutical effects of various applications including biomedical and agricultural fields. The thesis describes various mucoadhesive drug delivery platforms comprising of cellulose nanocrystals (CNC) and chitosan (CS) with different moieties. The scope of the research focuses on the development of mucoadhesive nanocomposite using green chemistry and facile synthesis methods through electrostatic gelation. To improve the functionality of the nanocomposite, colloidal behavior and mucoadhesive properties, various chemical modification techniques were employed to modify the functional groups and to decorate different moieties using nano-polysaccharide based materials.

Through this study, we found that the particle size CNC/CS nanoparticles was in the range of 200 nm to 2 μm, depending on the mass ratio of CNC and CS. The optimal mass ratio was 10:1 (CNC:CS w/w) yielding the smallest average particle size (~200 nm), highest zeta potentials (+40 mV), and highest drug loading efficiency. It was confirmed that polyvinylpyrrolidone (PVP) enhanced the colloidal stability of hydrophobic compounds by

making the system hydrophilic. Chitosan coating enhanced colloidal stability and drug encapsulation efficiency via electrostatic repulsion. The loading and encapsulation efficiency of CNC/CS nanocomposite was 11.6 and 65.6 %, respectively. CNC/CS nanoparticle exhibited good antifungal properties against *S. cerevisiae* and mucoadhesive studies confirmed that nanoparticles could bind to mucus surface of zebrafish. CNC/CS modified with quaternary ammonium groups (Gch) exhibited permanent positive charge at all pH values, resulting in enhanced solubility of CS. The optimal mass ratio was 1:4 (CNC:Gch w/w), and the shape of CNC/CS based nanocomposite depended on the synthesis order, reaction time, and sonication power. To produce nanocomplexes with a homogenous structure, polymeric CS solution should be added to the CNC to coat the surface. Finally, the optimal mass ratio of CNC/CS nanoparticles modified with catechol groups (cat) was 7:1 (CNC:CS-cat w/w). After functionalizing with poly(diallyldimethylammonium chloride) (PDADMAC), the colloidal stability was enhanced yielding a particle size of ~150 nm and a zeta potential of +50 mV. Mucoadhesive studies using confocal microscopy confirmed that CNC/CS nanoparticles modified catechol groups could bind to the zebrafish mucus after 30 mins exposure, as the fluorescence signals were significantly enhanced compared to control study without modification.

The significant discovery of this research are: (1) a facile and reproducible method to prepare CNC/CS based nanocomposite that encapsulate large amount of hydrophobic drugs via electrostatic gelation was developed, (2) the colloidal behavior and stabilization effect of CNC/CS based nanocomposites were elucidated, (3) mucoadhesive nano-drug delivery systems by incorporating bio-inspired active compounds were produced, and (4) the potentials of mucoadhesive CNC/CS based nanocomposite for the treatment of livestock's parasitic diseases by demonstrating mucoadhesive capabilities of prepared nanoparticles on zebrafish

was demonstrated.

With these findings, it is expected that CNC/CS based nanoparticles can serve as targeted drug delivery agents for the delivery of hydrophobic molecules, increasing colloidal stability, drug efficacy, and bioavailability. Furthermore, CNC/CS based nanocomposite will be applied for the treatment of various mucosal infections in agricultural and biomedical fields. This research establishes the foundation for the design and development of mucoadhesive delivery systems for the treatment of sea lice and other parasites found in fish farms in Canada.

Acknowledgements

Above all, I would like to thank to GOD almighty for the wisdom he bestows on me, the motivation to carry out the project, creativity, and good health to complete this research at the University of Waterloo.

I thank my parents whom I love and respect the most. Without their endless love and support, I could never reach this stage. My family went through some hardship during my master's degree. Facing the sudden news that my dad was diagnosed with stomach cancer was difficult. But thankfully my dad recovered, and through this incident, he even gave me a strong motivation to provide effective medical solutions that can truly help patients, rather than merely doing "research for research". I thank my dad (Hong Kyu Kim), mom (Eun Hee Kim), younger sister (Kyung Min Kim), and brother-in-law (Hyu Seung Park) for being awesome family members, giving all the patience and support.

I would like to express my deepest appreciation to my supervisor, Dr. Michael Tam. This thesis would not be possible without his careful supervision. I truly respect him as a scholar. During my master's training, Dr. Tam carefully supervised every detail of my research. Having one-on-one meeting biweekly, I could achieve my research goals step by step. Whenever I encounter research problem, his door was always open for discussion. Every week I experienced walking out of his room with meaningful advice. I am lucky to meet Dr. Tam in my life as he became my role model and a life-long mentor. If I can become a faculty member in the future, I would like to become one exactly like Dr. Tam. Thank you very much professor.

I thank to all the members of Tam's research group. I especially thank Jiyoo Baek for being a great colleague and a friend during my journey at University of Waterloo. She is such a sweetheart who cheered me up all the time, supporting and feeding me regularly (I blame her

Table of Contents

List of Figures

List of Tables

Chapter 1. Introduction

1.1 Background overview and research motivation

The field of nanomedicine has emerged as an effective remedy for current biomedical technologies.[3] Endeavors to develop drug delivery systems have provided a substantial improvement in drug delivery technologies, such as cancer treatments. However, conventional drug delivery methods generate toxicity in the plasma due to the failure to control the administrated drug concentration.[3] To overcome this shortcoming, nanotechnology is being deployed to safely transport drugs to the targeted area. There are various design approaches to encapsulate drugs using nanomaterials and to permit the controlled release at the targeted site. This thesis will provide background information on advanced nano-drug delivery systems and showcase techniques for targeted drug delivery to the mucus layer using polysaccharide-based nanomaterials.

Cellulose nanocrystals (CNC) have enormous potential in various sectors and applications because of their excellent mechanical strength, colloidal stability, abundant surface functional groups, biocompatibility, and biodegradability.[4] CNCs can be applied in nanomedicine, food, agriculture, energy, and wastewater treatment.[5] The number of publications involving CNCs has been increasing continuously. However, there are still significant discoveries to be made for their novel utilization in fields, such as targeted drug delivery.

Mucoadhesive drug delivery systems (MDDS) employ strategies for targeted drug delivery to the mucus membrane.[6] MDDS have received extensive attention due to the increasing demands for effective treatment at mucosal infection sites, such as the digestive, pulmonary, vaginal, oral, and optical tracts.[7] The motivation of this thesis is to develop a novel MDDS and explore its potential for the treatment of mucosal infections. This thesis will

showcase MDDS prepared using cellulose nanocrystals and chitosan (CS). The synthesis methods and optimal synthesis conditions for the system will be elucidated.

Another research motivation is to increase the stability of hydrophobic drugs in hydrophilic environments. Poor solubility of drug candidates has been a major challenge in the pharmaceutical research industry.[8] Despite their effective therapeutic capabilities, hydrophobic drugs cannot be utilized in various physiological environments that are hydrophilic in nature.[9] Liposomes or polymeric materials have been employed to address this challenge, but further investigation is still required. This thesis will investigate how to stabilize hydrophobic drugs in colloidal systems similar to physiological environments. In this study, nanopolysaccharide-based materials including cellulose nanocrystals and chitosan will be explored for drug delivery applications. CS has been extensively investigated for its mucoadhesive properties.[10] CS and chemically modified CS will be combined with cellulose nanocrystals to develop nanomaterials for MDDS. CS was modified with the catechol groups, a well-known bio-inspired underwater adhesive. Two CS derivatives were incorporated into the system to improve the mucoadhesive properties and colloidal stability. Emamectin benzoate (EMB), a widely used pesticide was used as a model for hydrophobic drugs. The mucoadhesive properties of the nanomaterials were analyzed using porcine mucin. Tests were also conducted using zebra fish as an animal model.

1.2. Research scope and methodology

This thesis focuses on the development of a mucoadhesive drug delivery system using natural polymers, such as CNC and modified chitosan. The research used the chemical modifications of nanomaterials, where the synthesis conditions were optimized to improve the

colloidal stability and mucoadhesive properties. The proposed systems were produced using facile synthesis methods and green chemistry. This involves the use of natural polymers to replace synthetic polymers in healthcare applications. To address all the therapeutic aspects, biological studies, both *in vitro* and *in vivo*, should be further conducted. Furthermore, since the experiments were designed at bench level, studies involving scale-up to the production level should be conducted.

1.3 Thesis outline & highlight

This thesis describes new mucoadhesive drug delivery systems prepared using CNC and chitosan that were functionalized with different moieties. The research was conducted in 4 sequential stages, with improvements being made at each stage. Firstly, the simplest formulation, comprising cellulose nanocrystals and chitosan, was prepared for drug delivery to the mucus membrane. The colloidal behavior of the cellulose nanocrystals and chitosan-based nanocomposite was analyzed, and the optimal conditions were determined. Next, quaternary ammonium groups were incorporated into the system to achieve a permanent positive charge at all pH values. Then, the chitosan surface was functionalized with the catechol group to induce covalent bonding with mucin. The interaction between chitosan-catechol and mucin will be evaluated to confirm that the functionalized nanocomposite could bind to the mucosal sites. Finally, the nano-formulation, functionalized with both positive quaternary ammonium groups and catechol groups, will be evaluated for the enhanced mucoadhesive properties and stabilized colloidal behavior of hydrophobic compounds.
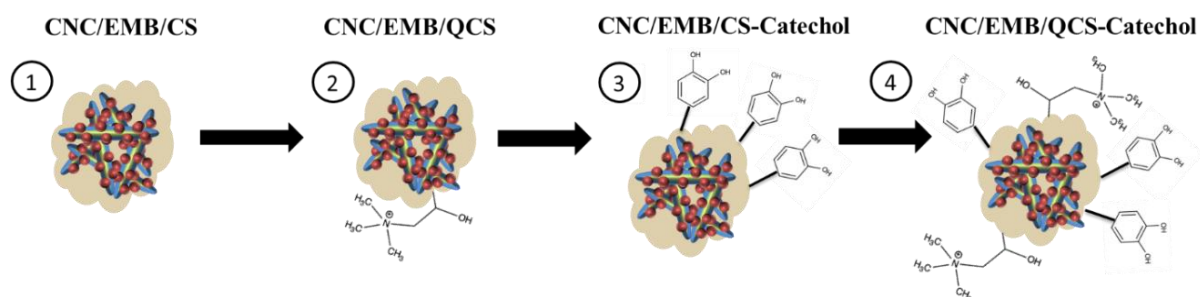
Figure 1-1. The stages of development of the nano-formulation for mucoadhesive drug delivery. 1) cellulose nanocrystals/emamectin benzoate/chitosan, 2) modified with quarternized chitosan, 3) modified with catechol groups, 4) modified with quaternized chitosan and catechol groups

Chapter 1 and 2: Introduction and literature reviews

Chapter 1 summarizes the general motivation of this research and provides an outline of the thesis. Chapter 2 describes the background knowledge of this master thesis research. An extensive literature review of the general drug delivery systems, MDDS, stabilization of hydrophobic compounds, composition of the mucus membrane, and materials used for the research including CNC, CS, and catechol groups will be discussed in Chapter 2.

Chapter 3: CNC/CS and CNC/EMB/CS nanocomposite

Chapter 3 investigates the fundamental structure of the mucoadhesive nanocomposite comprising CNC and CS. The synthesis method, colloidal behavior, physical and morphological properties, drug encapsulation and loading efficiency, and mucoadhesive ability will be discussed. This chapter explores the possibility of the CNC/CS based nanocomposites for the delivery of hydrophobic drugs. In order to examine the loading and delivery of hydrophobic drugs, emamectin benzoate was successfully encapsulated into the CNC/CS based nanocomposite. The drug loading test showed that the loading efficiency varied depending on the concentration of incorporated CS. Chapter 3 will discuss the optimal synthesis conditions

to achieve good colloidal stability. This study found that the mass ratio between CNC and CS is the most significant factor affecting the colloidal behavior and physical characteristics, including particle size and zeta potential. Finally, *in vivo* tests to determine the mucoadhesive properties were examined and elucidated.

Chapter 4: CNC/EMB/Gch nanocomposite

Chapter 4 describes the chitosan derivatives that were quaternized with glycidyltrimethylammonium chloride (Gch). We investigate the role of Gch on the mucoadhesive behavior of the drug delivery systems and explore how Gch can improve the functionality of the CNC/CS based nanocomposite for MDDS. The detailed synthesis process, optimal mass ratio between CNC and Gch, and morphological studies are discussed in this chapter. In particular, the morphology of the CNC/CS based nanocomposite was dependent on the order in which the synthesis steps were conducted.

Chapter 5: CNC/EMB/CS-Catechol and CNC/EMB/CS-Catechol/PDADMAC

Chapter 5 describes the utilization of chitosan functionalized with the catechol groups, which is well-known mussel-inspired adhesive compound. The catechol groups were incorporated into the CNC/CS based nanoparticles to improve the mucoadhesive properties. Chapter 5 outlines the synthesis of the CS-catechol and CNC/CS-catechol nanocomposites with improved adhesive properties. However, the application of CNC/CS-catechol was limited by its poor solubility above pH 6.5. To address this, synthetic cationic polymer, polydiallyldimethylammonium chloride (PDADMAC) was incorporated into the system to increase the colloidal stability of the nanocomposites. The detailed synthesis process, optimal synthesis conditions, morphological evaluation, and mucoadhesive properties of the CNC/EMB/CS-catechol/PDADMAC nanocomposite is discussed in Chapter 5.

Chapter 2. Literature Review

2.1. Introduction to drug delivery systems

2.1.1. Drug delivery systems using nano-polysaccharides

The methods of transporting molecules for pharmaceutical treatment are generally called "drug delivery". In order to administer pharmaceutical compounds, such as synthetic drugs, proteins, peptides, antibodies, and natural active compounds, various drug delivery formulations and novel approaches have been reported.[11] The concept of drug delivery is closely related to the dosage form and the route of administration. The minimum efficacious dosage of active pharmaceutical ingredients (API) or drugs is called minimum effective concentration (MEC). The administrated API must achieve MEC to have desired therapeutic effects, but the drug dosage must be less than the maximum safe concentration (MSC) to prevent damage of cells and tissues in the body. The duration of drug release is also important in order to increase the therapeutic effects with smaller drug dosages. Figure 2-1 illustrates the drug concentration in plasma using a conventional drug delivery system and a controlled drug delivery system.
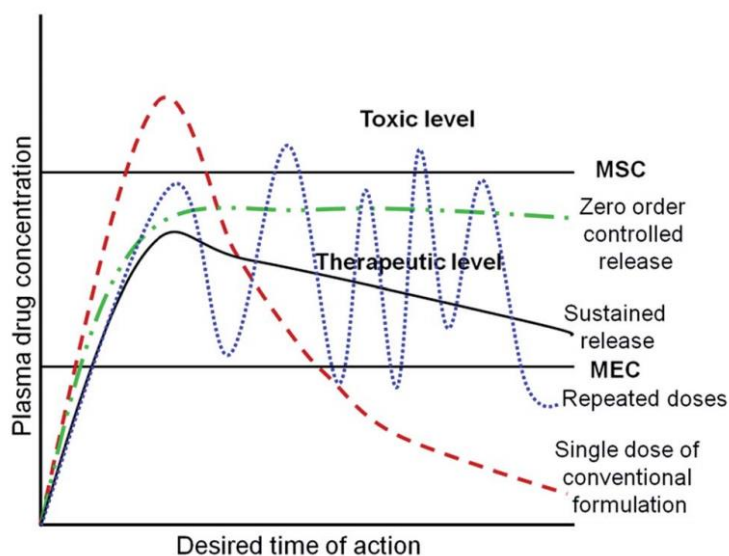
Figure 2-1. A schematic diagram of drug delivery. (adapted from [12])

Conventional drug delivery systems are designed for the immediate release of APIs or drugs for rapid absorption. However, these systems do not maintain the required drug concentration for an extended time. Frequent administration is necessary, and this increases the possibility of overdose that can have adverse effects on the patients. To address this concern, controlled drug delivery systems were developed to revolutionize the healthcare industries and drug delivery platforms. A controlled drug delivery system is designed to deliver API or drugs at a controlled rate as described in Figure 2.2. By utilizing controlled drug delivery techniques, the desired therapeutic effects could be achieved with a smaller dosage and APIs can be sustainably released over a longer duration. Also, this novel approach addresses patient compliance issues, minimized side effects, and reduces drug accumulation.[12]
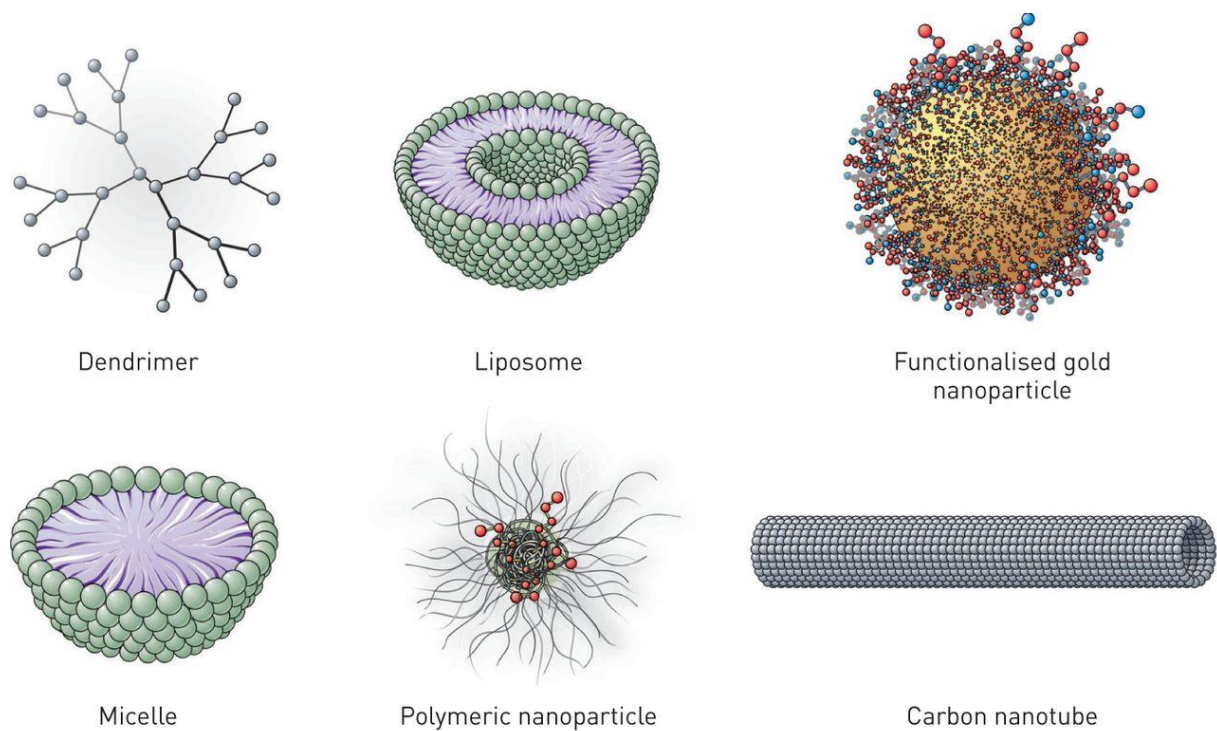
Figure 2-2. The structure of nanocarriers for drug delivery (adapted from Van Rijt et al.[13])

Nanotechnology provides many advantages to various drug delivery platforms in many ways; such as (1) increasing surface area, (2) enhancing solubility, (3) increasing rate of dissolution, and (4) improving bioavailability.[14] The particle size reduction of the drug carriers plays a significant role in improving the colloidal stability, bioavailability, solubility, and drug loading and release, while also reduces toxicity. For these reasons, the development of 'nano' sized materials has been extensively investigated for drug delivery applications.

Polysaccharides composed of long chain carbohydrates possess various derivable groups that can be modified to possess diverse physiochemical characteristics including molecular weights, functional groups, chirality, and solubility. The presence of reactive functional groups on their backbone, such as hydroxyl, carboxyl, and amino groups facilitates various chemical modifications, such as (1) oxidation of primary alcohols to aldehydes or carboxylic acids, (2) enzymatic oxidation of primary alcohols, (3) nucleophilic extraction of hydroxyl groups to generate ester and ether bonds, (4) amide linkage between carboxyl groups, and (5) nucleophilic reactions of amines.[15] In the past several decades, polysaccharide-based nanoparticles have been exploited as novel drug carriers for various APIs and drugs due to their favorable characteristics, such as renewability, sustainability, unique physiochemical properties, biocompatibility, and biodegradability.[16] Also, nano-polysaccharides possess mucoadhesive properties arising from their abundant hydroxyl surface groups, that resulted in enhanced *in vivo* drug residence times and pharmaceutical effects. Natural polysaccharides, such as chitosan, cellulose, and cyclodextrin can be incorporated with other types of nanomaterials including synthetic nanoparticles, such as PLGA and quantum dots for theranostic application, where both therapeutic and detection capabilities are combined in a single nanoparticle.[17] Polysaccharide-based nanoparticles can be synthesized by self-assembly, chemical crosslinking, or physical crosslinking with other polymers or nanoparticles. The strategies for

nano-polysaccharide synthesis can vary depending on the environment (i.e. pH, temperature, or the presence of specific proteins or enzymes) of the targeted area.

2.1.2. Drug delivery strategies for hydrophobic molecules

The poor solubility of drug candidates has been one of the major challenges encountered in the drug development and pharmaceutical fields. Despite the effective pharmaceutical effects, the poor solubility of drug candidates can reduce bioavailability, resulting in suboptimal drug delivery. It has been reported that around 90 % of compounds in the discovery pipeline of current drug development and nearly 40 % of drugs with market approval are insoluble in water.[18] To address this, various strategies, such as pH modification, surfactant stabilization, polymeric micelles, inclusion complexation, solid nanoparticles, nano-emulsions, and liposomes, have been investigated to improve bioavailability, efficacy, safety, and patient compliance.[18]

Nanotechnologies have been widely adopted for the delivery of hydrophobic compounds since reducing the particle size of drug candidates enhanced intercellular uptake and improved stabilization. In the pharmaceutical field, reducing the drug particle size to less than 1 µm is regarded as "nanonization". Amphiphilic polymers and micelle nanocarriers have been examined for hydrophobic drug delivery applications. Nanocarriers can be self-assembled by a number of driving forces, such as hydrogen bonding, hydration, electrostatic interaction, π-π interaction, steric interaction, and depletion interaction.[19] Amphiphilic nanoparticles possess both hydrophilic and hydrophobic domains, and the hydration of the hydrophilic region causes spontaneous phase separation when the critical micelle concentration is exceeded. In water suspensions, amphiphilic nanocarriers can encapsulate hydrophobic drugs in the hydrophobic region (the core of the nanocomposite), while the hydrophilic component extends

to the water phase. (Fig. 2-3). As hydrophobic drugs are encapsulated in the core of the nanocomposite, they can be safely delivered in aqueous environment. However, the loading efficiency of polymeric nanoparticles for hydrophobic molecules is low (usually less than 10 %). In order to increase the drug loading efficiency, a number of studies have been conducted using various methods including drug-core-polymer-shell nanocomposite techniques.[20]
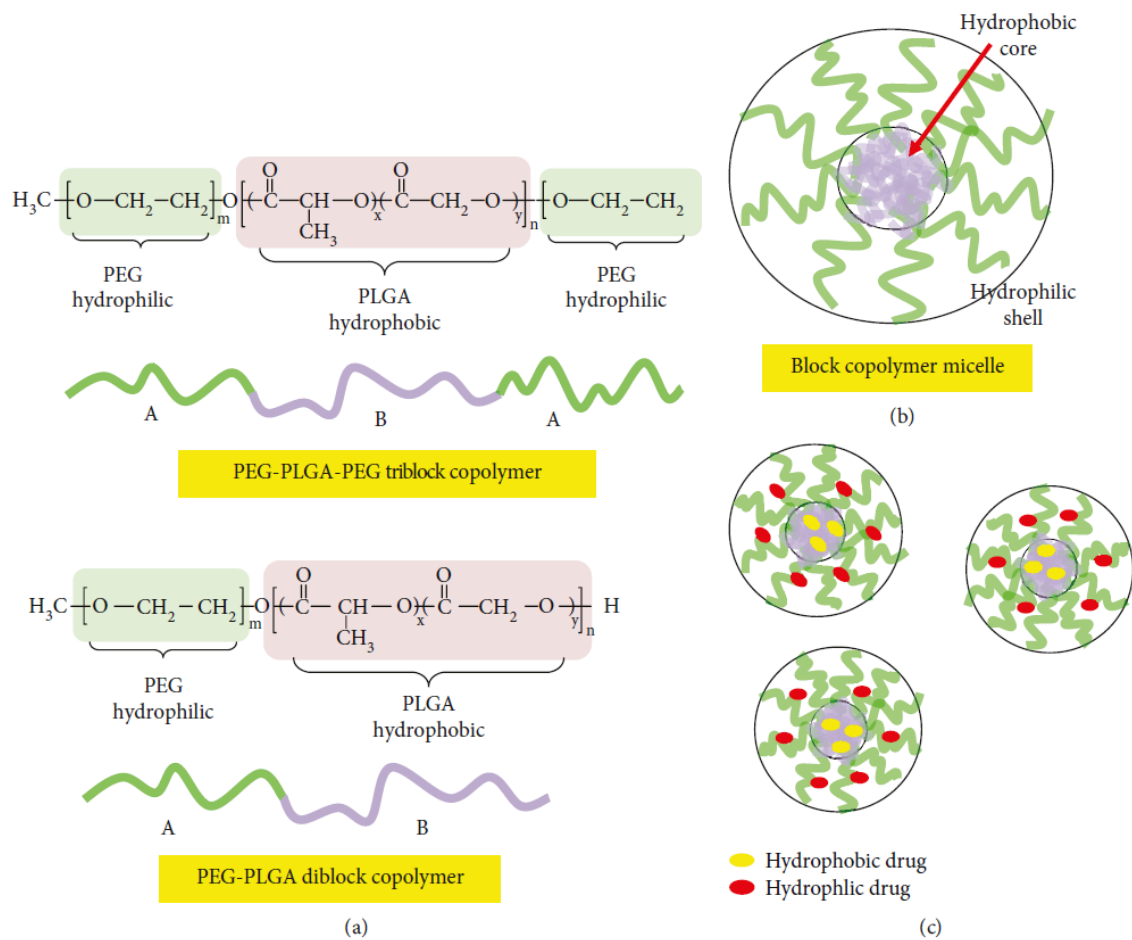
Figure 2-3. Nanoparticle drug delivery for hydrophobic drugs (adapted from Lombardo et al.[18])

Nano-emulsion (NE) is a system consisting of water and oil, which is stabilized by an interfacial film of surfactant with a droplet size of less than 100 nm. NEs are

thermodynamically stable and transparent nano-dispersions in water, and low-energy emulsification (LEE) techniques can be used for their synthesis.[21] NEs possess advantageous features over emulsions, liposomes, and nanoparticles, such as higher solubilization capacity, smaller droplet size, lower viscosity, easier preparation, enhanced physical stability, and improved bioavailability.[21] It was reported that oil-in-water (o/w) NEs have a higher loading capacity of hydrophobic molecules in their oil phase, resulting in improved solubilization and bioavailability.[22]

Liposomal drug delivery has been widely used to transport hydrophobic molecules since the liposomes can stabilize drugs, overcome barriers to cellular/tissue uptake, and achieve targeted drug delivery to specific sites. Liposomes consisting of membrane lipid layers surrounding aqueous components, are uni-lamellar or multi-lamellar vesicles containing phospholipids and cholesterol (CHOL).[8] Liposomes can encapsulate hydrophobic molecules within the lipid membrane and stabilize them in aqueous suspensions. It has been reported that nanoliposomes with a droplet size of less than 300 nm could carry hydrophobic molecules, resulting in a more effective therapeutic effects with smaller nanoliposomes (less than 200 nm).[23,24] Lipid-based nanoparticles are comprised of a solid lipid core with triglycerides, glyceride mixtures, or waxes. The particle size of drug encapsulated lipid-based nanoparticles ranges from nano to submicron scale (50 to 1000 nm) and they are composed of biocompatible components that can be synthesized without the need of organic solvents. The drug loading capacity is dependent on the crystalline structure of the lipid core.[8] Lipid-based polymeric systems are also developed using hydrophobic polymers, such as poly (D,L,-lactic-co-glycolic acid) (PLGA). Lipid-based micelle structures have been synthesized utilizing polyethylene glycol (PEG) or other hydrophilic segments. Modification with PEG provides many benefits by stabilizing the colloidal system through secondary interactions between polymeric particles,

13

and increasing the circulation time of drug carriers in blood.[8]

Cyclodextrin (CD), a hydrophilic water-soluble oligosaccharide consisting of a macrocyclic ring of glucose subunits connected by α-1,4 glycosidic bonds, has been examined as a solubilizer of hydrophobic drugs because CD can accommodate hydrophobic molecules in its hydrophobic cavity. The enclosed hydrophobic compounds (guest molecule) can be entrapped within the hydrophobic cavity of CD (host molecule) without altering the structure. The number of glucose units determines the type and size of the hydrophobic cavity of CD and various chemical modifications have been reported to increase its aqueous solubility.[25]

Apart from the drug delivery platforms described above, other interesting strategies have been proposed for the delivery of hydrophobic molecules. For example, a highly hydrophilic polymer containing guanidinium that can transport aromatic conjugated hydrophobic drugs via π- π interactions between the planar faces of guanidinium moieties and the aromatic rings of hydrophobic compounds.[9] The prepared drug delivery platform enhanced the (a) solubilization of doxorubicin, (b) stability of protein, (c) cellular uptake, and (d) endosomal permeation.[9] Drug delivery systems for hydrophobic compounds can also be prepared by electrospinning. Li et al. developed a poly(ethylene oxide) (PEO) nanofibrous membrane functionalized with cetyltrimethylammonium bromide (CTAB) and sodium dodecyl-benzenesulfonate (SDBS) for hydrophilic and hydrophobic drug delivery using electrospinning.[26] Gu et al. reported the use of hydrogels for the delivery of hydrophobic drugs. Hydrophobic polymeric chains and a hydrophobic crosslinker were used to form the hydrogel matrix. Various nanoparticles and molecules, such as CD were incorporated within the hydrogel matrix to enhance the functionalities of the hydrophobic drug delivery system.[27]

2.2. Mucoadhesive drug delivery system

2.1.1. Mucosa

A mucus membrane or mucosa is a membrane that covers the surface of various internal cavities and organs, such as the digestive, respiratory, nasal, buccal, vaginal, and ocular tracts. The total surface area of mucosa is about 400 square meters while the surface area of the skin is about 2 square meters. The composition of mucosa is mainly water (95 %), along with mineral salts (0.5-5 %), lipids and glycoproteins (1 %) and other free proteins (0.5-1 %).[28] The structure of mucosa is composed of one or multiple layers of epithelial cells and lamina propria of loose connective tissues.[28] The thickness of mucosa varies depending on the physiological site. The functions of mucosa are; (1) to protect the physiological systems (2) to keep the internal cavity moist, and (3) to absorb and transform nutrients. The epithelial cells in the mucous membrane secret mucus that serves as a primary barrier between the exterior and the interior of the body. [28] The type of mucus varies depending on the type of cells in the mucosa.
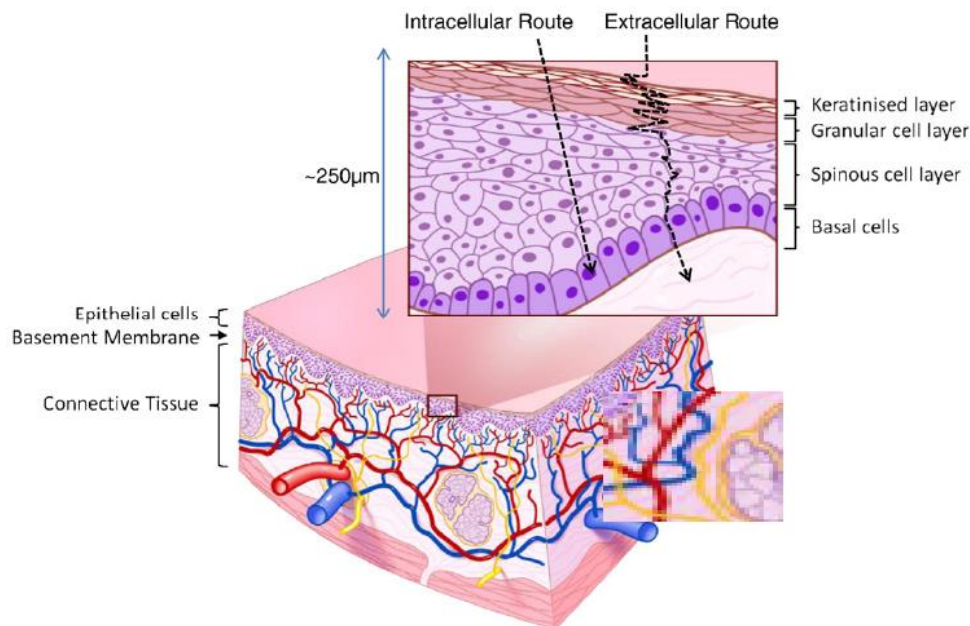
Figure 2-4. The structure of the oral mucous membrane. (adapted from Hearnden et al.[28])

2.1.2. Principle of mucoadhesion

The mucoadhesion process can be described by several theories including adsorption, diffusion, electronic, and wetting theories. Based on the adsorption theory, the adhesive forces of mucoadhesive materials are generated from physical interactions with the functional groups. These interactions include hydrogen bonds, van der Waals forces, electrostatic interactions, and hydrophobic interactions, resulting in strong global adhesion with the mucus membrane.[29] The wetting theory, which is one of the oldest theories for adhesion, is based on the embedding process of the adhesive materials.[29] Thermodynamic work of adhesion and contact angle measurements are used to determine the adhesive forces as mucoadhesion is related to the surface tension of the substrate and adhesive materials according to Dupre's equation:

$$W_A = y_b + y_t - yb_t$$

where W_A is the specific thermodynamic work of adhesion, and y_b, y_t, and yb_t represent the surface tension of mucoadhesive materials, substrate, and the interfacial tension, respectively.[29] The diffusion theory for adhesion involves the interpenetration degree of polymers into the glycoprotein mucin chain. The polymer chains and mucin generate semi-permanent adhesive bonds. The penetration degree of polymers in the mucus is dependent on the diffusion coefficient and the duration of contact. A depth of $0.2 \sim 0.5$ µm is necessary to achieve effective adhesive bonds.[29] The electronic theory is based on electron transfer upon contact of mucoadhesive polymers with the mucus surface due to differences in their electronic structures. This results in the formation of an electrical double layer at the interface. Mucoadhesive forces can be generated from the attractive forces across the double layer.[30]

There are several factors that affect mucoadhesion. Depending on the molecular weight, surface charge, spatial conformation, viscosity, chain length, concentration, swelling

factor, stereochemistry, and flexibility of polymers, the mucoadhesive capabilities can be altered. Also, the physiological conditions, such as pH, mucin turnover rates, and temperature can change the mucoadhesive properties.

Various methods have been proposed to evaluate mucoadhesion, such as the use of a texture analyzer, a modified surface tensiometer, a tensile stress tester, or an atomic force microscope (AFM).[31] The amount of polymer adhered to the mucin particles can be measured by rheology, ellipsometry, the colloidal gold staining method, the flow channel method or the falling liquid film method.[31] Texture analyzer is the most common method used to measure mucoadhesive properties, and to evaluate the detachment force and the total work of adhesion. Tensile stress measurements are used to compare the interaction of various formulations comprised of gelatin, pectin, and carmellose with mucin. The interaction with mucin particles increases the elongation rate (mm/min), leading to an increase in the tensile strength. AFM can analyze the surface properties and can quantify the adhesive forces between the mucus surface and the AFM tips treated with mucoadhesive materials.[31]

2.1.3. Materials for MDDS

Mucoadhesive drug delivery systems have been utilized for various infection sites, such as the oral, nasal, intestinal, ocular, and vaginal tracts, which are covered by a mucus layer.[32,7,33,6,34] Mucoadhesive polymers are classified according to their surface charge and functional groups. Conventional polymers interact with the mucus membrane through hydrogen bonds, hydrophobic interactions, or electrostatic interactions.

Figure 2-5 summarizes the classification of various materials that have been employed for MDDS. Mucoadhesive polymers can be classified into charged polymers and uncharged polymers in terms of their surface charge. Anionic polymers have carboxyl and sulphate

functional groups that generate strong hydrogen bonds with the mucus surface. Anionic polymers, such as poly (acrylic acid) and carboxymethyl cellulose are widely used due to their strong mucoadhesive properties and minimal toxicity to normal cells. Cationic polymers have been used for mucoadhesive purposes as they can interact with the mucus membrane mainly via electrostatic interaction. Chitosan is the most common cationic polymer employed for mucoadhesive applications because it has advantageous features, such as good biocompatibility, biodegradability, and antimicrobial effects. There are also uncharged mucoadhesive polymers, such as poloxamer, hydroxypropylmethylcellulose (HPMC), methyl cellulose (MC), poly(vinyl alcohol) (PVA), and poly(vinyl pyrrolidone) (PVP).[35] In terms of their sources, mucoadhesive polymers can be classified as natural or synthetic.
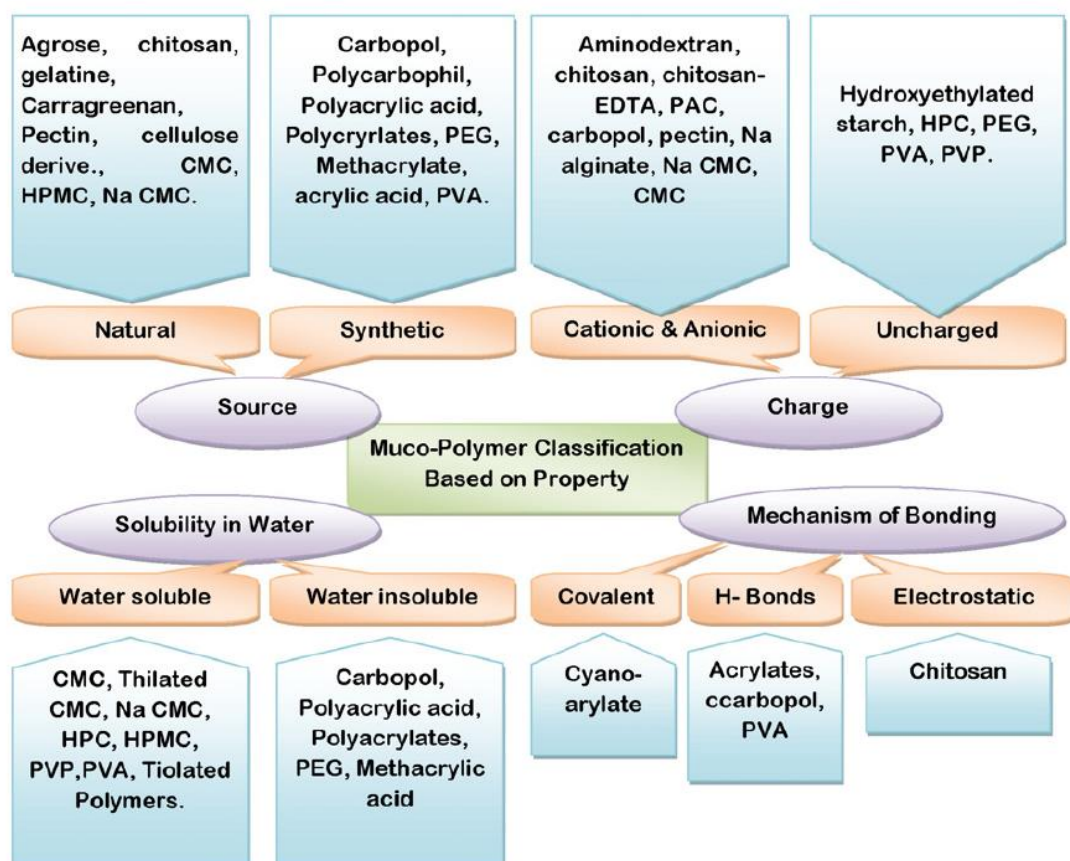
Figure 2-5. Classification of mucoadhesive polymers. (adapted from S. Mansuri et al.[6])

2.3. Cellulose nanocrystals

Cellulose, the most abundant and renewable polysaccharide in nature, can be readily utilized in a wide spectrum of industries and applications. Cellulose nanocrystals (CNC) that are extracted from cellulosic biomass via acid hydrolysis, have received unprecedented attention due to their inherent unique and advantageous properties, such as high surface area ($\sim$250 m^2/g), high aspect ratio, high tensile strength ($\sim$7500MPa), high stiffness (young's modulus: 140 GPa), good colloidal stability, abundant hydroxyl surface groups, biocompatible, and biodegradable properties. This section will examine the chemical structure, unique characteristics, and the characterization method of CNC.[36]

2.2.1. The physiochemical characteristics of CNC

The chemical structure of cellulose is composed of long repeating chain of anhydro-D-glucopyranose unit (AGU) and cellobiose connected by β-1,4 glycosidic linkage, serving as energy storage, and also define the physical structure of the polysaccharide. Cellulose has a linear chain structure due to β-1,4 glycosidic linkage while other polysaccharide, such as glycogen has different physical structure. The degree of polymerization (DP) of cellulose indicates the number of AGU in the structure, and it usually ranges from several hundred up to 20,000 depending on sources and extracting methods.[37]

CNC can be extracted from cellulose via acid hydrolysis, where high concentration of sulphuric acid (H_2SO_4) and hydrochloric acid (HCl) are used. Acid hydrolysis breaks the glycosidic bonds in amorphous region of cellulose microfibrils leading to a rod-like structure. Sulphuric acid hydrolysis imparts many anionic sulfate ester groups onto the CNC's surface by generating electrostatic repulsion in colloidal system, leading to good stabilization at all pH values. Hydrochloric acid hydrolysis maintains large amount of reactive primary hydroxyl

groups so that versatile chemical modification of CNC can be achieved. Other acids, such as phosphoric and hydrobromic acids have been reported for CNC treatment. Depending on the source of nanocelluose and its morphology, various nomenclatures have been used, such as cellulose nanocrystals (CNC), nanocrystallites of cellulose (NCC), cellulose nanowhiskers (CNW), cellulose nanofiber (CNF), nanofibrillated cellulose (NFC), nanofibrous cellulose (NFC), and bacterial nanocellulose (BNC). Despite the fact that nanocellulose has similar chemical structure, the morphology and mechanical behavior can be different. This section will focus on the morphology and crystalline characteristics of CNC.[36]

There are various instruments and characterization techniques that could be used to study the morphological structure of CNC. The most common characterization method is electron microscopy and light scattering techniques. The electron microscopy, such as transmission electron microscopy (TEM), scanning electron microscopy (SEM), atomic force microscopy (AFM), can provide direct morphological information, such as geometrical size and shape of nanomaterials with high-resolution. Also, light scattering techniques, such as small angle neutron scattering (SANS) and dynamic scattering (DLS, DDLS) can be used to analyze the morphological structure of CNC.[36]

The morphological dimensions of CNC can vary depending on the source of cellulose and hydrolysis techniques. As shown in the table, the length (L) and width (W) of CNC can be ranged from 50-1000 nm, 3-50 nm, respectively, and the aspect ratio (L/W) of CNC ranges depending on the extracted source. The aspect ratio of CNC derived from cotton ranges from 10-30 and around 70 for CNC derived from tunicate. This high aspect ratio of CNC can provide beneficial features by increasing the drug binding efficiency and percolation degree in matrix.[38]
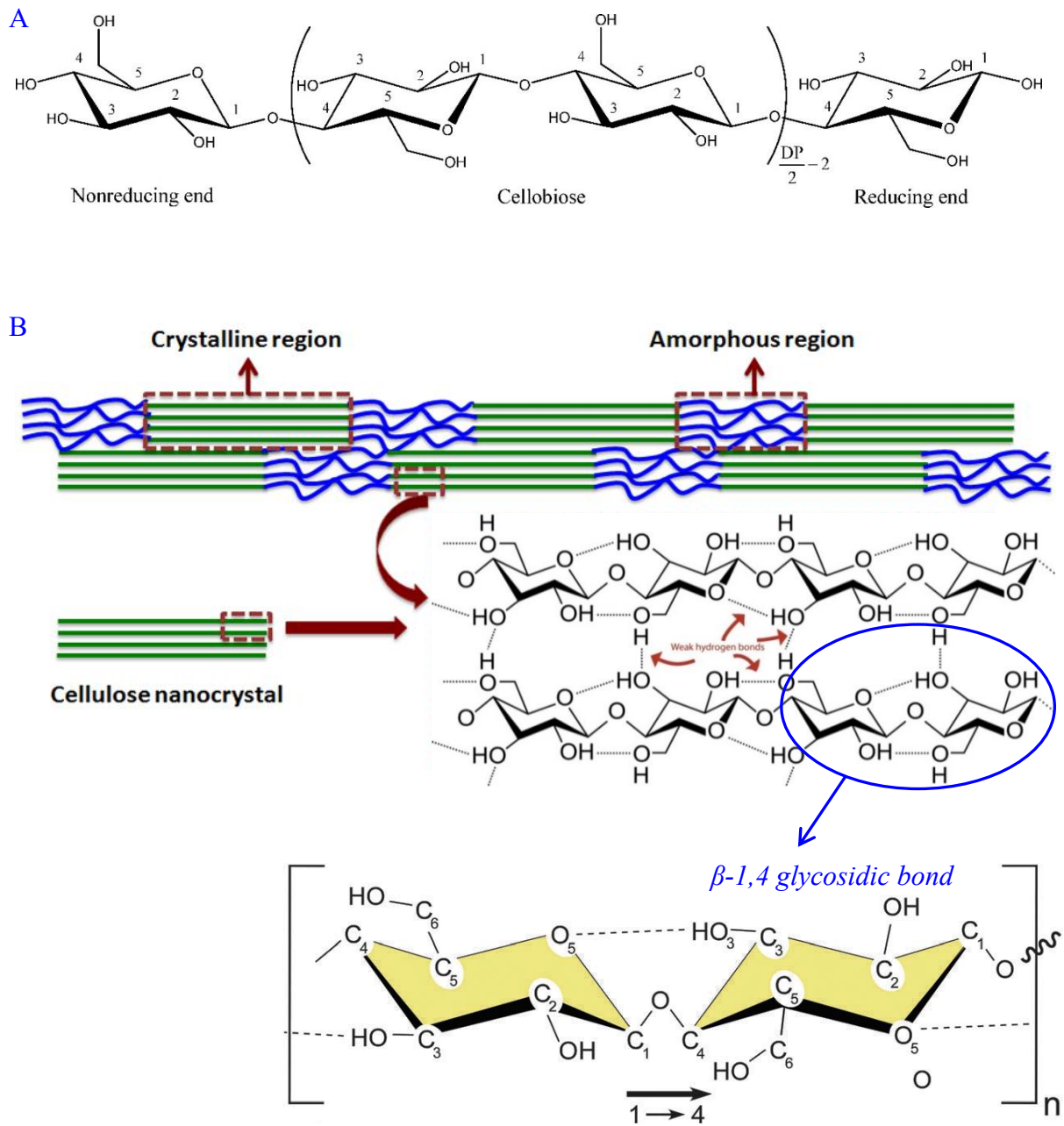
Figure 2-6. A) The Chemical structure of cellulose. (adapted from[39,40]), B) The physical structure of cellulose microfibrils: crystalline region and amorphous region and the interchain hydrogen bonding (dotted line). (adapted from[41])

Table 1. Comparison of the length (L) and width (w) of CNCs derived from different sources. (adapted from George and Sabapathi[38])

| Source | Size distribution | | Aspect ratio (L/w) | Technique | Preparation method |
	L (nm)	w (nm)			
Bacterial	100−1000	10−50	2−100	TEM	Acid hydrolysis
	100−1000	30−50	2−33	TEM	Acid hydrolysis
Cotton	100−150	5−10	10−30	TEM	Acid hydrolysis
	70−170	~7	10−24	TEM	Acid hydrolysis
	200−300	8	25−37.5	TEM	Acid hydrolysis
	255	15	17	DDL	Acid hydrolysis
	150−210	5−11	13.6−42	AFM	Acid hydrolysis
MCC	35−265	3−48	0.7−88	TEM	Mechanical
	250−270	23	10.7−11.7	TEM	Acid hydrolysis
Ramie	150−250	6−8	18.6−41.7	TEM	Acid hydrolysis
	50−150	5−10	5−30	TEM	Acid hydrolysis
Sisal	100−500	3−5	20−166.7	TEM	Acid hydrolysis
	150−280	3.5−6.5	23−80	TEM	Acid hydrolysis
Tunicate	1160	16	72.5	DDL	Acid hydrolysis
	500−1000	10	50−100	TEM	Acid hydrolysis
	1000−3000	15−30	33−200	TEM	Acid hydrolysis
	1073	28	38	TEM	Acid hydrolysis
Valonia	>1000	10−20	50−100	TEM	Acid hydrolysis
Softwood	100−200	3−4	25−66.7	TEM	Acid hydrolysis
	100−150	4−5	20−37.5	AFM	Acid hydrolysis
Hardwood	140−150	4−5	28−37.5	AFM	Acid hydrolysis

2.4.2. The mechanical properties of CNC

CNC possesses remarkable mechanical properties that can be served as reinforcement in polymeric matrix. High mechanical strength of CNC can be achieved due to their high stiffness, reactivity of cellulose, and high aspect ratio of nanocellulose. To prepare the highest mechanical reinforcement, CNC can be modified by casting and evaporating methods from a homogeneous CNC solution.[42] There are several ways to predict the reinforcement of CNC in a polymer matrix. Halpin–Kardos theory is conventionally used to assess reinforcement analysis of short fiber composite. However, the modified series–parallel model of Takayanagi has been adopted as it is more accurate than Halpin–Kardos theory by considering the percolation effect of blended matrix.[43] Based on Takayanagi's method, the infinite aggregates of CNC play an important role in imparting the stiffness to the nanocomposites. There is a percolation threshold above which the cellulosic nanoparticles may bind to each other and form a 3-D network within the nanocomposite film. This cellulosic network can effectively enhance the reinforcement features of the nanocomposite by establishing strong interactions between the nanocrystals.[43]

The high aspect ratio and modulus of the percolating CNC network are the most effective parameters that enable the formation of rigid network of the CNC. The modulus of the percolating CNC network can be experimentally obtained by performing tensile tests on the films prepared by removing the water from a suspension of CNC via evaporation. The modulus correlated to the aspect ratio of the CNC and typically ranges from 1 to 15 GPa.[44] There are three key factors that can significantly impact the mechanical properties of the composites, such as morphology and geometry of the nanoparticles, the fabrication process, and nanostructure of the polymer matrix and matrix-filler interactions. Various factors can

influence the formation of the percolating CNC network that can dramatically change the mechanical properties of the composite.[45] The percolation phenomenon of CNC within an organic or in-organic polymer can be employed to fabricate biomimetic, stimuli-responsive nanocomposites by incorporating CNC as high-modulus filler and a low-modulus polymeric matrix. Indeed, the capability of CNC in shaping and decoupling of the 3D rigid networks of individual nanocrystals within the polymeric matrix by specific chemical or thermal stimulation can make CNC an ideal candidate for reinforcing the physical properties of low-modulus polymers.[46]

2.4.3. The rheological properties of CNC

In terms of characterization as well as the processing of the systems, a good understanding of the rheological properties of CNC in nanofiller network is important. In CNC-polymer mixture, the rheological features of aqueous dispersion play a key role in preventing mixture from extreme aggregation.[47] It has been reported that the addition of CNC enhance the rheological properties of biomaterials as they exhibit shear-thinning, gel-like features, and viscoelastic behavior.[48] Markstedt et al. showed that the addition of CNC enhanced the shear-thinning properties of CNC-alginate hybrid matrix, which is a significant factor in maintaining the shape of bio-ink materials.[49] The rheological properties of a CNC dispersion can be controlled by the nanocellulosic components, dimensions and surface characteristics. Also, CNC can form liquid crystalline domains that influences the flow behavior, depending on the concentration and shear rate. At low shear rates, there was a reduction in the viscosity with shear rates, in the intermediate shear rates, the viscosity curve became constant, and at high shear rates the viscosity again decreased with upward trend in shear rate.[50]

2.4.4. The chemical modification of the Surface of CNC

There are many versatile modification methods of CNCs, such as esterification, etherification, phosphorylation, silytion, amidation, oxidation, and polymer grafting techniques. Among all the modification methods, polymer grafting is known to be an effective method to control the interfacial features of solid surfaces, particularly in the fabrication of biomedical devices and stimuli-responsive surfaces that require a durable and stable polymer film.[51]

In general, 'grafting to' and 'grafting from' are the two main methods commonly used to graft polymers onto solid surfaces. In the first method, a pre-synthesized polymer is covalently bonded to a functional group on a solid surface. Grafting a long polymer chain to the surface of the substrate can restrict the grafting density due to the steric hindrance occurred of the polymer chains.[52] In the 'grafting from' approach, polymer chains are directly synthesized from the solid substrate by covalently attaching a small molecular initiator to the surface prior to the incorporation of a catalyst/monomers.[53] Compared to 'grafting to' approach, 'grafting from' can provide a higher polymer grafting density and controllable polymer film thickness making it more favorable for modifying the surface of CNC.[50] Of all the controlled polymerization strategies, those governed by transition metal complexes, such as copper, can be considered as the most widely used techniques due to the simple fabrication process and tolerance of the different functional groups. To conduct a copper-mediated polymerization, an alkyl halide initiator is covalently immobilized on the surface of CNCs. For example, Zoppe et al. grafted α-bromoisobutyryl bromide (BiBB) to the hydroxyl groups of CNC by dispersing CnC in DMF or THF. Subsequently, these initiator-modified CNCs were used to grow polymer chains, such as poly(N-isopropylacrylamide) (PNIPAM) and poly(N,N-dimethylacrylamide) (PDMAM).[54] They have also reported that high surface charge of CNCs can effectively provide

25

greater surface bound initiator, but this can also have a negative effect on the dispersity of the polymer grafts due to the partial dissociation of copper complexes in aqueous media.[54]

2.4.6. Nanocellulose for drug delivery application

As one of the nanomaterials for drug delivery, nanocellulose has been extensively investigated due to their favorable characteristics, such as biocompatible, biodegradable, high aspect ratio, good mechanical strength, and good colloidal stability. Nanocellulose have the capabilities to encapsulate both hydrophilic and hydrophobic drugs on their amphiphilic surface nature and abundant hydroxyl groups on surface of nanocellulose can be modified for specific controlled drug delivery systems.[11] Previously, conventional drug delivery agents were mainly served to deliver the drugs and released at specific targeted area, but current drug delivery systems have been improved to control the released time and rate contingent by environmental condition, such as temperature, pH, and radiation. Qian et al. prepared redox-sensitive nanogels composed of carboxymethyl cellulose for the delivery of doxorubicin and near-infrared fluorescence imaging. The synthesized nanogels possessed around 192 nm particle size, negative zeta potential, and exhibited better targeted drug accumulation in tumor site through cellular uptake of cancer cells.[55] Tan et al. developed dual-stimuli sensitive nanogels composed of thiolated hydroxylpropyl cellulose (HPC-SH), where they displayed potentials in stimuli-responsive drug delivery applications by exhibiting reversible thermal and redox sensitivities and non-cytotoxicity to MG-63 cells.[56]

CNC-based hybrid systems containing both organic and inorganic compounds have been investigated for theranostic applications which can serve both therapeutic treatment and diagnose of disease with a single formulation. Mianehrow et al. incorporated reduced graphene oxide into hydroxyethyl cellulose and chitosan matrix (rGO-CS-HEC) for controlled drug

delivery applications. The fabricated rGO-CS-HEC was highly stable at all pH range and ionic environments for the delivery folic acid.[57]

Bacterial nanocellulose (BNC) is one of the cost-effective and renewable nanomaterials that is produced by aerobic strains of Gluconacetobacter xylinus, and it has received attentions for its outstanding properties for drug delivery applications. Muller et al. fabricated hydrogels composed of BNC loaded with albumin, where the hydrogel showed good swelling, mechanical properties, and controlled release profile of bovine serum albumin.[58] Moritz et al. developed BNC-based active wound dressings loaded with octenidine and it was stable for up to 6 months with controlled drug release characteristic.[59] Muller et al. fabricated BNC-based drug delivery system with shape memory effect and it possesses improved re-swelling, rehydrate behavior as poor re-swelling ability after drying process limits the applications. The controlled drug delivery could achieve through this shape memorized BNC hydrogel.[60]

CNC, a rod like structure of crystalline region of cellulosic materials have been shown to possess suitable characteristics for drug delivery applications. It can be employed as drug carrier by incorporating with other renewable polysaccharides, such as chitosan, cyclodextrin, and etc. CNC can be easily modified due to its hydroxyl surface group and extremely stable in aqueous systems because of its negative surface charge. Ntoutoume et al. studied CNC-based nanocomposite incorporated with cyclodextrin for anticancer drug delivery systems. The internal cavity of cyclodextrin can carry hydrophobic drugs which is well-known as host-guest interactions. The CNC-cyclodextrin showed good anticancer effect against colorectal and prostatic cancer cell lines by slowly releasing curcumin. Chitosan was incorporated with CNC to form polyelectrolyte macroion nanocomplex for drug delivery application.

2.3. Chitosan

2.3.1. The characteristics of chitin and chitosan

Chitin, the second most abundant natural polymer, is a primary component of cell walls fungi and the exoskeletons of arthropods, such as crabs and shrimps. Chitin has poor solubility due to strong intermolecular bonds that limit their applications.[61] Chitosan (CS), which can be obtained from chitin via deacetylation process, has been extensively studied for biomedical applications, such as antimicrobial, wound dressing, drug delivery agents, bioimaging, and tissue engineering material.[62] CS has a linear polymeric structure consisting of glucosamine (2-amino-2-deoxy-β-d-glucopyranose) and N-acetyl glucosamine (2-acetamide-2-deoxy-β-d-glucopyranose) units via β- (1→4) linkage.[63] The degree of deacetylation (DD) and the degree of polymerization (DP) determine the molecular weight and physical properties of polymeric structure of CS. Even though molecular structure of chitin and CS are similar, the physiochemical properties of both polymers are quite different. Both chitin and CS have reactive hydroxyl and amino groups, but chitin is more crystalline than CS, hence CS is more accessible to various reagents. CS is soluble in weak acid below a pH of 6.3 as their primary amino groups are protonated and become positively charged. Above the pH of 6.3, the primary amino groups are deprotonated and lose their surface charge, and CS became insoluble. The solubility of chitin and CS is also dependent on the degree of acetylation. Water soluble CS derivatives with various salts, such as formate, acetate, lactate, citrate, glyoxylate, pyruvate, and ascorbate, have been reported.[64] The degree of acetylation of chitin is usually 0.90 with presence of some amino groups (5 to 15 %). CS is the N-deacetylated derivative of chitin (usually less than 0.35) indicating that CS is comprised of glucosamine and N-acetylglucosamine. [65]
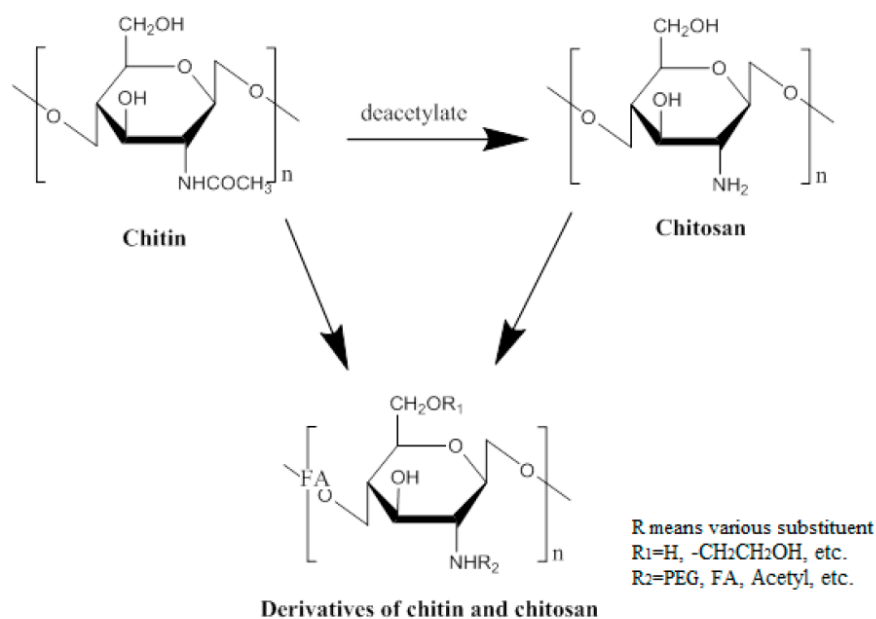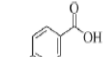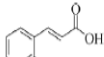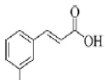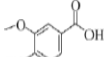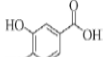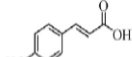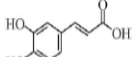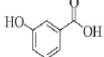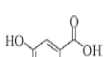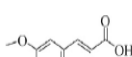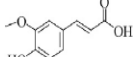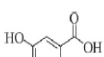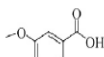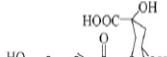
Figure 2-7. The chemical structure of chitin and chitosan. Adapted from Xing et al. [66]

2.3.2. Chitosan derivatives with phenolic compounds

Phenols are known as aromatic organic compounds consisting of a phenyl group (C_6H_5) bonded to hydroxyl group and more than 8000 natural compounds belong to this category of phenolics.[67] Phenolic compounds are the most abundant secondary metabolites that can be extracted from the plant kingdom, such as fruit, cereals, vegetables, olives, cocoa, tea, coffee, and wine. Phenolics have been employed in biomedical applications due to their favorable biological activities, such as antioxidant, antimicrobial, anti-inflammatory, antidiabetic, anticancer, iummunomodulatory, and metabolic regulatory properties.[68] As one of the categories of phenolics, phenolic acids that possess carboxyl groups and two carbon frameworks can be classified into hydroxybenzoic and hydroxycinnamic structures. Table 1 summarizes the classification and structure of phenolic acids. Phenolic acids also exhibit beneficial properties such as antimicrobial, antiviral, antitoxidant, anti-inflammatory abilities.

29

Table 2. Classification and structure of prominent phenolic acids (adapted from J. Liu et al.[67])

Chitosan grafted with phenolic acids have been studied because it significantly enhances biological activities without changing physiochemical properties of chitosan, such as stability, crystallinity, and rheological properties. Phenolic acids, such as ferulic acid [69] [70] [71], hydroxycinnamic acid[72], gallic acid[73], protocatechuic acid[74], caffeic acid[75] were grafted with chitosan to prepare novel biomedical applications. In order to incorporate phenolics with chitosan, various chemical modification methods have been employed. Carbodiimide based coupling reactions are the most common method to graft phenolic compounds onto the chitosan backbone. 1-ethyl-3-(3-dimethylaminopropyl) carbodiimide (EDC) and dicyclohexylcarbodiimide (DCC) are examples of carbodiimide based coupling agents that have been used to chemically conjugate primary amino groups to carboxyl acids. The carbonyl group of phenolic compounds attack the carbodiimide of coupling agents leading to a subsequent proton transfer. Then, primary amino groups of chitosan attack carbonyl carbon of the phenolic acids yielding a chemical conjugate by generating new amide form and urea derivatives. The urea derivatives can be easily purified after dialysis process. Carbodiimide based coupling reaction usually occur in acidic environment and mild reactions. Other methods

to graft phenolic acids to chitosan include enzyme catalyzed grafting and free radical mediated grafting. Free radical initiator system using potassium persulfate, ceric ammonium nitrate, and ascorbic acid/hydrogen peroxide have been reported to introduce phenolic acids to chitosan. Ascorbic acid/hydrogen peroxide redox pair systems have been widely used because it is less toxic, can be conducted at room temperature, cheaper and can prevent oxidation of phenolic acid compared to enzyme catalytic reaction and carbodiimide coupling reaction method.[67]

2.4. A mussel-inspired adhesive material: a catechol group

Marine mussels possess the capability to bind to various type of surfaces under seawater using protein-based adhesives. Mussel use a network of threads to anchor their soft invertebrate body to foreign surfaces.[76] The microstructure of mussel is described in Figure 2-8. The byssus of mussel consists of four components: attachment plaques, threads, stem, and root. Each byssus is comprised of bundles of threads containing adhesive plaques.[77] The expanded plaques at thread ends are used to bind to foreign surface.[77] The mussel foot proteins (Mfps) generate adhesive plaques with high interfacial binding strength, durability, and toughness by rapidly curing themselves. 3,4-Dihydroxyphenylalanine (Dopa) is one of the major components in Mfps. The catechol side chain of Dopa can generate various chemical interactions and crosslinking to bind tightly to foreign surfaces. Due to their remarkable binding abilities for both dry and wet conditions, the design of Mfps with catechol groups have been incorporated into various applications to develop novel adhesive material.[78]
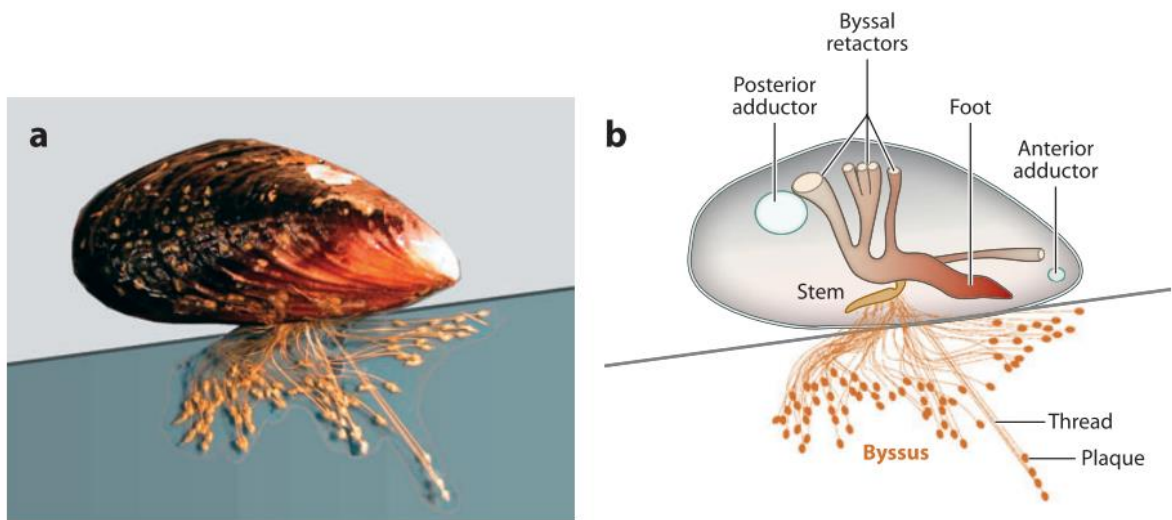
Figure 2-1. Adhesion of marine mussel *Mytilus californianus*. (a) Adult mussel (5cm length) with extensive byssus, (b) Schematic of mussel structure (adapted from Lee et al.[77])

Catecholic amino acid, Dopa, plays a role in forming interfacial bond and the solidification of the adhesive proteins. Catechol groups can bind to both organic and inorganic surfaces via reversible non-covalent including hydrogen bonds, π-π interaction, cation-π interaction, or irreversible covalent bonds. The hydroxyl groups of catechol form hydrogen bonds that can improve the interaction with mucus containing water and hydroxyapatite surface. The benzene ring of catechol can react with aromatic rings via π- π interaction and the aromatic rings can react with cationic ions through cation- π interaction. Catechol chelates metal ions including Cu^{2+}, Zn^{2+}, Mn^{2+}, Fe^{2+}, V^{3+}, Ti^{3+}, and Ti^{4+} to generate strong and reversible complexes.[78]

One of the advantages of using Dopa is the presence of catechol groups which can be commercially conjugated with other compounds containing carboxyl and amino groups. Furthermore, above pH 7, catechol groups can be oxidized to form o-quinone which possess

ability to generate irreversible covalent bonds with thiols and amines group. Utilizing bio-inspired catechol groups into MDDS will improve the mucoadhesion dramatically by inducing strong covalent bonds with mucin polymers which contain thiols and amines group.
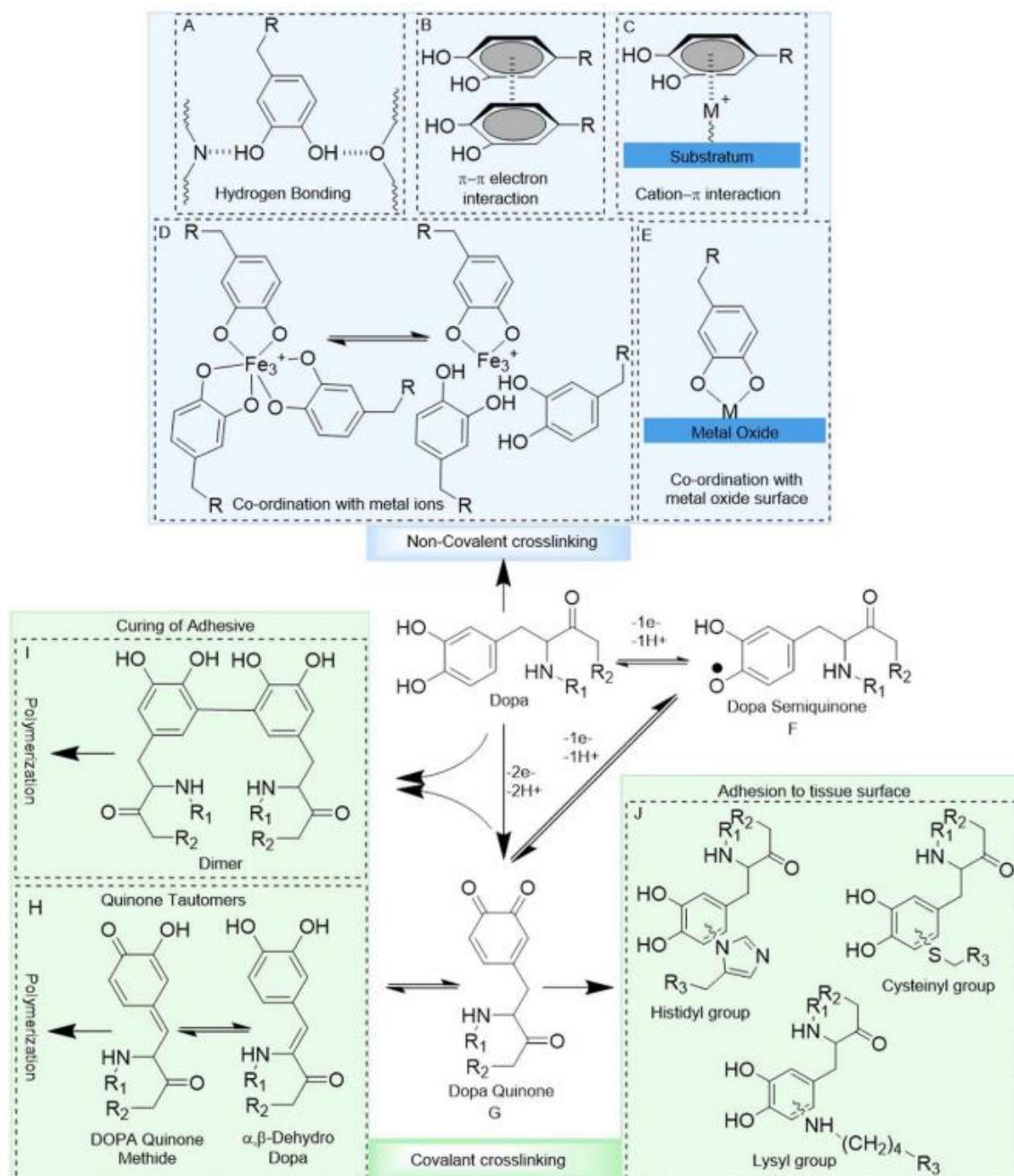
Figure 2-2. Catechol chemistry (adapted from Forooshani and Lee[78])

2.5. Drug delivery systems to control sea louse

Lepeophtheirus salmonis, commonly known as a sea louse is a member of small crustaceans, within the order of Siphonostomatoida, and family of Caligidae. They are marine ectoparasites that attach to the mucus membrane and epidermis tissue of host marine fish.[79] The two main species of sea louse on the east coast of Canada are *Lepeophtheirus salmonis* and *Caligus elongatus*.[79] Sea lice browse on the skin of salmon, increasing its susceptibility to secondary infections that can lead to death of large populations of fish.[79] Over the decades, the temperature of sea water has been increasing due to effects of global warming, resulting in an increased number of sea lice on the fish farming sites. This rising number of sea lice is a serious issue for marine fish farming industries since it causes significant declines in sea survival of wild salmon population and financial damage to global pisciculture market.[80]

To combat infections and retain commercial viability, several strategies are employed as treatments to control sea lice. Conventional treatment has been relying on using chemotherapeutants or bath treatment.[79] However, the development of parasite resistant to the current chemotherapeutants reduces the drug efficacy and toxic compounds pose an environmental risk to non-target organisms in the marine environment.[80]

Fish are vulnerably exposed to hazardous aquatic environment that contains bacteria, viruses, parasites, and pollutants. The secretion of mucus plays a significant role in protecting them from pathogenic microenvironments, forming a barrier between fish and the environment.[81] Fish is surrounded by a continuous mucus surface that represents a physical, chemical, and biological barrier. There are abundant antibacterial compounds secreted by fish's skin cells, such as immunoglobulins, lectins, lysins, agglutinins, and lysozymes. These compounds discriminate between pathogenic and microorganisms to protect fish from invading

the pathogens.[82]

Recently, mucoadhesive nanoparticles composed of CS were employed to enhance the protection of fish mucus. Costa et al. tested mucoadhesive properties of CS on fish skin.[83] Two weeks old tambaqui, *Colossoma macropoum,* was tested as an animal model using fluorescence labelled CS nanoparticles, and the result showed that CS nanoparticles could adhere to both gills and skins. Another study was conducted by Charlie-Silva et al. for CS coated PLGA nanoparticles for fish immune system modulation.[1] They evaluated the mucoadhesive properties of CS coated PLGA nanoparticles on zebrafish mucus; and confirmed that nanoparticles could adhere to zebrafish mucus for 3 hours (Fig. 2-10).[1]
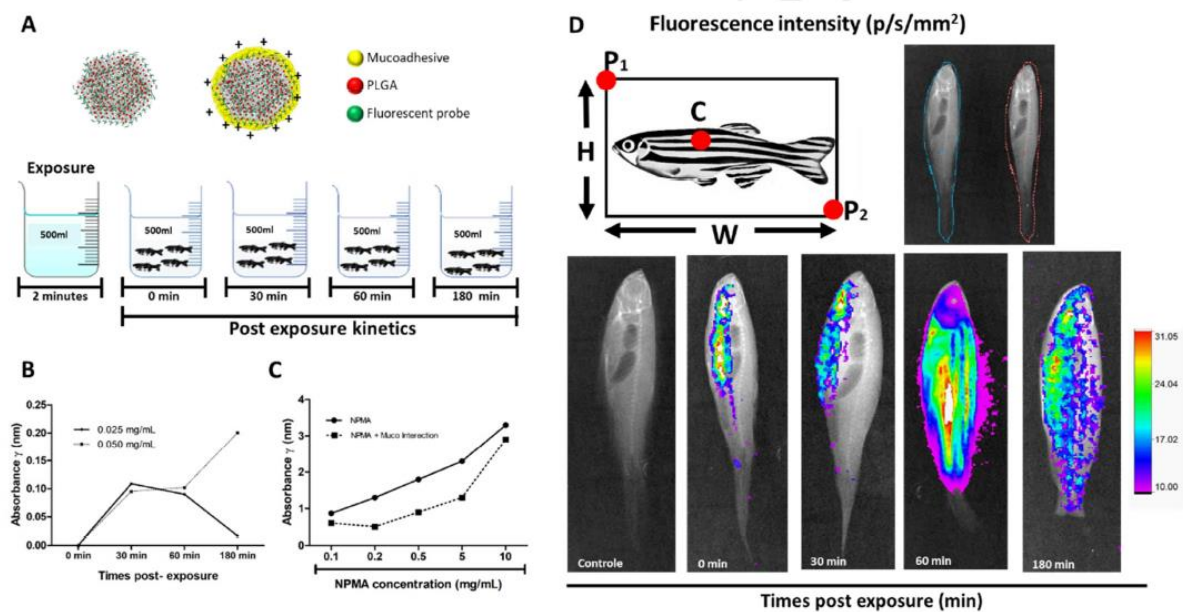
Figure 2-10. Mucoadhesive system in zebrafish. A) preparation of mucoadhesive studies for zebrafish, B, C) Absorption spectra of pure water and mucoadhesive nanoparticles, and mucus (2 mg), D) Green fluorescence image of zebrafish at different exposure times *$(p/s/mm^2)$= photon/second/milimeter^2 (adapted from Charlie-Silva et al.[1])

Emamectin benzoate (EMB), a macrocyclic lactone biological insecticide produced from avermectin B_1 via fermentation process, has an ultra-high efficiency, wide spectrum, low toxicity, environmental pollution, enhanced thermal stability compared to avermectin.[84] Due to these favorable characteristics, EMB has been used in wide range of agricultural industries as an effective insecticide. EMB is extremely active to the leipidoptera insect lavae and many other pests and mites, while it is not harmful to beneficial insects. However, despite the effective insecticide performance, EMB has poor water solubility ($\sim$ 24 mg/L^{-1}), resulting in decrease of bioavailability in the target sites. To enhance water solubility, various nanotechnologies have been employed. Yang et al. prepared solid nanodispersion containing 15 % (w/w) of EMB using solidifying nanoemulsion method.[84] The solid nanodispersion exhibited high dispersible and stability, similar to surfactants and it decreased the particle size and improve dispersity of the solid nanodispersion. The reduced particle size (96.6 nm), high zeta potential (31.3 mV), and stable crystalline state of solid nanodispersion resulted in good and homogeneous dispersion with excellent storage behavior of EMB.[84] Shoaib et al. prepared EMB nanoformulation using polymeric nanocapsules (PNC), mesoporous nanosilica (MCM-48), and silicon dioxide nanoparticles (SNPs). They confirmed that nanoformulation enhanced UV stability and colloidal behavior. The encapsulation efficiency of EMB was 92.84 % (PNC), 87.45 % (MCM-48), 71.19 % (SNPs) with good insecticidal activity against *Plutella xylostella*.[85] Wang et al. fabricated EMB slow-release microsphere using various surfactants via microemulsion polymerization method. PVA was also used as a emulsifier to tune the morphology, average size, dispersity, and stability of the EMB microsphere.[86]

The potential of mucoadhesive drug delivery platforms for the treatment of fish parasitic disease has been recently suggested in two short communications.[1,79] However, there are still many unexplored issues. First, it is unknown that how these nanoparticles behave in

the colloidal system. Understanding colloidal behavior of nanoparticles is important as colloidal suspensions are subjected to several types of instability, such as aggregation, coagulation, flocculation, deposition, and sedimentation. All these instability mechanisms can be counteracted by strong electrostatic repulsion, which can be parameterized by zeta potential measurements. Strong electrostatic repulsion can prevent aggregation by separating the nanoparticles from each other in the colloidal system.[87] To increase colloidal stability for nano drug delivery carriers, this thesis will elucidate colloidal behavior of CNC and CS based nanoparticles and provide several stabilization techniques for targeted drug delivery system using electrostatic and steric stabilization effects. Second, understanding mucoadhesion in colloidal behavior is important. Chitosan has been extensively utilized for mucoadhesive materials because its cationic surface can react with anionic surface of mucus membrane by electrostatic interaction.[88] However, the salts concentration and pH can disrupt the counterions mediated interaction between chitosan and mucus.[89] To address these issues, nanoparticles were functionalized with catechol group that can generate irreversible covalent bonding with the mucus layer, thereby enhancing the mucoadhesive properties both in acidic and alkaline environment as well as in the presence of salt concentrations. This novel utilization of MDDS to control fish parasitic diseases will improve the functionality of current drug delivery platforms. Furthermore, this thesis will describe the development of CNC and CS based nanoparticles to encapsulate EMB, which is belong to ivermectin family of compounds. Ivermectin has been approved by food and drug administration (FDA) and widely used for various sectors to control nematodes, arthropods, and other pests. Recently, it was reported that ivermectin can inhibit the replication of SARS-CoV-2 which shows great potential to commercialize for biomedical applications.[90] This thesis will demonstrate EMB encapsulation using CNC and CS based nanoparticles that possess high drug encapsulation efficiency, good

antifungal activity, and enhanced colloidal stability. The detail synthesis process, optimal condition, colloidal behavior, drug efficacy, and morphological structures of CNC/CS based nanocomposite will be discussed. It is expected that prepared CNC/CS based nanocomposite can be applied in various applications encountered in the agricultural to biomedical sectors.

Chapter 3. Cellulose nanocrystals and chitosan nanogels
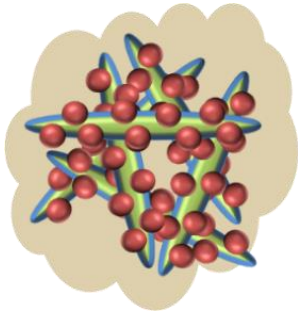
3.1. Introduction

Recently, nanotechnology-based drug delivery systems have played an important role in various therapeutic applications by providing advantageous features These features include: 1) increasing the drug utilization by delivering drugs to targeted areas including cells, tissues, and organs, which can result in decreasing side effects 2) improving colloidal stability of both hydrophilic and hydrophobic drugs, and 3) delivering biomacromolecules such as DNA, RNA, proteins to specific areas where acute therapeutic treatment is required. Since the 1960s, biodegradable synthetic polymers, such as poly (glycolic acid) (PGA), poly (lactic acid) (PLA), poly (lactic-co-glycolic acid) (PLGA) have been explored for drug carrier applications.[91]

Nano-polysaccharides have received much attention for biomedical applications due to favorable features, which include great biocompatibility, biodegradability, mechanical strength, colloidal stability, and effective antimicrobial effects. Cellulose nanocrystals (CNC), produced from cellulosic fibrils via strong acid hydrolysis are hydrophilic and colloidally stable due to abundant hydroxyl surface groups. In addition, CNC can be modified with different functional groups that can bind with drugs, DNA, or proteins. Chitosan, a linear polysaccharide produced from chitin, has novel characteristics for biomedical applications. These natural polymers are ecofriendly and possess more biocompatible characteristics than synthetic polymers, making them ideal materials for the treatment of various diseases.[11]

A Mucoadhesive drug delivery system (MDDS) is a targeted delivery platform to deliver drugs to the mucus layer covering the mucosal epithelial surface. The MDDS interacts with the mucus and mucin proteins and it offers several advantages for therapeutic treatment by localizing the dosage at a specific site with controlled drug release. Mucoadhesive polymers that possess abundant hydrophilic groups including hydroxyl, carboxyl, amide, and sulfate

groups, have been employed in MDDS as they can interact with the mucus surface by forming hydrogen bonds.[29] The increasing demands for mucoadhesive drug delivery systems have been reported for their therapeutic effect at various mucosal infection sites including gastrointestinal, ocular, oral, nasal, vaginal, and pulmonary tracts.

The poor solubility of hydrophobic drug candidates constitutes one of the major challenges in drug development and pharmaceutical research. About 90 % of molecules in the drug discovery pipeline and 40% of approved drugs have poor water solubility, resulting in lower bioavailability.[18] To address this, numerous hydrophobic drug delivery formulations such as synthetic polymeric micelles, amphiphilic polymers, and liposomes have been developed to stabilize molecules. Further advancement in drug delivery technologies for poorly water-soluble drugs will be promising in future drug development.

In this study, we developed a mucoadhesive drug delivery system that can encapsulate poorly water-soluble molecules by using cellulose nanocrystals (CNC) and chitosan (CS) based nanogels prepared via electrostatic gelation. The potential of a CNC-CS based drug delivery platform for mucosal infection sites will be explored. Synthesis and experimental conditions, colloidal behavior, and potential therapeutic effects of CNC-CS based nanogels will be discussed in detail.

3.2. Experimental section

3.2.1. Materials

Low to medium molecular weight chitosan (50-190 kda with 75-85% deacetylated), polyvinylpyrrolidone (average Mw ~ 1,300,000) (PVP), fluorescein isothiocyanate (FITC), yeast extract (for use in microbial growth medium), phosphate buffered saline (PBS, pH 7.4), and (3-Chloro-2-hydroxypropyl) trimethylammonium chloride solution (60 wt. % in H_2O)

(GTMAC) were purchased from Sigma Aldrich (St. Louis, USA). Cellulose Nanocrystals were supplied by Celluforce (Montreal, Quebec). Emamectin benzoate (purification 95%) was purchased from Wellgreen technology (Xian, China).

3.2.2. Synthesis of CNC/CS nanogels

To evaluate the fundamental physical structure and colloidal behavior of the CNC-CS based nanocomposite, CNC/CS nanogels were prepared using a facile synthesis method based on electrostatic gelation. Briefly, 0.5 wt. % of CNC solution was prepared by dispersing CNCs in deionized water and various concentrations (0.2 to 1 wt. %) of CS solutions were prepared using 1% acetic acid solution. Then, CS solutions were slowly injected at a rate of 1.5 mL/min into the CNC solution using a syringe pump under probe sonication.

3.2.3. Synthesis of CEC and CPEC (drug encapsulation)

Briefly, 1g of CNC and 0.1g of PVP were mixed in 0.8 mL acetone and stirred overnight. Various amounts of EMB were dissolved in 0.2 mL of acetone. EMB (0.2 mL) solutions were slowly injected into the CNC/PVP solution (0.8 mL) under sonication for 5 minutes. Then, the mixtures were dried in the oven at 40 ˚C and re-dispersed in milli-Q water (200 mL). For CS encapsulation, various concentrations of CS were prepared in 1 % acetic acid solution. A similar amount of CS was slowly injected into the CE and CPE solutions with a syringe pump at a rate of 1.5 mL/min, while the solution was subjected to probe sonication.

3.2.4. Preparation of labelled chitosan

Briefly, various concentrations (0.1 to 1%) of CPEC nanoparticles labeled with flourescein isothiocyanate (FITC) were prepared according to the protocol reported by Ge et al.[92] with slight modifications. 30 mg of FITC in 30 mL dehydrated methanol was mixed with 30 mL of 1 % CS in 1 % acetic acid solution. After 3 h reaction in the dark at room temperature,

FITC-labelled chitosan was precipitated by increasing the pH using 0.5 M NaOH. The precipitated FITC-labelled chitosan was separated in a centrifuge and unbound FITC was washed with DI water several times until no fluorescence was observed in the supernatant. Then, the washed FITC-labelled chitosan was dissolved in 30 mL of 1 % acetic acid and dialyzed for 3 days in the dark at room temperature, and the water was replaced daily.

3.2.5. Particle size and zeta potential measurements

The particle size and zeta potential measurements were performed to examine the colloidal behavior of CEC and CPEC. Zeta-potential analyzer (Nanosizer ZS, Malvern, UK) was used to measure the particle size, surface charge, and their dispersion characteristics. The prepared CEC and CPEC suspensions of different concentrations were diluted with distilled water and 1.5 mL of diluted sample was transferred to the measuring cell (folded capillary cell, Malvern) for the measurement at 25 °C.

3.2.6. TEM analysis

The size and morphology were analyzed with a transmission electron microscope (TEM) (Philips CM10 electron microscope, acceleration voltage of 60 kV). To prepare the sample grid for TEM measurements, the CEC and CPEC suspensions (0.05 %) were diluted 10 times with ethanol. Then, a drop of diluted sample was placed on a carbon coated copper grid, and the excess liquid was carefully removed using a small piece of Kimwipe. The sample was then left to dry overnight.

3.2.7. Drug binding and encapsulation tests

Briefly, various concentrations of EMB (10 ppm to 200 ppm) were prepared and the absorbances were measured with a UV-vis spectrophotometer. to prepare An EMB calibration curve. Four samples with different CNC:CS mass ratios and stable colloidal behavior after

synthesis were selected for the drug binding study. The synthesized CEC and CPEC suspensions were carefully washed with ethanol and filtered with a 100 nm pore size membrane. Filtered solutions were measured with UV-vis spectroscopy to calculate unbound drug concentration based on the EMB calibration curve. The drug loading and encapsulation efficiency were calculated based on the following equations:

$$Drug\ Loading\ Efficiency\ (\%) = \frac{Weight\ of\ drug\ in\ nanoparticles}{Weight\ of\ nanoparticles} \times 100$$

$$Drug\ Encapsulation\ Efficiency\ (\%) = \frac{Weight\ of\ drug\ in\ nanoparticles}{Weight\ of\ total\ drug\ added} \times 100$$

3.2.8. Antifungal test using yeast

In order to assess the antifungal activity of CPEC nanoparticles, antimicrobial evaluation was conducted by using *Saccharomyces cerevisiae* as a model organism. CO_2 production from *S. cerevisiae* was measured and compared with a control group that contained only yeast. The experimental setup was as shown in Figure 3-1. Briefly, a 10 mL volumetric flask was connected with a graduated cylinder using a 0.1 mm diameter tube, and the system was completely sealed to prevent any gas leakage. The yeast medium was prepared by mixing 0.1 g of *S. cerevisiae* and 0.25 g of D-(+)-glucose with PBS buffer (pH 7.4). EMB was dissolved in dimethyl sulfoxide (DMSO) to add into yeast medium. Finally, various concentrations of CPEC nanoparticle suspensions were introduced into the yeast medium and the volume was adjusted to 10 mL using PBS buffer (pH 7.4). Treated yeast medium was implanted in the experiment setup at 42°C. After confirming the gas generation in the graduated cylinder, the volume of CO_2 produced by *S. cerevisiae* was recorded every 5 minutes.
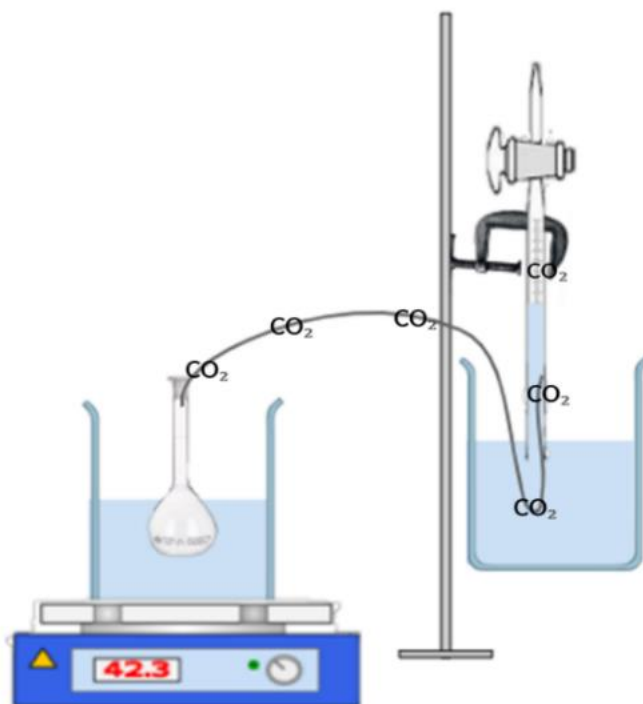
Figure 3-1. The experiment setup for testing antifungal abilities of CPEC

3.2.9. Mucoadhesive tests

To assess the mucoadhesive capabilities of CPEC nanoparticles, zebra fish was chosen as the animal model. The test protocol was evaluated and approved by the animal care committee (ACC) at the University of Waterloo. Briefly, the zebra fish was transferred to 200 mL water and the prepared fluorescence-labelled nanoparticles (50 mg/L) were slowly released into the water. After 30 mins, the zebra fish was anaesthetized with a buffered 100 mg/L solution of MS222 and washed several times with water to remove unbound fluorescence-labelled nanoparticles from the mucus surface. Fluorescence at 460 nm range on the zebra fish mucus was quantified in a fluorescence microscope (Nikon Eclipse Ti-S, Nikon Instruments Inc., USA). After the test, the zebra fish was released back to the aquarium.

3.3. Results and discussion

The detail characteristics of the CPEC nanoparticles, such as the synthesis condition (with and without drugs), colloidal behavior, morphological structure, drug binding efficiency, and their antifungal ability against *S. cerevisiae* are reported here. To finalize and optimize the nanoparticles for the mucoadhesive drug delivery system, we prepared and tested four formulations: 1) CNC-PVP (CP), 2) CNC-PVP-CS (CPC), 3) CNC-EMB-CS (CEC), and 4) CNC-PVP-EMB-CS (CPEC). This section will examine the characteristics and various properties of the formulations for mucoadhesive drug delivery applications.

3.3.1. Synthesis of materials
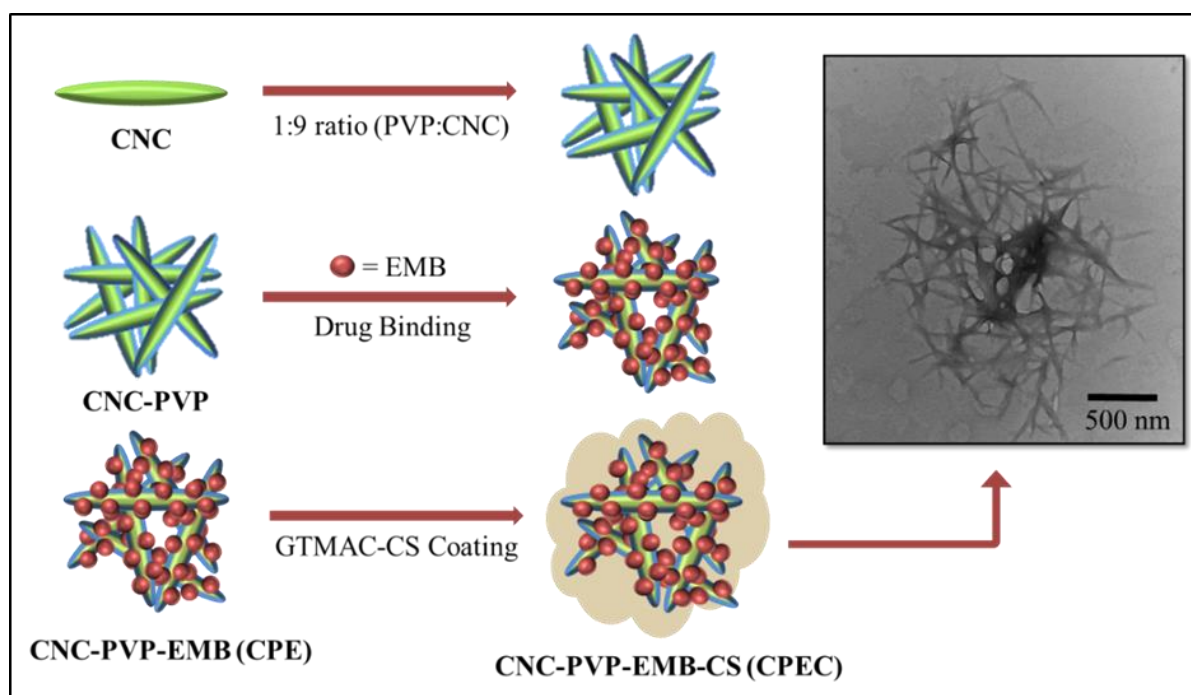
Figure 3-2. Brief synthesis scheme of nanoparticles

The synthesis of CNC-PVP-EMB-CS (CPEC) nanoparticle is described in Figure 3-2. In order to understand the fundamental behavior of the nano-formulation composed of CNC and CS, CPC without drugs was prepared. When the CS solutions were introduced into 0.5 wt.%

of CNC aqueous dispersion, a thick gel was formed due to the strong electrostatic interaction (ionic gelation) between CS and CNCs as shown in Figure 3-3, and these gels were not dispersible in water. Therefore, a probe sonication was employed to disperse the nanoparticles as the CS solution was slowly injected into the CNC solution via a syringe pump. A probe sonication process reduced the particle size, stabilizing the colloidal systems that yielded a homogenous particle size. Without probe sonication, the thick gel remained aggregated, and we found that the bath sonication was insufficient to disperse the aggregated complex that remained as a gel. It was observed that the mass ratio between CNC and CS was a critical factor in preparing a stable CNC/CS nanogel, and this will be discussed in depth later.
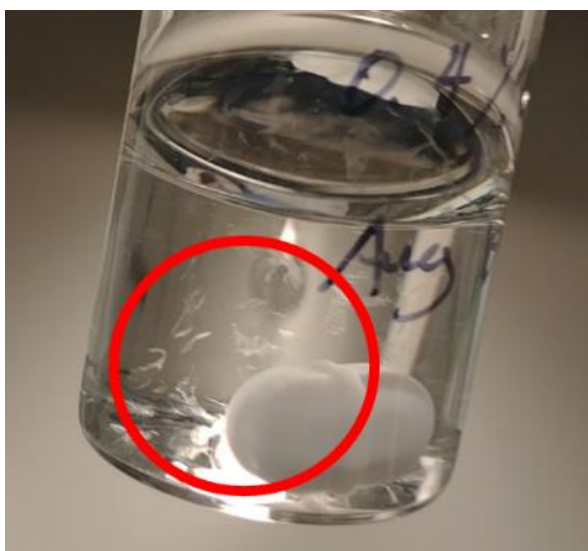
Figure 3-3. Ionic gelation (red circle) of cellulose nanocrystals and chitosan

3.3.2. Characterization of CNC/PVP/CS (CPC)

Particle size, zeta potentials, and TEM were conducted to characterize the CNC/PVP/CS systems. Amphiphilic PVP was coated onto the CNC surface to increase the hydrophobicity of CNC, to enhance the binding of the hydrophobic drug to CNC. It was

previously reported that a 1:9 mass ratio of PVP and CNC was optimal to cover the surface of CNCs with polypyyrole for conductive ink application.[93] Initially, CNCs possessed high negative zeta potentials (around -48 mV) and it was decreased to -30mV after PVP coating.

As shown in Figure 3-4, the particle size and zeta potentials were measured to evaluate the colloidal behavior of CPC in an acidic environment (pH 3). Initially, the particle size of CNC/PVP was less than 200 nm, and after chitosan was introduced, the particle size of CPC increased. The agglomeration of CPC was due to the hydrogen bonds generated between carbonyl groups in the pyrrolidone rings of PVP and hydroxyl groups in CS. The range of CS concentrations was set from 0.2 to 1 %, and the result showed that the 1 % CS concentration yielded a CPC nanoparticle particle size greater than 1 μm, which is undesirable for delivery through the mucus membrane. Achieving a higher degree of mucus penetration is dependant on the particle size and their surface properties. The ideal particle size to penetrate the the mucus membrane is between 20 to 100 nm.[94] When coated with 0.2 % CS, the zeta potential of CPC was maintained at around +48 mV. Since mucus possesses negative charges, nanoparticles for mucoadheisve drug delivery should have postive surface charge to induce electrostatic interaction with the mucus membrane. Based on the particle size and zeta potential analysis, we confirmed that the chitosan concentration is an important factor to produce favorable particle size and zeta potentials of the CPC nanocomplex. The detailed CS concentration and mass ratio between CNC will be discussed in the next chapter.
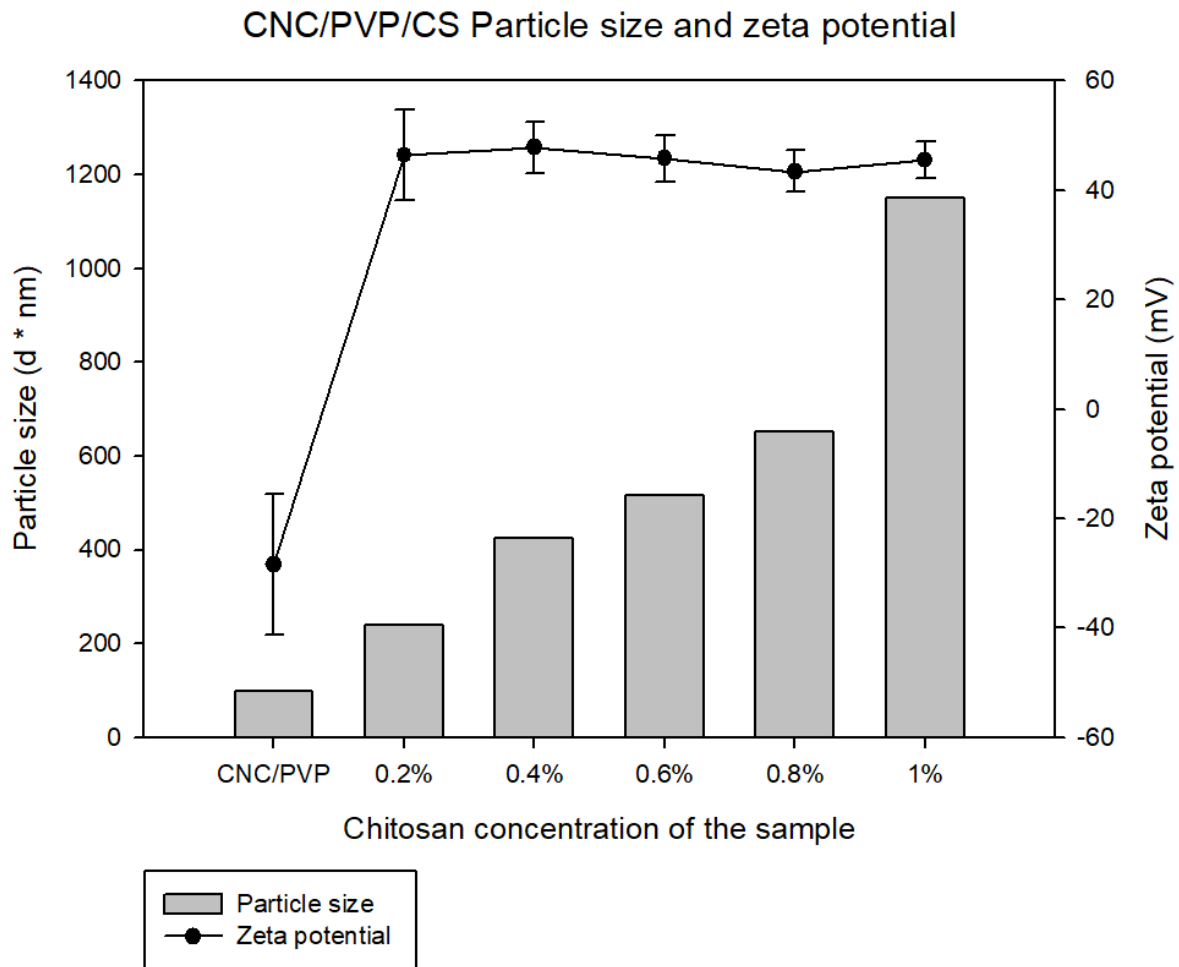
Figure 3-4. Particle size and zeta potential of CNC/PVP/CS

As shown in Figure 3-5, TEM images of CNC/PVP/CS confirmed a randomly coiled structure between cellulose nanocrystals (negative) and chitosan (positive) via strong electrostatic interaction. By using a probe sonicator, the particle size was reduced. However, the particle size of CPC nanoparticles was approximately 1 μm, which is much larger than the results from DLS (dynamic light scattering) measurements. It is believed that the CPC nanoparticles were aggregated when dried on the TEM grid. In order to prevent the aggregation for size evaluation, advanced TEM techniques could be employed.
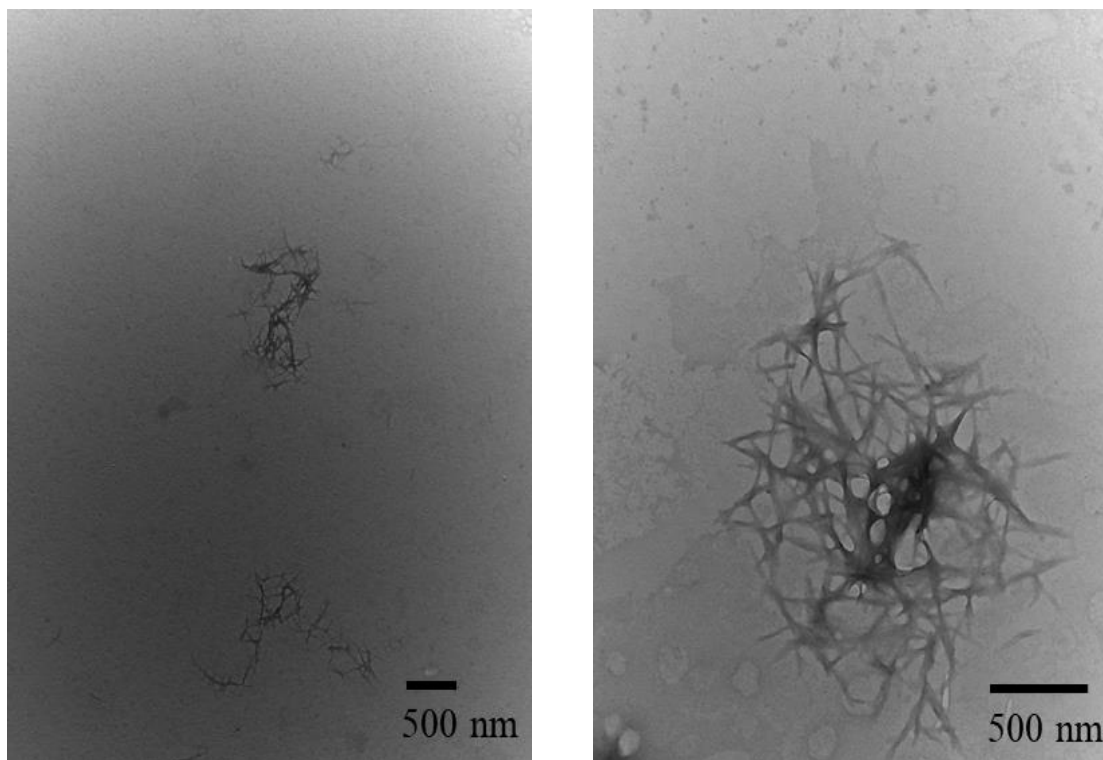
Figure 3-5. TEM images of CNC/PVP/CS

3.3.3. Stabilization of hydrophobic compounds by CPC

CNC has received increasing attention as a drug carrier due to its amphiphilic surface, containing both hydrophilic (hydroxyl groups) and hydrophobic regions (glucose units) on its surface. In addition to drug binding capability, CNC can serve as a stabilizer in aqueous systems because they possess excellent colloidal stability in water. With this attractive characteristic, CNC can stabilize hydrophobic drug compounds, such as doxorubicin, that have poor water solubility. As shown in Figure 3-6, EMB existed as a separate phase, and is not miscible with water due to its hydrophobicity. However, when EMB was bound to CNC (middle), CNC/EMB (CE) was somewhat miscible in water, although the suspension agglomerated and settled to the bottom when stored overnight. Depending on the amounts of EMB bound to CNC, the degree of agglomeration varied as will be discussed later by examining the DLS results. After binding

50

EMB to CNC, the stabilization of the CNC/drug complex by the coated PVP was evaluated. CNC/PVP was blended with EMB (CPE), and this was compared with CE. Both CE and CPE samples were stored overnight to assess the amounts of agglomerate at the bottom of the 50 mL plastic tube. As shown in the Figure 3-6 (right), the amount of agglomeration was reduced in CPE after the introduction of PVP, which promoted the steric stabilization of the complex.[95] The alkyl groups on PVP interacted with EMB, which was then encapsulated by the nanogels. Additionally, the pyrrolidone groups on PVP stabilized the complex particles due to their hydrophilic character.
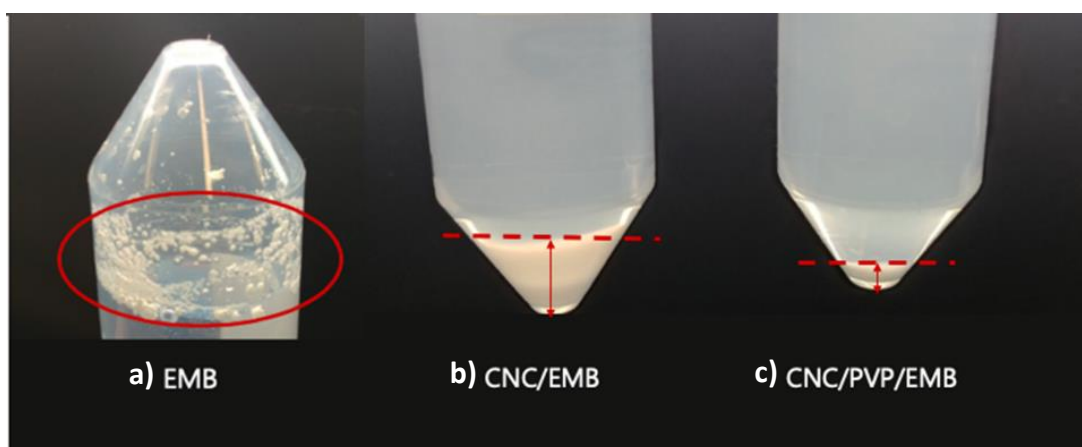
Figure 3-6. The steric stabilization effect by PVP in colloidal system. a) phase separation of EMB with water, b) CNC/EBM, c) CNC/PVP/EMB

The hydrophobicity of EMB before and after binding with CNC/PVP nanoparticle was evaluated by measuring the contact angles on a flat substrate (Fig. 3-7). EMB was dissolved in ethanol and CPE nanoparticles were dispersed in water. Films comprised of EMB and CPE were fabricated on clean glass slides by drying in room temperature overnight. For pure EMB particles a contact angle of approximately 90 degrees was observed due to their hydrophobic

nature. However, when the EMB was encapsulated within the CNC/PVP, the contact angle was reduced to around 48 degrees, indicating the hydrophilic nature of the CNC/PVP/EMB system. From the contact angle analysis, the observed stability (Fig. 3-6C) can be associated with the hydrophilic character of the CNC/PVP complex. The hydrophobic EMB interacted with the hydrophobic domains of the CNC/PVP, which was masked by the hydrophilic pyrrolidone groups resulting in a stable dispersion.
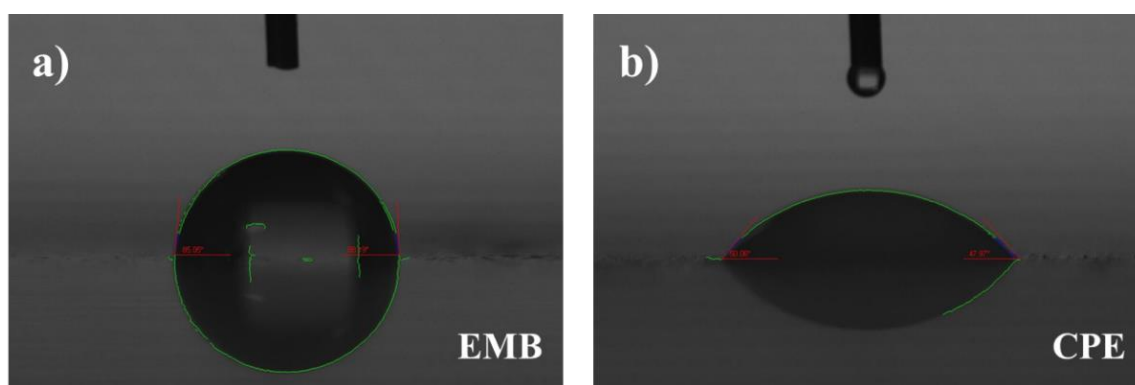
Figure 3-7. The contact angle of a) Emamectin benzoate (EMB) and b) CPE

The particle size and zeta potential of CNC/EMB were quantified to elucidate the drug binding capabilities of the CNC nanocomposite. EMB is not soluble in water (less than 20 ppm), however it is highly soluble in organic and polar solvents. Binding interaction in ethanol would be more favorable than in water as EMB molecules could bind to the surface of CNC in ethanol. In order to study the binding capacity of CNC, various amounts of EMB (10 to 100 mg) were dissolved in ethanol (0.2 mL) and mixed with 1g of CNC dispersion in ethanol (0.8 mL) under probe-sonication for 5 minutes. After drying in the oven, the CE solutions were re-dispersed in 200 mL of water. The colloidal behavior of samples with 0.5 wt. % CNC but different amounts of EMB were examined.   Figure 3-8 shows the dispersion of CE in water containing different amounts of EMB. For simplicity, CE containing 'x' mg of EMB will be

defined by CE-x; for example, CE with 10 mg of EMB is CE-10. The pure CNC 0.5 wt. % solution (control) appeared clear and well-dispersed in water. However, the CE solutions became more opaque with increasing amounts of EMB owing to the aggregation of the CNC/EMB complex.
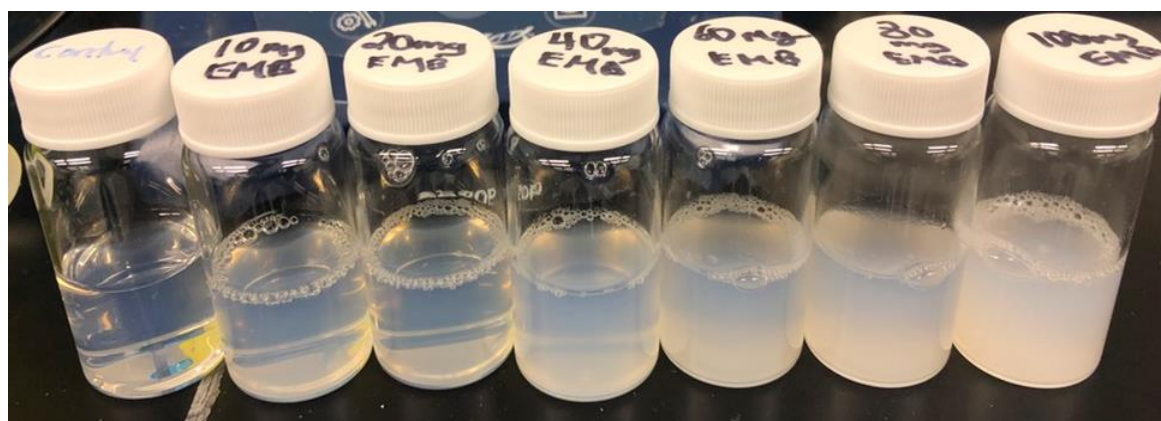
Figure 3-8. CNC/EMB in water (10 mg - 100 mg EMB) (label clearly the EMB content)

In addition to the visual assessment of the colloidal behavior (Fig. 3-8), the particle size and zeta potential were quantified and shown in Figure 3-9. Both CE and CPE were evaluated to determine the effect of PVP on the colloidal system. The average particle size of pure CNC particles was around 100 nm and CNC/PVP displayed a larger particle size (around 200 nm) due to the PVP coating. The particle size of CE gradually increased as the amount of EMB was increased from 10 to 80 mg. As shown in Figure 3-9, samples with a higher content of EMB became opaque, implying that the CNC surface became highly hydrophobic after the binding of excessive amounts of EMB. The colloidal behavior of CPE nanocomposite was similar to CE (without PVP), where the average particle size increased gradually upon the addition of increasing amounts of EMB. In particular, when 80 mg of EMB was added, PVP was capable of reducing both the particle size and aggregation.
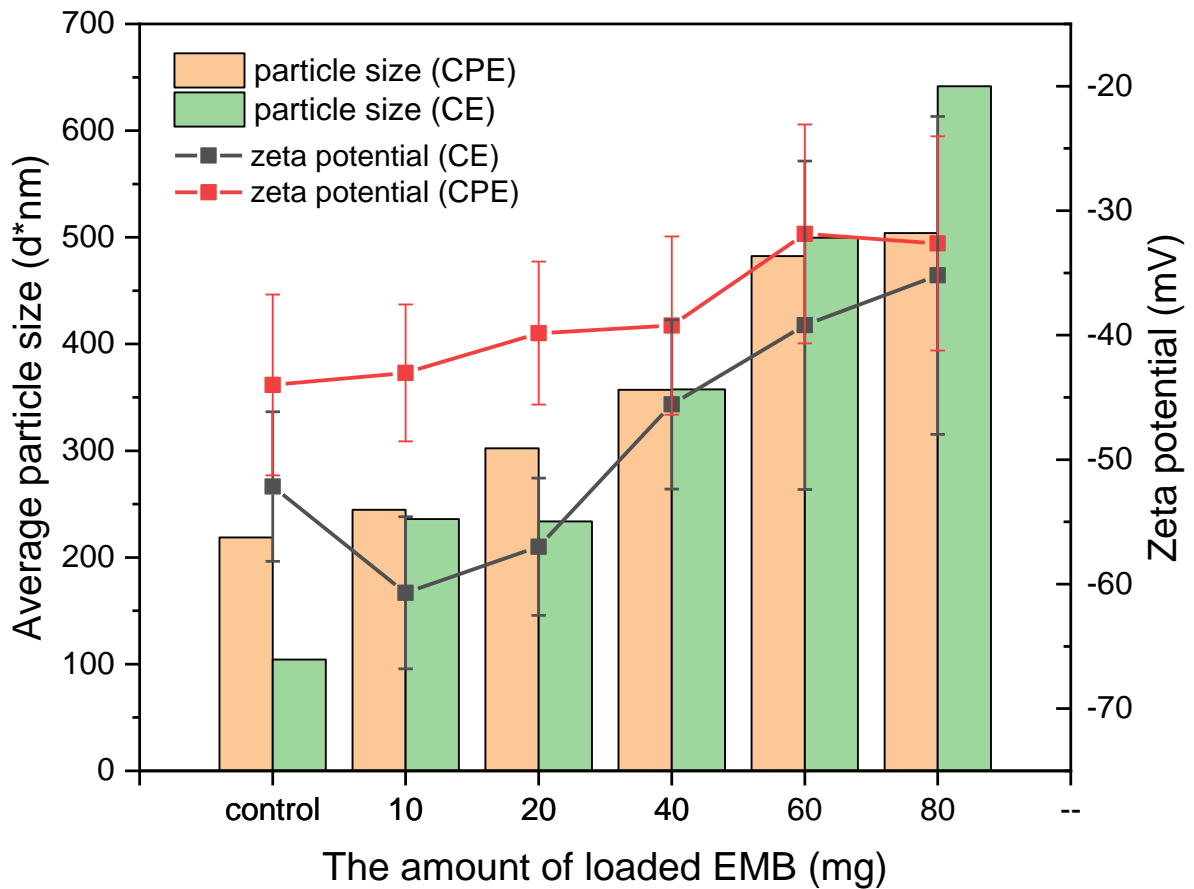
Figure 3-9. Particle size and zeta potentials of CP and CPE

The zeta potential of CNC and CNC/PVP was determined to be -50 and -40 mV, respectively. After introducing PVP, the zeta potential increased due to the non-ionic PVP. Also, the zeta potential gradually increased EMB was added to both CE and CPE due to the hydrophobicity of EMB. When 80 mg of EMB was added, the zeta potential of CE and CPE was increased to -35 and -33 mV, respectively. As the zeta potential approached the isoelectric point (zero surface charge), the system was sterically stabilized by the PVP. Overall, the average particle size and zeta potential of CE and CPE showed that the addition of EMB increased the particle size resulting in an unstable colloidal system.

3.3.4. Chitosan coating

In the design and development of the controlled antifungal delivery system for the control of sea lice in salmon, chitosan coating was introduced to improve its mucoadhesive properties. After analyzing the nanocomposite structure and the stabilization effect, chitosan was incorporated into CE and CPE. Chitosan is only soluble in acidic environment below its pKa (< 6.5). The poor solubility of chitosan limits its applications despite its many advantageous characteristics. To address this, we prepared chitosan-based nanomaterials that showed excellent colloidal stability, this modified formulation will be discussed in Chapter 4.

CEC and CPEC were synthesized in the acidic condition of pH 4 and 20 mg of EMB was encapsulated within the nanogels. Various concentrations of chitosan ranging from 0.01 to 0.6 wt. % were coated onto CE and CPE to prepare a mucoadhesive nanocomposite (CEC, CPEC). Figure 3-10 shows the colloidal property of CPEC with different amounts of chitosan. CPEC was well-dispersed and stable when 0.01 % chitosan solution was added. However, the system aggregated in the presence of 0.02 to 0.03 wt. % chitosan. Interestingly, the system was stabilized when a larger amount of chitosan (0.6 %) was added, and this colloidal behavior is associated to the electrostatic charge of the system. The addition of increasing amounts of chitosan to the system resulted in a shift of the zeta potential from negative to positive.
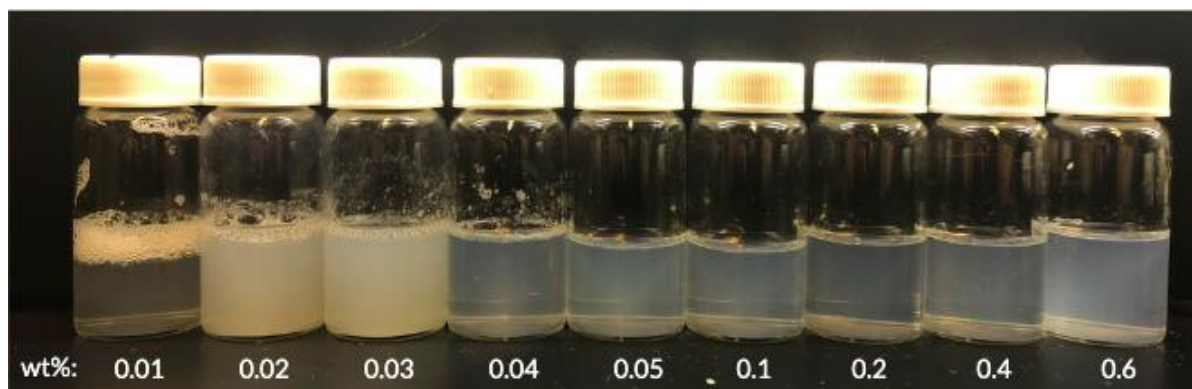
Figure 3-10. Optical image of CPC at various chitosan concentrations (0.01 to 0.6 wt.%)

In order to further study this colloidal phenomenon, the average particle size and zeta potential of CEC and CPEC were determined as shown in Figure 3-11. Since the chitosan solutions were injected into 0.5 wt. % CNC solutions, the mass ratio between CNC and chitosan could be determined as shown in Table 1:

Table 3. Mass ratio between CS and CNC

Sample	1	2	3	4	5	6	7	8
CNC (wt. %)	0.5	0.5	0.5	0.5	0.5	0.5	0.5	0.5
Chitosan (wt. %)	0.01	0.02	0.03	0.04	0.05	0.1	0.2	0.4
Mass ratio (CS:CNC)	1:50	1:25	1:17	1:13	1:10	1:5	1:2.5	1:1.3

*working volume = 10 mL, all samples contain 20mg of EMB

The average particle sizes of pristine CNC and CNC/PVP were 100 and 200 nm, respectively. When anionic CNC and CNC/PVP were coated with cationic chitosan polymer, the particle size steadily increased due to strong electrostatic interactions.[96] When 0.01% of CS

(1:50 CS:CNC) was introduced, the system was stable with a small particle size and negative zeta potential. However, the system aggregated at 1:25 mass ratio, forming a macro-gel with an average particle size greater than 2 μm. The sample at 1:17 mass ratio exhibited similar aggregation where the particle size was larger than 1 μm. This aggregation was associated to the zeta potential of the system approaching 0 mV, where the nanoparticles became neutral and aggregated due to the loss of the electrostatic repulsion. However, when more chitosan (1:13 CS: CNC w/w) was added to the system, the zeta potential became positive, approaching +35 mV, thereby stabilizing the complex and yielded an average particle size lower than 700 nm. Interestingly, the average particle size became smaller than 200 nm at a mass ratio of 1:10 (CS: CNC), maintaining a positive zeta potential of ~ +40 mV. This is optimal for the mucoadhesive drug delivery system due to stable particle size and electrostatic interaction with the negatively charged mucus membrane. The particle size increased slightly to 600 nm at a 1:10 mass ratio, and the zeta potential remained positive at +50 mV. These results indicated that the mass ratio played a significant role in controlling the particle size and zeta potential of CPC and CPEC. In order to determine the optimal synthesis conditions for CEC and CPEC, other aspects, such as drug binding and encapsulation efficiency should be considered, and this will be discussed in subsequent chapters. In terms of physical characteristics of CEC and CPEC, a 1:10 mass ratio between CS:CNC was the optimal condition for targeted drug delivery to the mucus membrane due to colloidal stability and particle size. If a larger particle size is desired for a specific purpose, CPC or CPEC of up to 500 nm could be prepared by increasing the amounts of chitosan, while maintaining good colloidal stability. It was shown that PVP participated in reducing the particle size at various mass ratios, particularly for the 1:25 and 1:17 CS:CNC where significant aggregation occurred.
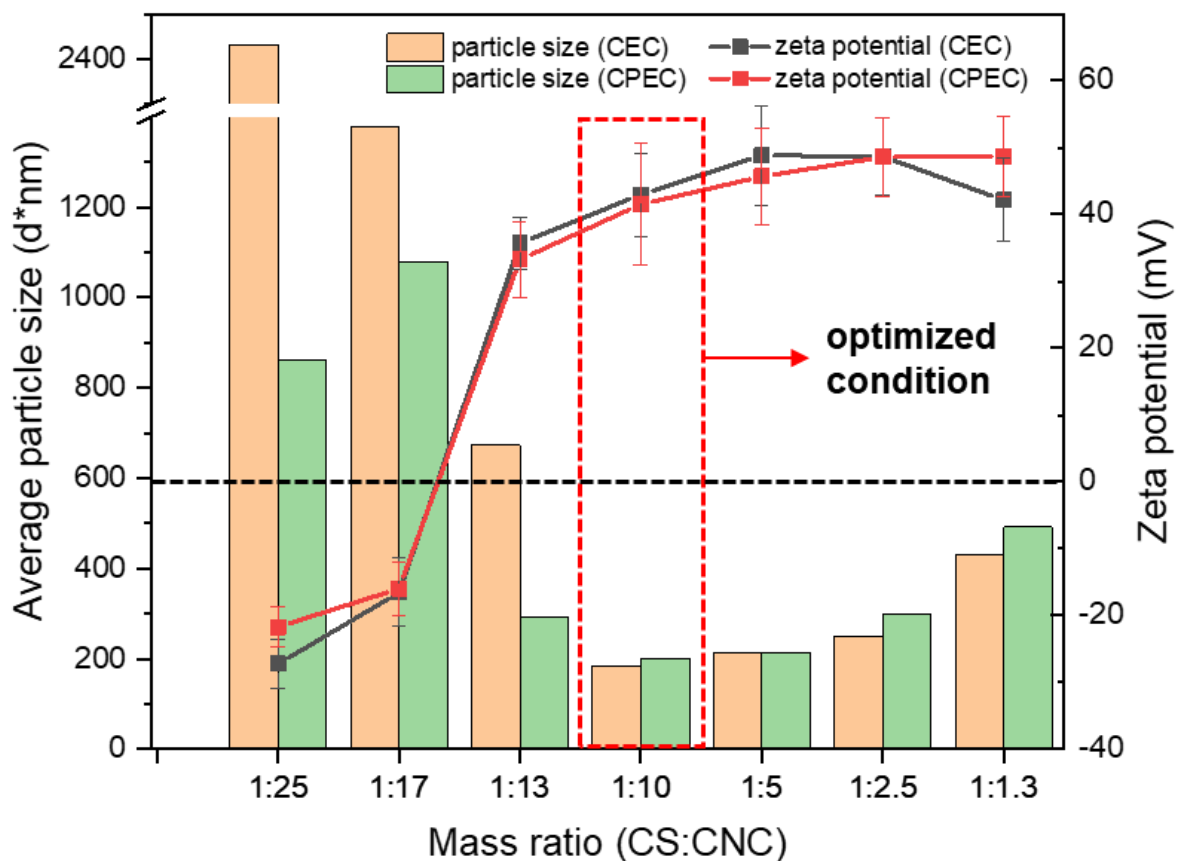
Figure 3-11. The average particle size and zeta potentials of CEC and CPEC

The colloidal behavior of CEC and CPEC nanocomposites was assessed with 20 mg of EMB. To determine the maximum loading amount of hydrophobic EMB into CEC and CPEC, a larger amount of EMB was introduced. As shown in Figure 3-12, CPE-20 was clear and stable in aqueous solution suggesting that EMB was successfully bound to the hydrophobic region of the CNC. The CNC/PVP was not saturated with 20 mg of EMB, however, when 80 mg of EMB was loaded to CNC/PVP, the solution became very opaque, an evidence of some aggregation of the free EMB in the aqueous suspension. Interestingly, the unstable CPE-80 system was stabilized when coated with chitosan, and Figure 3-12 shows that the CPEC-80 sample was clear and well-dispersed in water. This is because the chitosan was successfully

coated onto the hydrophobic CPE-80 particles, and these coated cationic chitosan particles electrostatically repelled each other and stabilized the colloidal system. Intramolecular repulsion of cationic chitosan polymer on nanocomposite plays an important role in generating electrostatic stabilization for CPEC in water. Based on these findings, chitosan could potentially be utilized as an electrostatic stabilizer for various hydrophobic drugs in the pharmaceutical industry.

CPE with 20mg EMB loading **CPE with 80mg EMB loading** **CPEC with 80mg EMB loading**

Good dispersion in water | Poor dispersibility due to increased hydrophobicity | Enhanced colloidal stability due to electrostatic repulsion (+) of coated CS
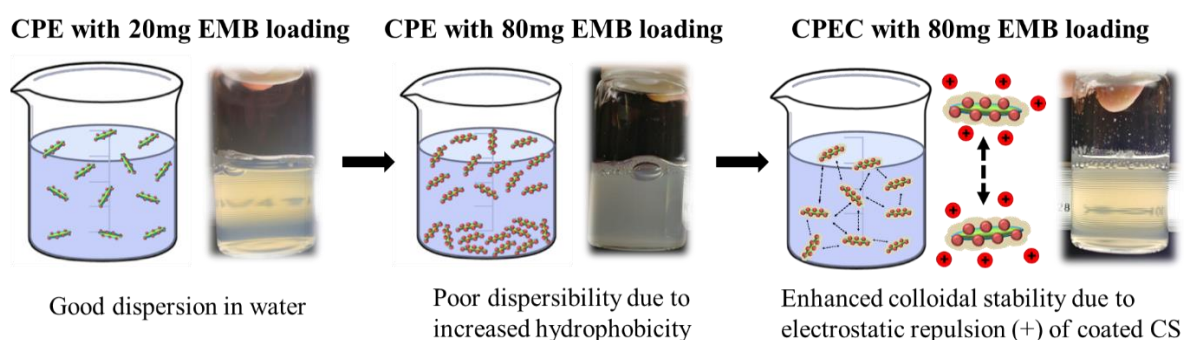
Figure 3-12. Colloidal behavior of CPE-20 (left), CPE-80 (middle), and CPEC-80 (right)

3.3.5. Drug binding and encapsulation efficiency

According to the Beer-Lambert law, $A=\varepsilon*l*c$, the optical attenuation of physical material (A) is proportional to the absorptivity of the attenuating species (ε), the optical path length (l), and the concentration of species (c). Based on the Beer-Lambert law, the concentration of EMB could be determined for computing the drug binding and encapsulation efficiency of nanoparticles. UV-vis spectroscopy was used to determine the drug binding and encapsulation efficiency as EMB has a distinctive UV-absorbance spectrum, with peaks at 237 nm and 245 nm. The UV spectra of EMB concentrations of between 10 to 200 ppm are shown in Figure 3-13A. All the spectra from 10 to 100 ppm exhibited peaks at 237 nm and 245 nm,

and the intensity increased with increasing EMB concentration. However, the measurement after 100 ppm was "noisy" due to the high absorptivity, so the range of EMB concentration for the drug binding study was kept to between 10 and 100 ppm. The calibration curve of EMB was plotted according to the Beer-Lambert law as shown in Figure 3-13B. The calibration curve is linear with absorptivity coefficient of 0.0281 from which the unknown concentrations of EMB were calculated and used to compute the binding and encapsulation efficiency of CEC and CPEC nanocomposites.

Drug loading efficiency and encapsulation efficiency are important parameters for nanotechnology-based drug carrier platforms. Drug loading efficiency (DLE) reflects the amount of drug loaded onto a single nanocomposite particle. Drug encapsulation efficiency (DEE) represents the percentage of drug successfully encapsulated into the nanocomposites. DLE can be affected by the physical and chemical structure of the drug carrier, while DEE can be affected by the concentration of drugs and carriers in the system, the drug loading mechanism, and other environmental conditions in the nanomaterial synthesis. Drug loading processes via physical and electrostatic adsorption usually result in low DEE, while drug loading through crystallization and covalent bonding exhibits higher DEE. Nano drug carriers with high DLE can be prepared using the desired synthetic protocol to achieve high DEE because physical structure of nanocomplex is an important factor to encapsulate sufficient amount of drug. [97]

In order to test the drug binding abilities of CEC and CPEC nanoparticles, four samples of CE and CPE containing different mass ratios of chitosan to CNC (1:10, 1:5, 1:2.5, 1:1.3) were selected and purified using a 100 nm membrane. As particle sizes of CE and CPE were greater than 100 nm, only unbound EMB was removed, and characterized by UV-vis to

determine EMB concentration. Figures 3-14 A and B show the UV-vis spectra of unbound EMB in the filtrate recovered from the CEC and CPEC. It was confirmed that the unbound EMB had distinct peaks at 237 and 245 nm, similar to pure EMB. Interestingly, it was observed that the absorbance peaks gradually decreased with increasing amounts of chitosan in the CEC and CPEC nanocomposites, which indicated that the drug encapsulation efficiency was reduced at higher chitosan concentrations. The calculated DLE and DEE based on the absorbance of filtered EMB contents are shown in Figure 3-14C. Increasing the EMB:CS ratio from 0.03 to 0.25 decreased the DLE from 11.6 to 1.2 %, and the DEE also decreased from 66.1 to 48.2 % for CPE and from 65.6 to 46.8 % for CPEC with increasing EMB:CS ratios. When the EMB:CS ratio was 0.03, the maximum DLE and DEE of 11.6 and 65.6% were obtained. A similar reduction in the DEE of chitosan nanoparticles with increasing amounts of chitosan in the system was observed by Jiang et al.[98] These results show that excessive amounts of chitosan hinder the drug-loading process of the nanoparticles. Interestingly, when the EMB:CS ratio was 0.03, the CS:CNC ratio was 1:10, where the most stable colloidal behavior was observed (Figure 3-14). We concluded that the amounts of all components (CNC, CS, EMB) can affect the drug loading capabilities of the nanocomposite. The optimal CPEC colloidal stability and DLE was observed when the CS:CNC ratio was 1:10 and the EMB:CS ratio was 0.03.

A)

B)
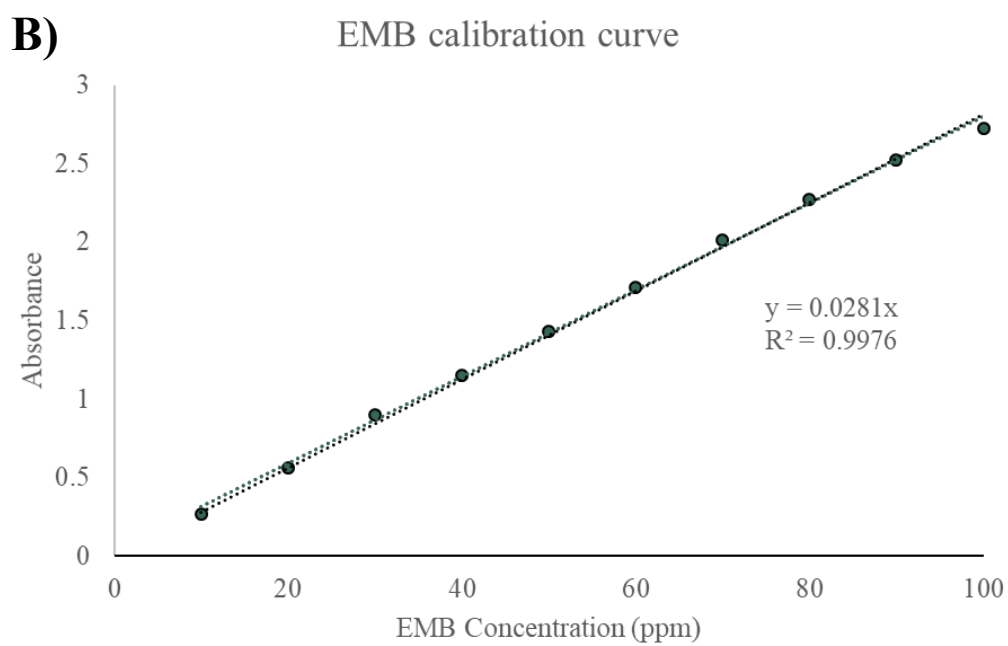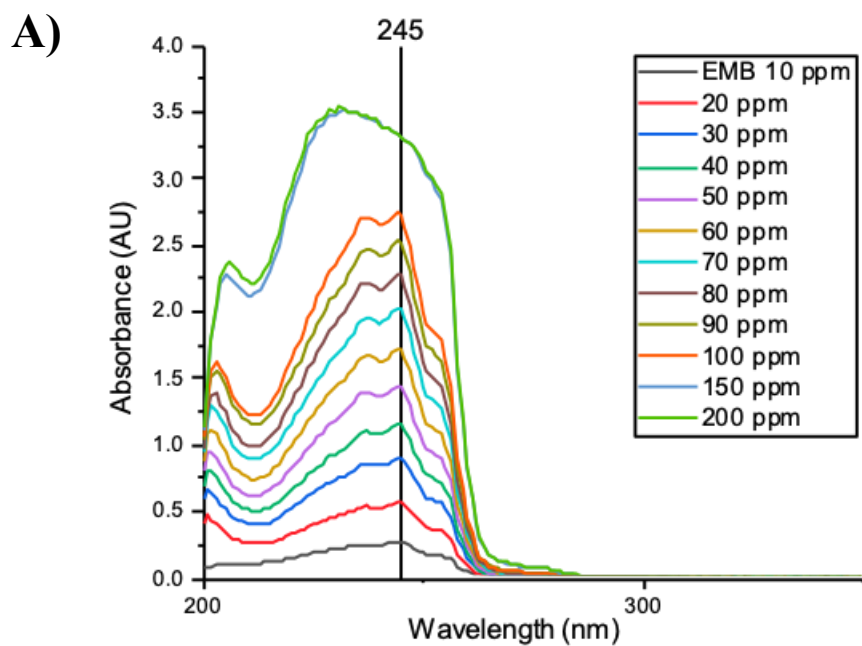
Figure 3-13. A) UV-vis spectra of Emamectin benzoate (10 ppm to 200 ppm), B) EMB

calibration curve
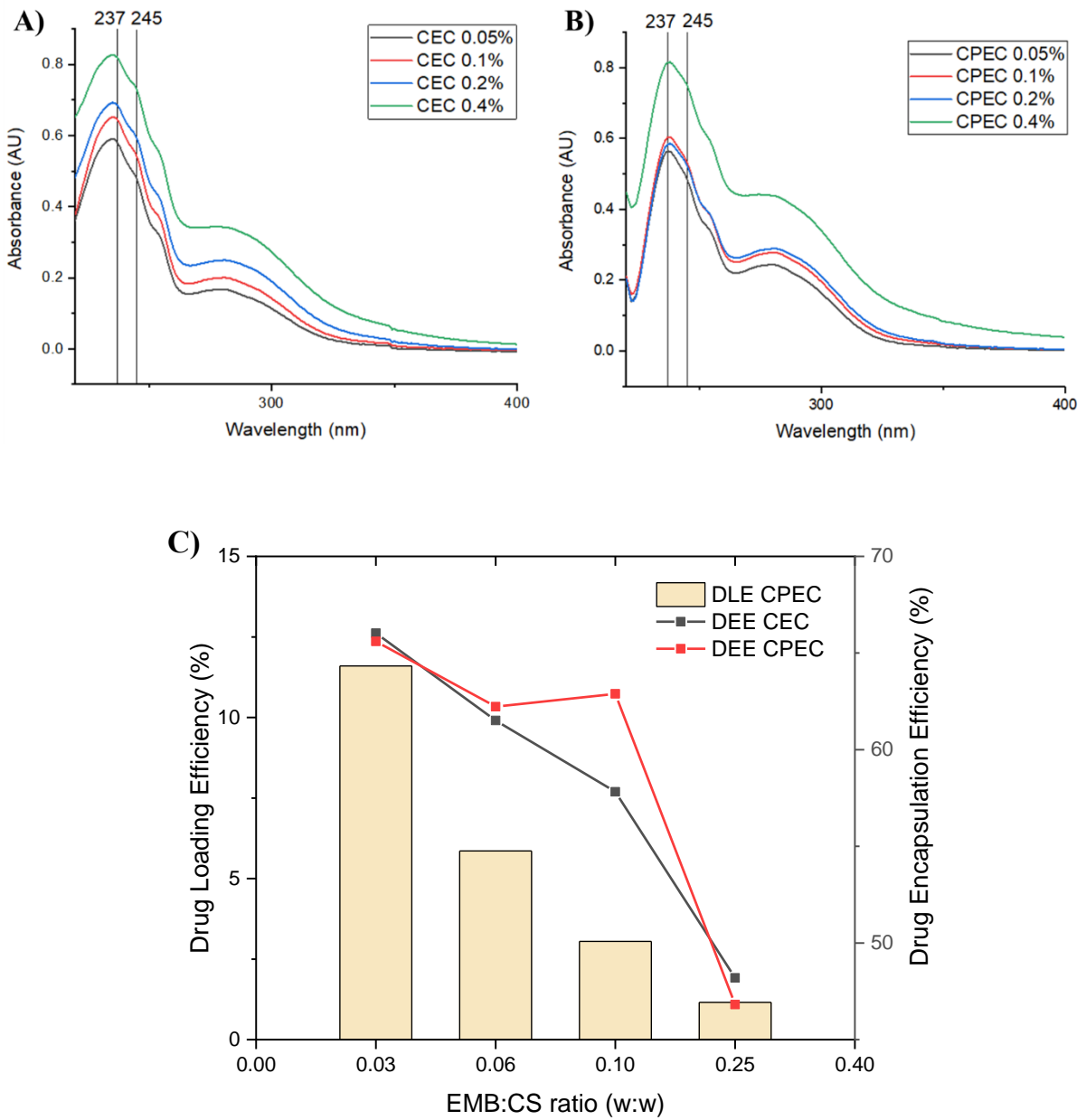
Figure 3-14. UV-vis spectra of unbound EMB after filtering from CEC (A) and CPEC (B) and C) Drug loading and encapsulation efficiency of CEC and CPEC at different mass ratios of EMB to CS.

3.3.6. Antifungal activity

The antifungal ability of CPEC nanoparticles was evaluated by measuring the production of carbon dioxide, which is a product of sugar metabolism by *S. cerevisiae*. The rapid conversion from sugars to ethanol and carbon dioxide is the most prominent characteristics during metabolisms of S. cerevisiae, where CO_2 was produced through oxidative phosphorylation and fermentation and this process is dependent on the environmental conditions. In aerobic conditions, pyruvate is broken down into CO_2 and adenosine triphosphate (ATP) through oxidative phosphorylation. However, in anaerobic conditions, sugars are converted to ethanol and CO_2 by fermentation, a process described by the Gay-Lussac equation: $C_6H_{12}O_6 \rightarrow 2CH_3CH_2OH + 3CO_2$.[99] Therefore, analyzing the volume of CO_2 production provides an indicator on the anti-fungal activity of the compounds against *S. cerevisiae*. Table 2 shows the specific components (CNC, EMB, and CS) and their concentrations for each test.

Table 4. The components of tested groups for antifungal activity

	CNC (µg/mL)	EMB (µg/mL)	CS (µg/mL)
Control	0	0	0
EMB	0	240	0
CPEC-1	250	20	25
CPEC-2	500	40	50
CPEC-3	1000	60	75

*working volume = 5 mL

The control group comprising of pure yeast without treatment, showed the highest rate of CO_2 production (~ 0.3 mL/min). EMB (240 µg/mL) was introduced to the yeast medium

and the production rate of CO_2 decreased to $\sim$ 0.175 mL/min. Considering its high concentration, the inhibition degree of metabolic activity of S. *cerevisiae* was not satisfactory. To test the antifungal activity of CPEC nanoparticle, different doses of CPEC loaded with EMB were introduced to the S. *cerevisiae* medium (Table 2). The addition of CPEC 1 to CPEC 3 successfully diminished the yeast metabolism as shown in Figure 3-15. It was observed that CPEC-1 inhibited CO_2 production; and the antifungal activity were almost similar to EMB. CPEC-1 exhibited better antifungal efficiency considering that only contains 20 µg/mL of EMB, which is 12 times lower than EMB. CPEC-2 inhibited more than half of yeast metabolism activity and CPEC-3 completely inhibited the metabolic activity of S. *cerevisiae*. It was observed that CPEC nanocomposite exhibited much stronger antifungal properties than pure EMB; and antifungal capabilities of CPEC nanoparticles are due to addition of CS. In later chapters, the yeast plate tests will be discussed to provide a better understanding of the antifungal properties of the CPEC nanocomplex.
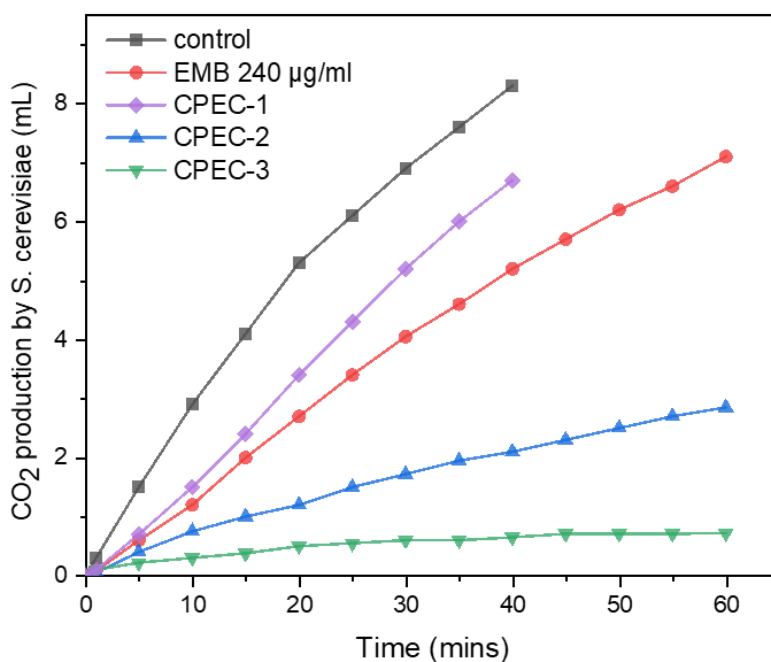
Figure 3-15. Antifungal activity of CPEC: accumulative CO_2 production by S.cerevisiae

3.3.7. Mucoadhesive properties on fish skin

To evaluate the mucoadhesive capabilities of the nanoparticles, chitosan labelled with FITC was used to prepare fluorescence labelled CNC-PVP-CS-FITC nanoparticles (CPC-f). The synthesis of CPC-f is based on the chemical conjugation between the primary amino groups of CS and the isothiocyanate group of FITC. The mucoadhesive properties of the nanocomposite were studied using the zebra fish as an animal model. After 30 mins of exposure to the CPC-f, the zebra fish were anesthetized and washed several times to remove unbound nanoparticles that may have remained on the surface of fish skin. As shown in Figure 3-16, the fluorescence image of zebra fish skin shows that labelled CPC bind well to zebra fish mucus. Zebra fish have horizontal lines on their surface. Interestingly, it was observed that CPEC nanocomposites specifically bound to the horizontal lines on zebra fish tails (Fig. 3-16a). CPEC binding was observed at other regions including the body (Fig. 3-16b) and the head (Fig. 3-16c). CPEC nanoparticles bind to the zebra fish surface via electrostatic interaction and hydrogen bonding. As mucus is composed of water, the abundant hydroxyl groups of CNC and CS form hydrogen bonds with the mucus. Furthermore, cationic CS polymers are attracted to the negatively charged mucin protein of zebra fish. In later chapters, the interaction between CS and mucin will be discussed in greater details. The fluorescence images were recorded in a transmitted fluorescence microscopy; therefore, only thin skins could be observed because light cannot be transmitted through thick fish skin. Scattered light microscopy will be conducted with different time exposures to CPEC in future studies.
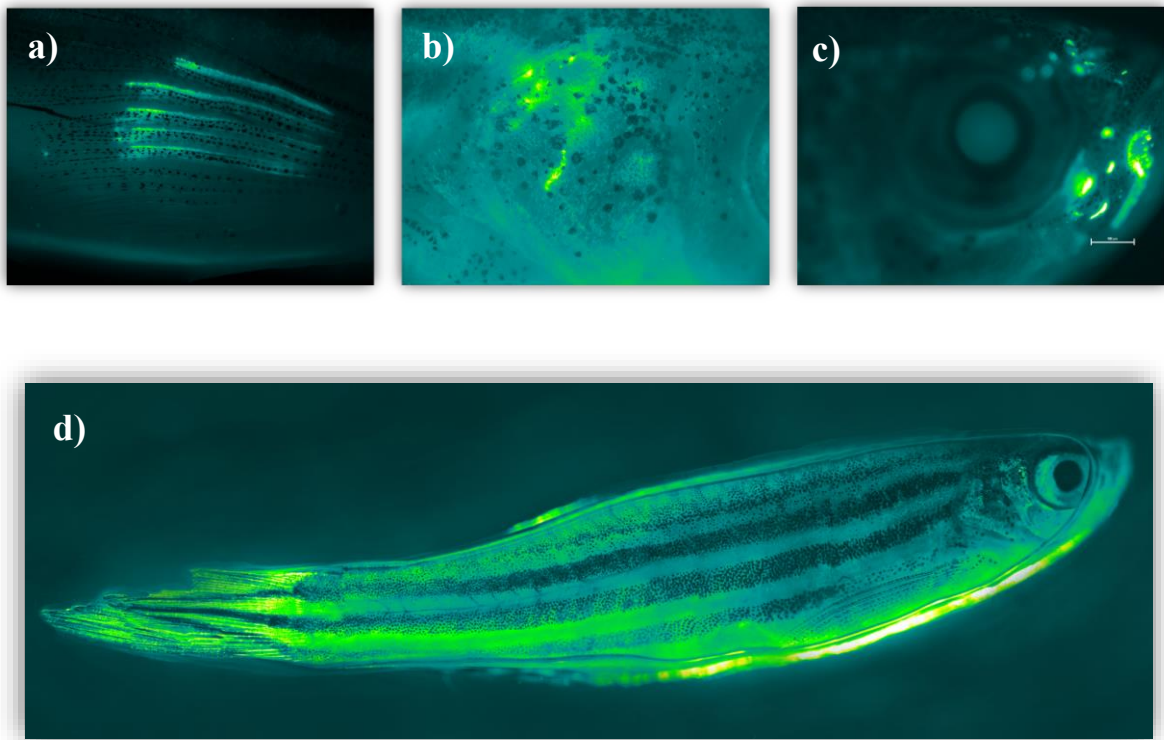
Figure 3-16. Fluorescence image of CPEC on zebra fish: a) tail, b) body, c) head; bar scale is 100 μm; d) fluorescence image of entire zebra fish skins after 30 mins of CPEC exposure.

Kovacs et al. (2009) studied the potential environmental risks of CNC nanotoxicity by performing a wide ecotoxicological evaluation through toxicity assays on rainbow trout hepatocytes and nine aquatic species including *Ceriodaphnia dubia*, *Daphinia magna*, and fathead minnow (*Pimephales promelas*).[100] There was no genotoxicity found after CNC exposure. In assays with nine species, there were no other effects on thesurvival and growth rate observed at CNC concentrations below 1 g/L, although CNCs affected the reproduction of the fathead minnow with an IC_{25} value of 0.29 g/L.[100] Therefore, CPEC nanocomposites will have fewer harmful effects on both fish and the environment, as the incorporated amounts of CS and CNC in the nanocomposites were less than 0.2 g/L, which will not impact fish survival and growth rate. Cytotoxicity tests on fish skin were not conducted. However, it was observed that fish can survive for more than a week after exposure of CPEC on their skins.

3.4. Conclusion

The particle size of the CPEC nanocomposite ranged from 200 nm to ~2 μm, depending on the mass ratio of CNC to CS. The optimized mass ratio (CNC:CS w/w) was 10:1 and exhibited stability in an aqueous system with a particle size of 200 nm and zeta potential of around +40 mV. Hydrophobic molecules (EMB) were successfully encapsulated in CPEC nanoparticles yielding a stable suspension due to increased hydrophilicity. PVP enhanced the colloidal stability of the nanocomposites during the drug encapsulation process. The drug loading and encapsulation efficiency of CPEC were 11.6 and 65.6 %, respectively. Both the DLE and DEE decreased as the CS concentration was increased with maximum binding properties achieved at a mass ratio of 10:1 (CNC:CS w/w). CPEC exhibited better antifungal activities than pure EMB against *S. cerevisiae*. The mucoadhesive properties of CPEC nanoparticle were demonstrated using a zebra fish, and the nanoparticles were successfully bound to zebra fish mucus and remained on the fish skin for several days.

Chapter 4. Synthesis and morphology of quaternized chitosan and cellulose nanocrystals nanogels
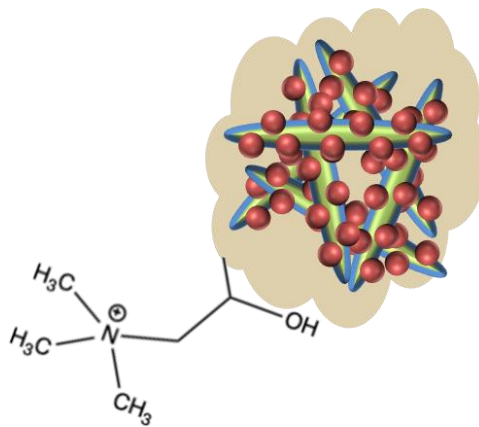
4.1. Introduction

Chitosan is one of several cationic polysaccharides found in nature, and due to its unique characteristics, chitosan has been incorporated in numerous biomedical applications. Furthermore, chemical modification techniques enable the functionality of chitosan to be enhanced. The poor solubility of chitosan above pH 6.4 is one of the major challenges limiting its applications. To address this, chitosan derivatives have been synthesized by converting the primary amino groups to other functional groups. The features of chitosan can be modified depending on the degree of deacetylation, molecular weight, and the sequence of repeating units, that significantly alter its innate physicochemical and biological properties.

Glycidyltrimethylammonium chloride (GTMAC), a quaternary ammonium compound (QAC), possesses strong antibacterial effects and can be coated onto various substrates. The epoxide rings of GTMAC can also react with the primary amino groups of chitosan. GTMAC modified materials have been utilized in various applications, such as surfactants, fabric softeners, and antibacterial agents. GTMAC has strong antimicrobial capabilities as its cationic ammonium groups can rupture bacterial cell surfaces. Additionally, the long alkyl chains of GTMAC can be used as antimicrobial agents and disinfectants.[101]

Previously, we prepared GTMAC-CS (Gch) for Pickering emulsion in functional food application to improve the solubility of chitosan[102]. From our understanding of previous studies, Gch plays three major roles in enhancing the functionality of nano drug carriers in mucoadhesive drug delivery applications: 1) increasing the colloidal solubility of chitosan-based nanomaterials, 2) providing a permanent positive charge for electrostatic interaction with the mucous membrane, and 3) improving antimicrobial effects.
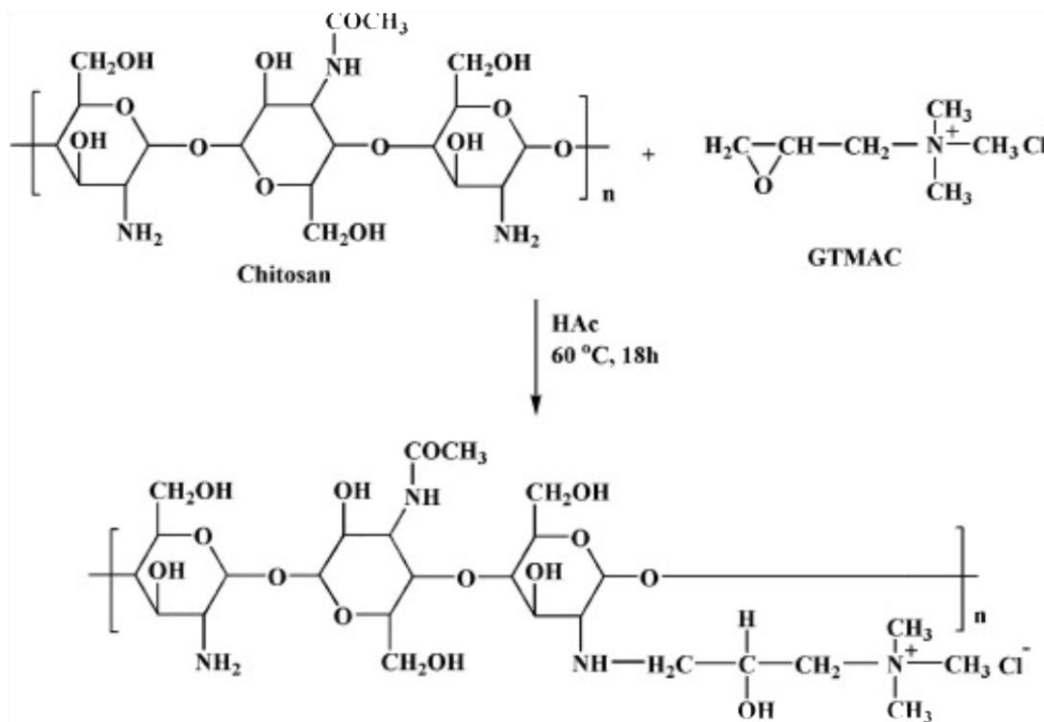
Figure 4-1. Synthesis scheme for GTMAC-Chitosan (adapted from Sajjan et al.[2])

We proposed three major mucoadhesive drug delivery mechanisms/stages to target the mucosal infection site: 1) proximity adhesion, 2) contact adhesion, and 3) drug release as described in Figure 4-2. First, the nanoparticle loaded with drugs should diffuse to the mucus layer for adhesion. To achieve proximity adhesion, attractive forces between the nanoparticle and the mucus layer are necessary, and the possible driving forces include electrostatic interaction and hydrogen bonding. The abundant hydroxyl surface groups of CNC can generate hydrogen bonds with the mucus layer, which is composed primarily of water. Furthermore, the positively charged nanoparticles can interact electrostatically with the mucus layer where the surface charge is negative. A stronger positive surface charge of nanoparticle will intensify the electrostatic interactions with the mucus layer and improve the binding. The second stage of our proposed delivery mechanism is contact adhesion. This is achieved by employing the catechol groups, which are well-known mussel-inspired active compounds for underwater

adhesion. The catechol groups will induce covalent bonds with the amino or thiol groups of the mucin protein, anchoring them to the mucus surface. Utilizing these bio-inspired active compounds for our nano drug delivery system will facilitate the sustainable drug release and a reduced dosage, and this will be discussed in Chapter 5. The final stage of the drug delivery mechanism is "mucus penetration" of the CPEC nanocomposite. As chitosan biodegrades at the target site, the encapsulated drug will be released from the pores of the chitosan polymeric structure. The CPEC nanocomposite was designed to penetrate the mucus layer that is highly hydrophilic. Amphiphilic PVP was used as a penetration enhancer to improve the diffusive properties and penetration of the hydrophobic molecules. Consequently, these PVP coated drugs will have an enhanced degree of penetration through the mucus layer, epidermis, hyper dermis, and dermis layer for therapeutic treatments.
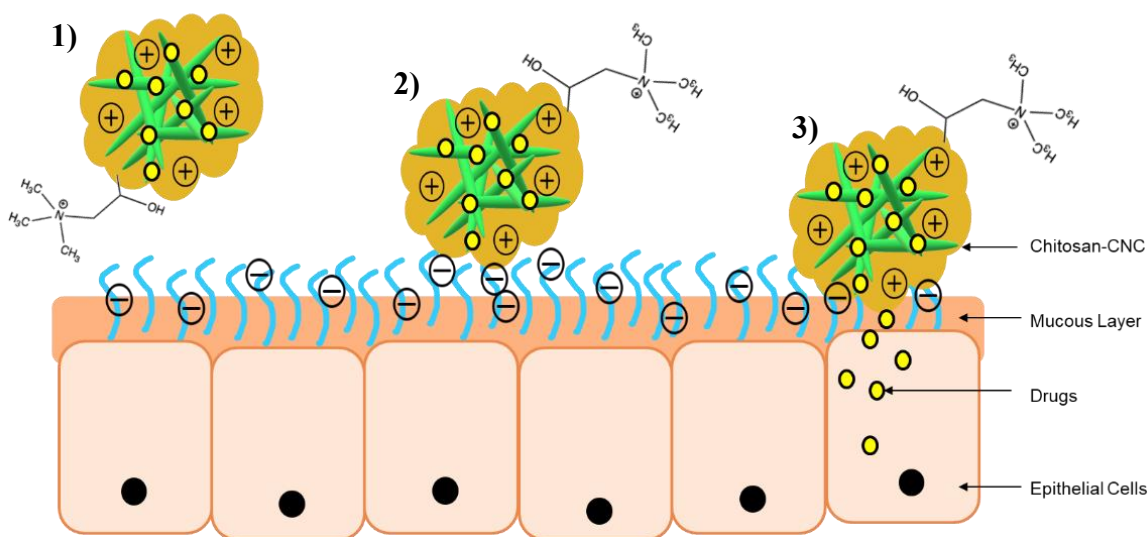
Figure 4-2. Mucoadhesive drug delivery mechanism of CPECg

In this chapter, the preparation of a nanocomposite comprising of CNC and GTMAC-modified chitosan for mucoadhesive drug delivery applications is described. The synthesis

method, optimized synthesis conditions, colloidal behavior, and morphological structure of the CNC/GTMAC-CS nanocomposite (CPCg) will be examined.

4.2. Experimental section

4.2.1. Preparation of GTMAC-chitosan (Gch)

1 wt.% chitosan (low molecular weight) solution was prepared by dissolving in 1% acetic acid solution. GTMAC and 1 wt.% of chitosan (0.6:1 mass ratio) were mixed at 60˚C for 18 hours under nitrogen purge with magnetic stirring. Then, Gch was washed several times with ethanol and dialyzed for three days to remove unreacted GTMAC. Finally, Gch powder was prepared by freeze drying for 24 h.

4.2.2. Synthesis of CPECg

Briefly, 1g of CNCs and 0.1g of PVP were mixed in 0.8 mL of acetone and stirred overnight. Various amounts of EMB (10 - 200 mg) were dissolved in 0.2 mL of acetone. EMB (0.2 mL) solutions were slowly injected into the CNC/PVP solutions (0.8 mL) under sonication for 5 minutes. Then, the mixtures were dried in an oven at 40 ˚C and re-dispersed in milli-Q water (200 mL). For CS encapsulation, various concentrations of CS and GTMAC-CS (Gch) were prepared in 1 % acetic acid solution. The Gch solution was slowly injected into CE and CPE solutions using a syringe pump at a rate of 1.5 ml/min under probe sonication.

4.2.3. Conductometric titration

In order to determine the degree of quaternization (DQ) of chitosan, conductometric titration was conducted as previously described by Li et al.[103] 20 mg of Gch was dispersed in 40 mL of water and titrated with 0.01 M $AgNO_3$ solution. DQ was calculated based on the

following equation:

$$Degree\ of\ Quaternization\ (DQ) = \frac{C \times V}{C \times V + \left(\frac{W - C \times V \times M_2}{M_1}\right)}$$

C: concentration of $AgNO_3$ (M), V: volume of $AgNO_3$ (L), M: weight of Gch (g), M_1:

Molecular weight of CS (g), M_2: Molecular weight of Gch (g)

4.2.4. Morphological studies of CPECg

The morphologies of CPEC prepared using two different protocols were analyzed. Firstly, chitosan solutions (with 1 % acetic acid) and CNC/PVP solutions (wt. 0.5 %) were prepared. The optimized mass ratio 1:10 (CNC: CS), which was found in earlier characterization studies, was used for the morphological studies of the CNC/PVP/Gch nanocomposite. Two different methods were used to synthesize the CPCg. First, the CNC/PVP solution was slowly injected into the Gch solution at a rate of 1.5 mL/min. Next, Gch solution was injected to CNC/PVP solution at the same rate. Then the morphology of the prepared samples was evaluated by transmission electron microscopy (TEM).

4.2.5. Antibacterial test against E coli

Anti-bacterial analyses of CS, Gch, CE, CEC, and CEC-g were conducted for two different concentrations against *Escherichia* coli (E. coli) as a model organism. Briefly, E. coli was grown for 24 hours diluted 100 times. CS, Gch, CE, CEC, and CEC-g suspensions were prepared and 40 µL of E. coli cells was added to each suspension. The final volume was adjusted to 1 mL using 1 x PBS buffer (pH 6.5). The tubes were incubated, and the number of colonies was incubated and counted on the agar plates.

4.3. Results and discussion

4.3.1. Degree of quaternization of Gch

Gch was prepared by converting the amino group of CS to GTMAC. The degree of quaternization is dependent on the molecular weight of chitosan, synthesis time, temperature, and the molar ratio of GTMAC to the amino groups on the chitosan.[102] In order to determine the degree of quaternization, conductometric titration was used to measure the amount of Cl^- counterions. $AgNO_3$ was injected to the Gch suspension and the silver ions combined with the chloride ions to form silver chloride. When the existing Cl^- ions were fully titrated with $AgNO_3$, the conductivity started to increase as shown in Figure 4-3, and the transition corresponded to the neutralization point. The degree of quaternization of the synthesized Gch was determined to be 36.8 % by conductometric titration, and it determines the solubility and antimicrobial capabilities of the compound. Increased solubility of Gch with a degree of quaternization of 48% was previously demonstrated.[102] We found that Gch with a degree of quaternization of 36.8% also showed better solubility in neutral and alkaline pH. Furthermore, the degree of quaternization determined antimicrobial abilities as the positively charged quaternary ammonium groups can rupture the bacterial cell wall.
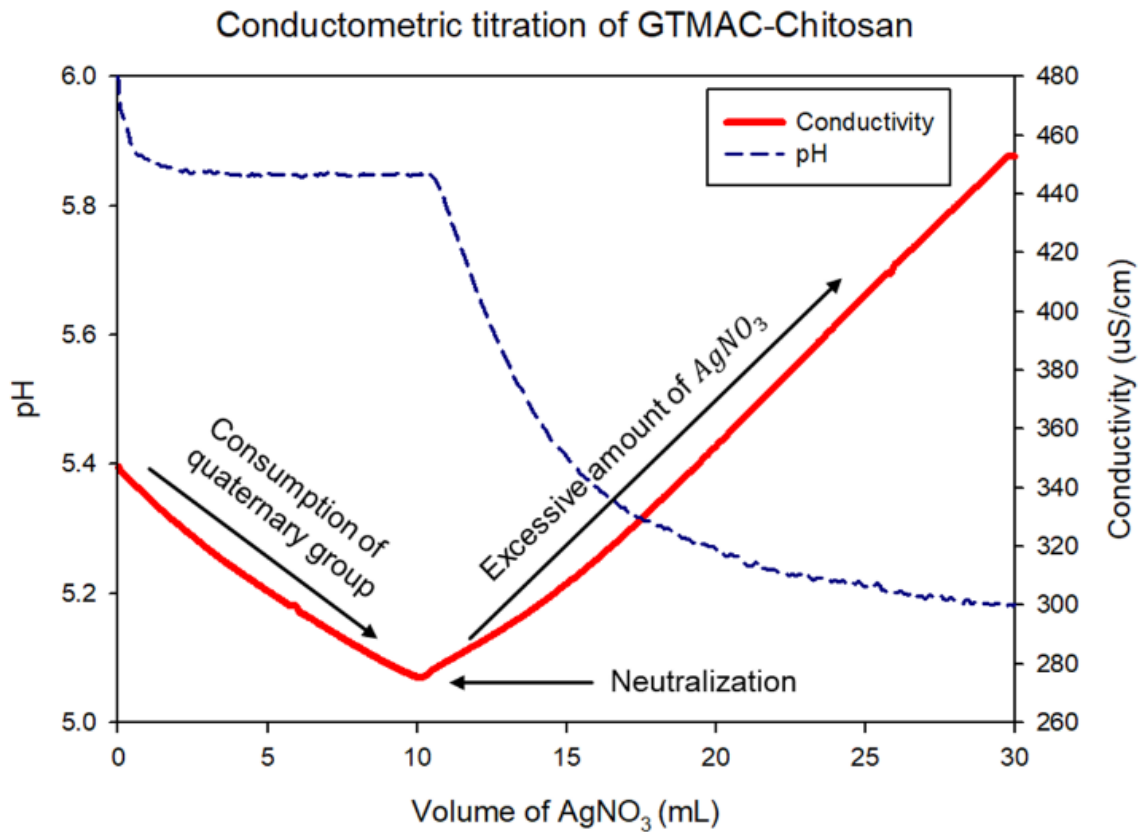
Figure 4-3. Conductometric titration of GTMAC-CS

4.3.2. Preparation of CNC/Gch nanogels

After quantifying the degree of quaternization of Gch, a nanocomposite consisitng of cellulose nanocrystals, PVP, and Gch (CPCg) was prepared following the same method used in the CPC preparation. Figure 4-4 shows the colloidal behavior of the synthesized CPCg. As observed previously with CPC, CPCg exhibited aggregation at a CS concentration of 0.05 % and became stable after 0.1 %. From 0.1 % to 1 % CS concentrations, the CPCg sample formed stable colloidal solutions. We observed that the system was stabilized upon the introduction of a specific concentration of CS to the CNC solution. This is because the positively charged CS coated the entire surface of the CNC, decreasing the interfacial tension between the particles resulting in enhanced electrostatic stabilization.
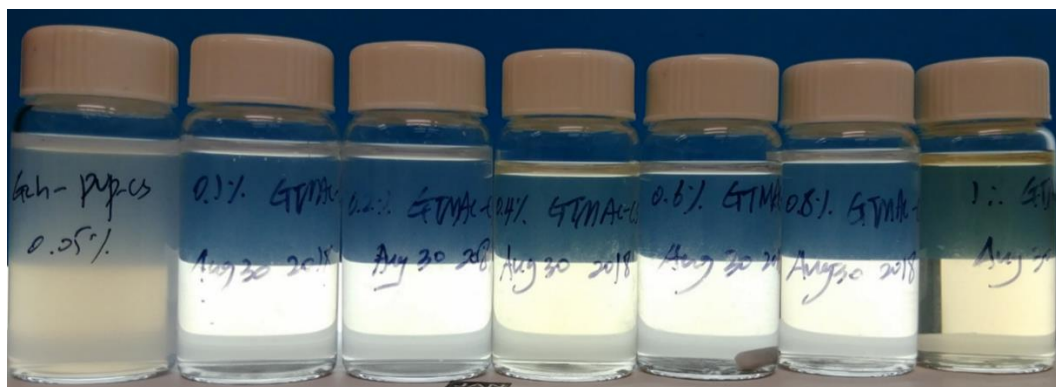
Figure 4-4. CPCg observed at different Gch concentrations

Conductometric titration (Fig. 4-5) was used to determine the content of GTMAC-CS in both aggregated (0.05 wt. % CS) and stabilized (0.2 wt. % CS) samples. If CPCg contains Gch, the conductivity should decrease as the Cl⁻ ions from GTMAC combined with silver ions to form insoluble silver chloride. Interestingly, no Cl⁻ ions were detected in CPCg at 0.05 wt. % as the conductivity increased as soon as the AgNO₃ solution was introduced (Figure 4-5A). However, it was confirmed that CPCg did contain some Cl⁻ ions at 0.2 wt. %. Figure 4-5B shows that the conductivity of AgNO₃ decreased due to precipitation with Cl⁻ ions from GTMAC. It was expected that both CPCg samples would contain Cl⁻ ions because Gch was incorporated into the system. However, the 0.05 wt. % sample does not show any detected Cl⁻ ions. Since this sample was aggregated, it is possible that the Cl⁻ ions were inaccessible due to interactions with the CNC.
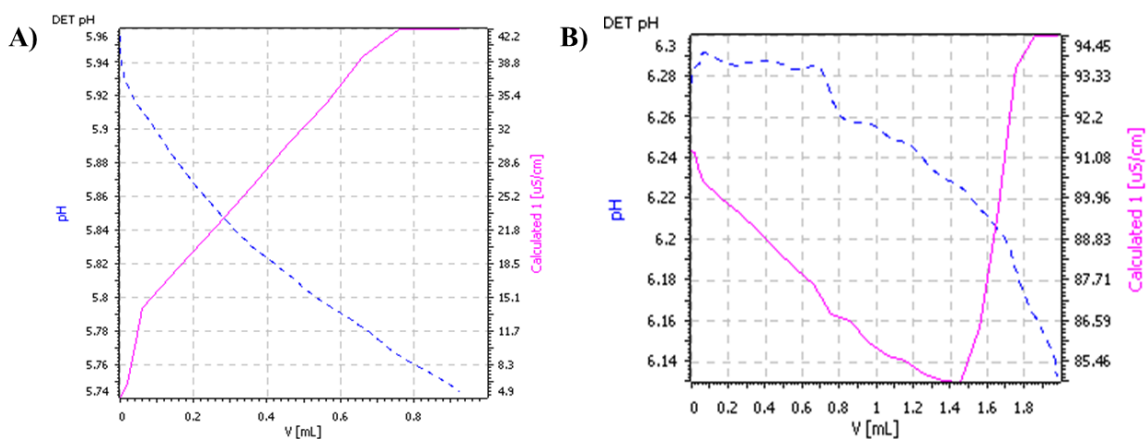
Figure 4-5. Conductometric titration to determine the existence of GTMAC in different concentrations. A) CS 0.05 wt. % and B) CS 0.2 wt. %

To determine the optimal mass ratio (Gch:CNC w/w) where the colloidal behavior of CPCg is the most stable, we analyzed the particle size and zeta potentials the CPCg of mass ratios between 0.05 to 0.1 %. Table 5 summarizes the mass ratios (Gch:CNC w/w) and the amounts of CNC and Gch, where the concentration of Gch in CPCg was increased from sample 1 to 7.

Table 5. **Calculation of mass ratio (CS:CNC)**

Sample	1	2	3	4	5	6	7
CNC (wt. %)	0.4	0.4	0.4	0.4	0.4	0.4	0.4
Gch (wt. %)	0.07	0.08	0.09	0.1	0.2	0.4	0.6
Mass ratio (Gch: CNC w/w)	1:5.7	1:5	1:4.4	1:4	1:2	1:1	1:0.7

*working volume = 20 mL

The particle size and zeta potentials of CPCg (Fig. 4-6) were assessed at pH 6.5. Due to the chemical modification of chitosan with GTMAC, the synthesis could be conducted at neutral pH. WE observed that CPCg exhibited similar colloidal behavior as CPC and CPEC.

The mass ratio between CNC and Gch is a key factor in determining the particle size and zeta potential. The particle size of CNC/PVP was less than 200 nm, and the addition of chitosan increased the particle size. At 1:5.7 and 1:5 (Gch:CNC), the system aggregated by forming macro-gels with particle sizes exceeding 2.5 μm and a zeta potential of close to 0 mV. The same aggregation was observed earlier for CPEC due to the loss of electrostatic charge when the system approached 0 mV zeta potential. However, at 1:4.4 (Gch:CNC), the particle size of CPCg began to decrease again achieving with a minimum particle size of 200 nm at a mass ratio of 1:4 . As the CS concentration was further increased, the particle size increased slightly, and no aggregation was observed. The zeta potential was maintained at approximately +20 mV. Based on these observations, we concluded that a mass ratio of 1:4 (Gch:CNC) was the optimal condition yielding a smallest particle size and a zeta potential of +20 mV. Compared to the CPEC nanoparticles, the optimized mass ratio shifted from 1:10 (Gch:CNC w/w) to 1:4 (Gch:CNC w/w). The colloidal behavior was different because CPEC contained hydrophobic drugs while CPCg did not, therefore, less chitosan was required to cover the surface of the CNCs, stabilizing the system via electrostatic repulsion. Furthermore, the zeta potential of CPEC was +40 mV while CPCg could achieve only +20 mV due to the different pHs where the measurements were conducted. CPEC was prepared and tested in an acidic environment and the amino groups of chitosan were protonated leading to a more positive zeta potential. However, CPCg was tested in pH 6.5 where the amino groups were less protonated.
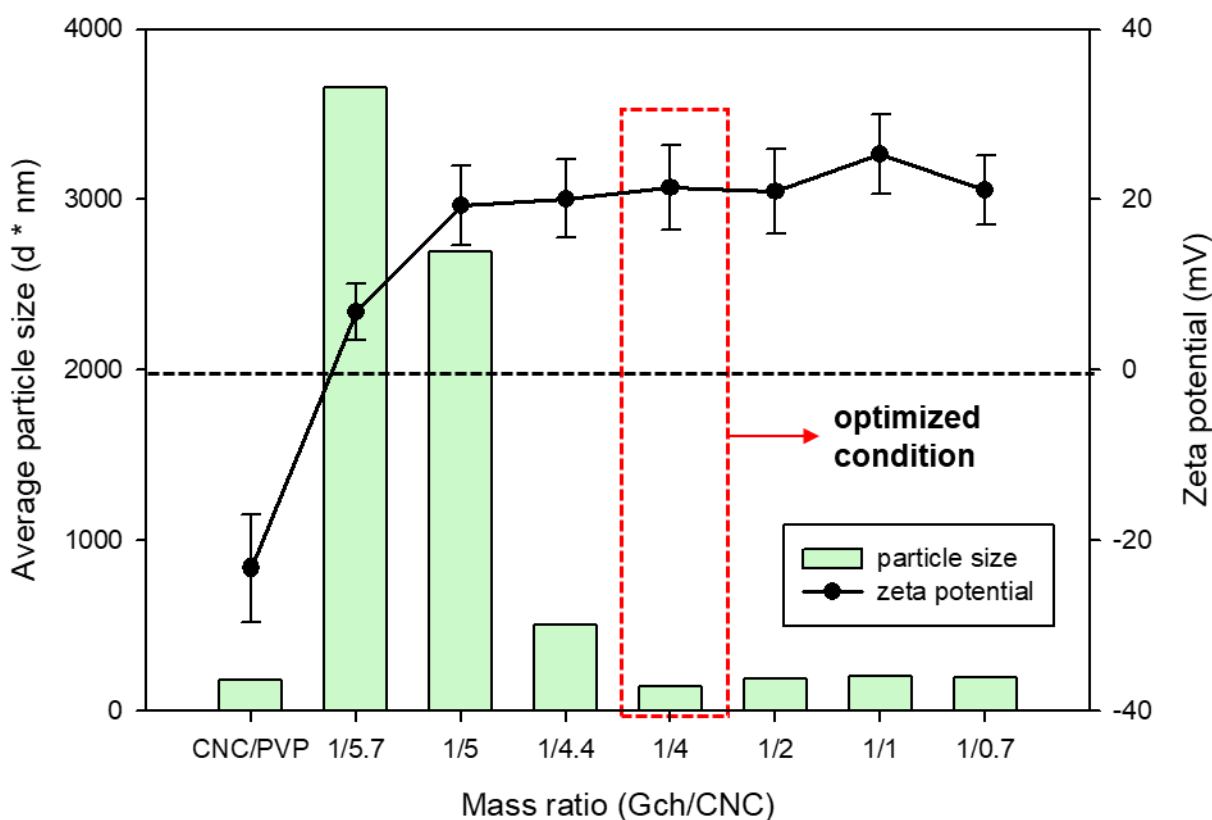
Figure 4-6. The particle size and zeta potential analysis of CPCg

4.3.2. The morphological properties of CNC/PVP/Gch

The morphology of the CPECg nanocomposite depended on the synthesis method, and two different protocols were used as shown in Figure 4-7. The same injection speed (1.5 mL/min) was applied in both synthetic protocols. When the CNC/PVP solution was slowly introduced into the CS solution under sonication, the TEM image of CPCg showed that the nanocomposite possessed an irregular random-coil structure (Figure 4-8 A, B). However, when CS solution was introduced into CNC/PVP solution at the same injection speed, the TEM image displayed a homogenous chitosan coating on the CNC/PVP nanoparticles as shown in Figure 4-8C, D. In method 1, the CNC/PVP nanoparticles exhibited a randomly coiled structure because the excess chitosan randomly coated the nanoparticles via strong electrostatic

interactions. However, when a small amount of CS polymer was injected into the CNC/PVP solution (method 2), chitosan evenly coated on the individual nanoparticles, suggesting that the order of adding the polymer played a significant role on the morphology of the nanocomposite. Introducing the chitosan polymer into the CNC/PVP nanoparticle solution is a better way to obtain a homogenous morphology. The concentration of the polymer and nanoparticles, sonication power, and injection speeds are several important factors to consider when preparing a homogenous coated nanostructure.
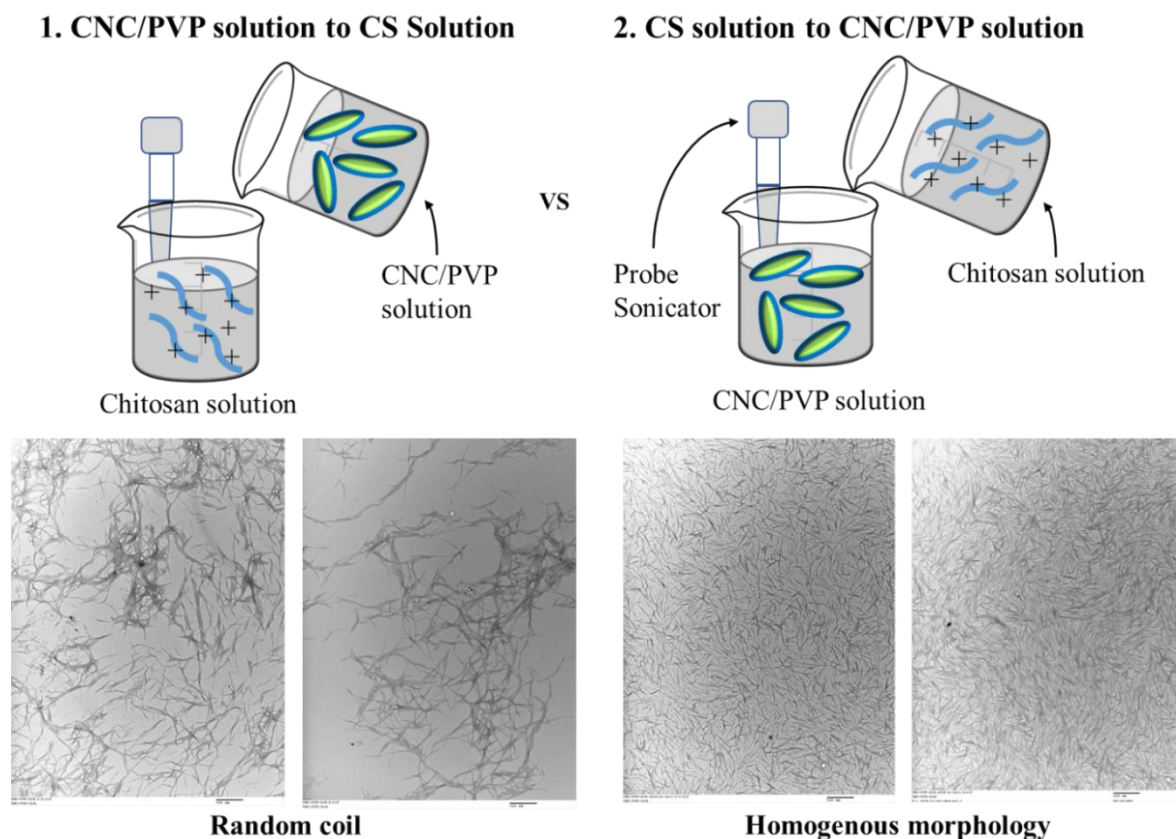
Figure 4-7. Different morphological structures of CPCg depending on the synthesis method. (1) CNC/PVP solution injected to CS solution; (2) CS solution injected to CNC/PVP solution. *Injection speed is 1.5 mL/min
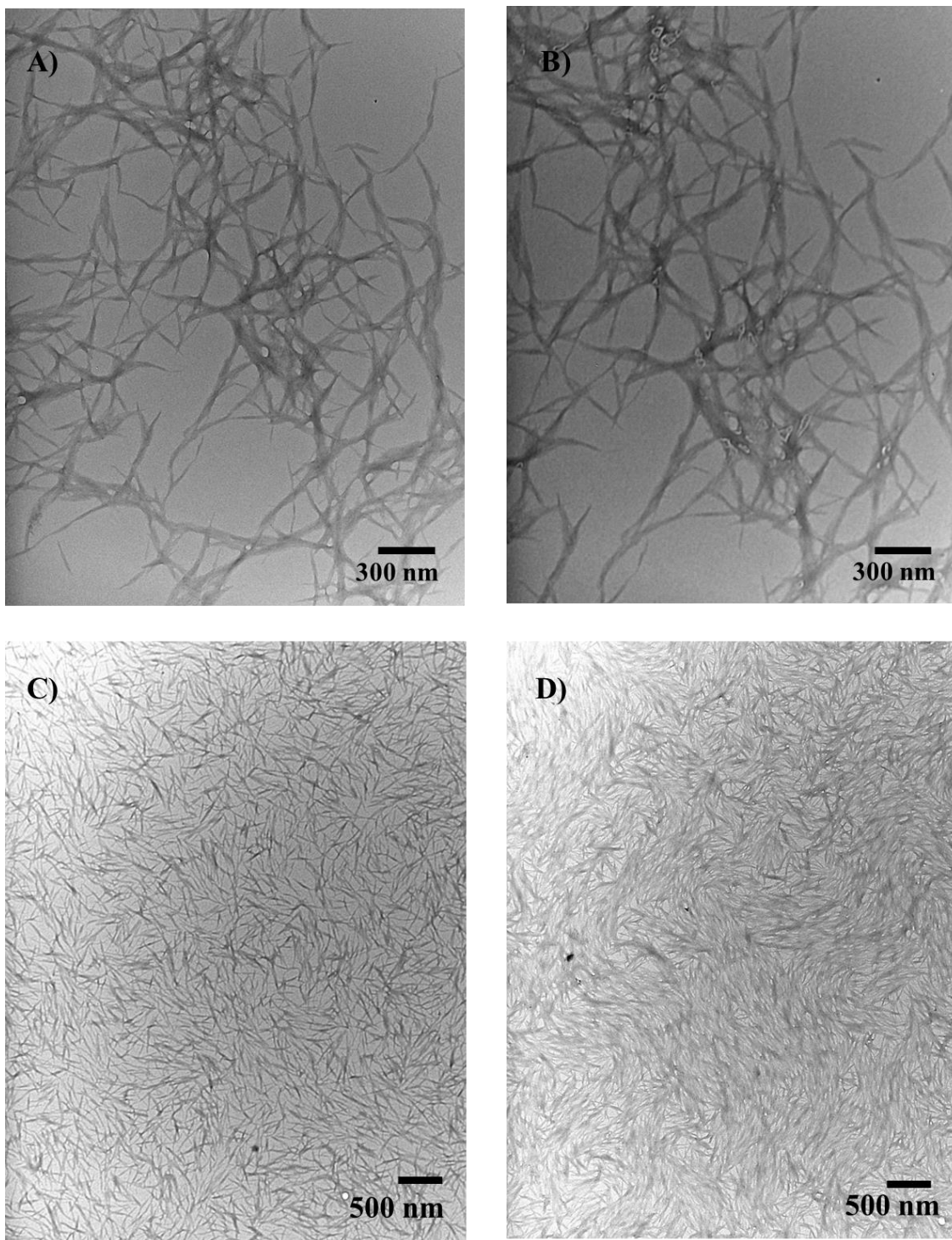
Figure 4-8. The different morphologies of CPCg depending on synthesis conditions. (A, B) random coiled structure; (C, D) homogenous coated structure

4.3.3. Antibacterial activity

The antibacterial mechanism of CS is based on interactions with the bacterial surface including the cell wall and outer membrane. Four models of antibacterial mechanism have been proposed.[104] The first and most widely accepted model for the antibacterial activity of chitosan is the electrostatic interaction between the negatively charged bacterial cell surface and the cationic groups of chitosan. The second proposed antibacterial mechanism of CS is the prevention of nutrient transport into the gram-negative bacterial cell by changing the permeability of the outer envelope due to the formation of ionic bonds. The third proposed mechanism is that CS inhibits the DNA transcription and interrupts mRNA and protein synthesis by perforating the bacterial cell. The fourth mechanism is based on chelation effects, where the amino group of chitosan interacts with the metal ions from bacterial surface.

The antibacterial capability against *E. coli* was evaluated. CS and Gch showed strong antibacterial activity at 80 µg/ml. However, CNC/EMB did not display antibacterial capability as shown in Figure 4-9. EMB is a derivative of emamectin, which is a common pesticide for treatment of nematodes, arthropods, and other pests in the agricultural sector. However, no effective antibacterial and antifungal activity of EMB has been reported. When CNC/EMB was coated with CS and Gch, CEC and CECg nanoparticles (Fig. 4-9) showed some antibacterial effects as evidenced by the plate test showing a reduced *E. coli* colony. The concentration of CS and Gch incorporated into the nanoparticles was 8 µg/ml. Therefore, we confirmed that CEC and CECg nanoparticles possessed antibacterial ability due to the presence of CS and Gch but the other components, including CNC and EMB, did not possess antibacterial abilities. The antiparasitic activity and the MIC value of the nanoparticles will be evaluated in future studies.
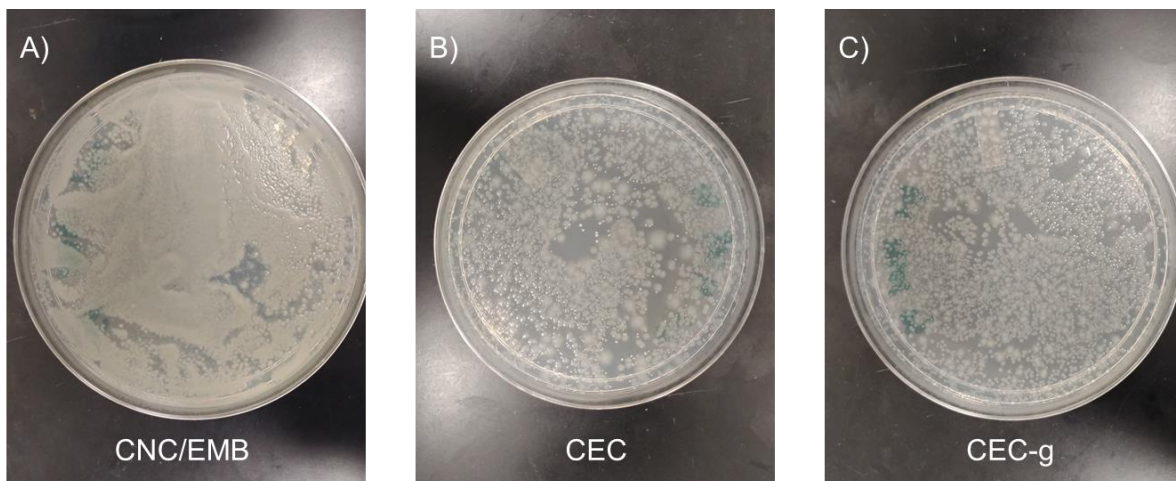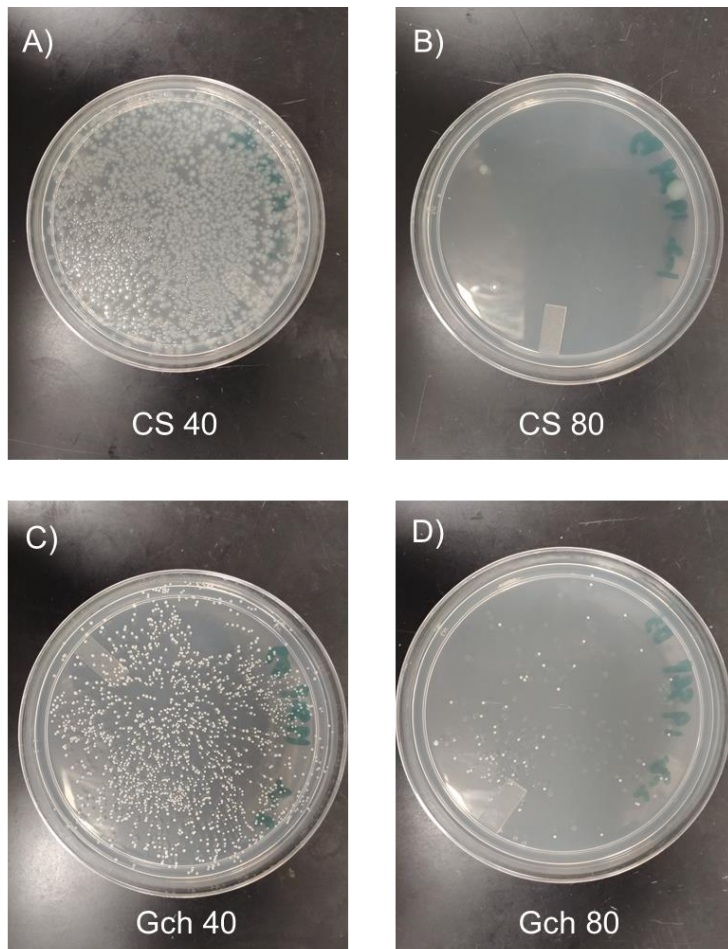
Figure 4-9. The antibacterial activity of CS and Gch against E. coli. A, B: chitosan, C, D:

Gch, Below: (A) CNC/EMB, (B) CNC/EMB/CS, (C) CNC/EMB/Gch

4.4. Conclusion

Mucoadhesive CPCg nanoparticles consisting of CNCs and GTMAC-CS (Gch) were synthesized via electrostatic gelation. The degree of quaternization of Gch was 36.8 % as determined by conductometric titration. The functionality (solubility and colloidal behavior) of CPCg was enhanced in neutral and alkaline pH compared to CPEC, which was not soluble in that pH range. The morphology of CPCg was dependent on the synthesis method, reaction time, and sonication power. Through morphological studies of CPCg, it was observed that suspension of nanocrystals should be introduced to sample containing the polymeric structure to generate a homogenously coated structure. When reversibly introduced from polymer to nanoparticle suspensions, irregular structure was observed. CS and Gch showed strong antibacterial and antifungal activity against *E. coli* and *S. cerevisiae*, whereas EMB did not exhibit antibacterial effects against *E. coli* and *S. cerevisiae*. CPCg showed some antibacterial and antifungal ability due to the addition of Gch, and the exact MIC would be determined in future studies.

Chapter 5. A bio-inspired catechol modified chitosan and cellulose nanocrystals nanogel
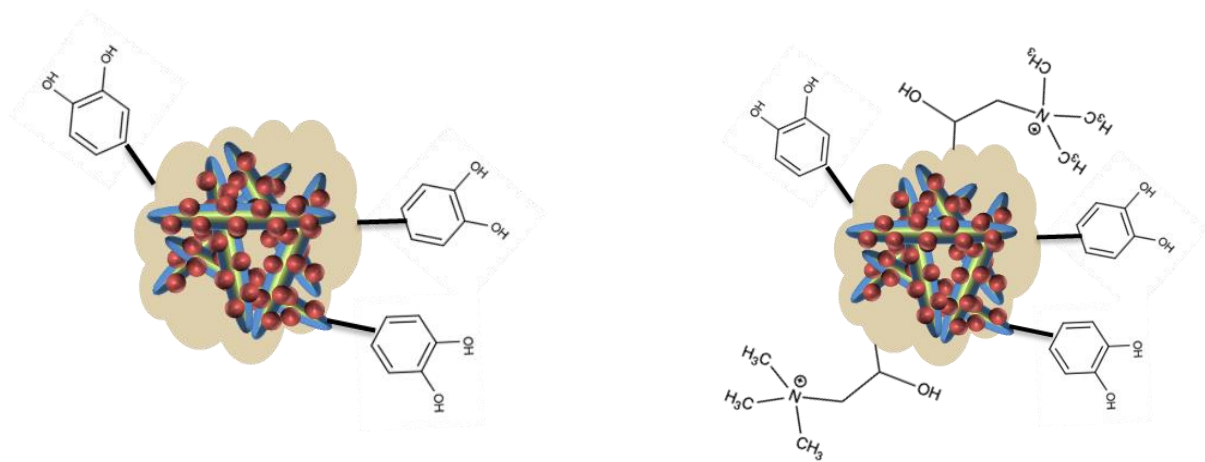
5.1. Introduction

Cellulose nanocrystals (CNC) are derived from forest and agriculture biomass, an abundant and renewable materials from nature. They possess attractive properties for use as drug carriers, such as excellent dispersibility in water, abundant surface hydroxyl groups, and colloidal stability. Moreover, due to their biocompatibility and non-toxicity, they have minimal environmental impact.[5]

Chitosan (CS), a linear polysaccharide composed of both deacetylated and acetylated units, has been extensively studied due to its strong mucoadhesive properties. CS can interact with the mucus layer by forming strong hydrogen and electrostatic interactions. Moreover, CS is biocompatible and has antimicrobial properties, making it an excellent candidate for use in drug delivery systems.[62] However, CS also has several drawbacks, and because of its deacetylated units, CS is only positively charged in acidic environment. As the pH of the ocean is slightly basic (pH 7.5 - 8.3), thus CS is not ideal for application in marine biology. Therefore, modification of CS is necessary to maintain the mucoadhesive properties and increase the stability/solubility of CS in an alkaline environment. Various attempts have been made to improve both its mucoadhesive properties and its solubility at higher pH.

The catechol groups present on the side chain of Levodopa (L-Dopa) offer a solution by providing the desired mucoadhesive properties and solubility.[10] Mussels possess an abundant catechol groups in the protein found on their foot-like structures. This group is the reason mussels can attach to most surfaces, ranging from the bottom of a ship to the side of a concrete dam. Catechol can form various types of bonds with different surface structures due to the two hydroxyl groups on the benzene ring. The examples of forces include metal oxide coordination, cation-π interaction, π- π interaction, and electrostatic interaction. The ability to form irreversible covalent bonds with functional groups like thiol or amine makes catechol

attractive for mucoadhesive applications. Since catechol is found in nature, it is biocompatible, making it a perfect candidate for marine drug delivery.

Quaternary ammonium groups (QAG) are also advantageous in mucoadhesive applications due to their positive charges. Glycidyltrimethylammonium chloride (GTMAC) has been used in previous studies to enhance the solubility of chitosan.[102] GTMAC has been used for the cationization of starch and in other starch/pulp related applications, and to increase antibacterial properties of the nanocomposite.[101] Poly(diallyldimethylammonium chloride) (PDADMAC) is also used in the pulp/paper industry to control the papermaking process or in the water purification process. Though PDADMAC exhibits some cytotoxicity, it is approved by the Food and Drug Administration (FDA) for use as an additive in wound dressings.[105] PDADMAC is also a good candidate for mucoadhesive applications due to its positively charged QAG.

Kim et al. developed chitosan functionalized with catechol groups (CS-cat) for long lasting mucus interactions.[10] They confirmed that CS-cat enhanced the interaction with mucin protein compared to only chitosan. The amine and thiol groups on the mucin proteins formed covalent bonds with o-quinone, which is the oxidized form of the catechol groups. The role of the catechol group in this nanocomposite is to enhance the mucoadhesive properties, enabling sustainable drug release at the targeted mucus site. The driving forces for interaction between nanoparticles and mucin depend on the environmental conditions, especially pH. The catechol groups are not oxidized below pH 6.5 so the nanoparticles mainly interact with the mucus via electrostatic interactions due to the protonated primary amino groups on the chitosan. However, above the pH of 6.5, where the catechol groups are oxidized, they transform into o-quinione groups resulting in the formation of irreversible covalent bonds between the amine and thiol

groups of mucin. The covalent bonds allow the nanoparticles to remain in the mucus layer for a longer period, releasing the drug in a sustainable manner. As described in Figure 5-1, chitosan-catechol will enhance the mucoadhesive properties by forming both covalent and physical bonds with the mucus layer compared to pure chitosan that forms only physical bonds.

Despite the mucoadhesive properties, the poor colloidal stability of the quinone groups is a major challenge. To address this, PDADMAC was introduced to stabilize the colloidal system. It is also expected that the introduction of PDADMAC will enhance the colloidal stability via electrostatic repulsion, which also improves the antibacterial capabilities of the nanocomplex. This chapter will discuss the synthesis method, colloidal behavior, physical structure, and mucoadhesive properties of CNC-CS-cat and CNC-CS-cat-PDADMAC nanocomposites.
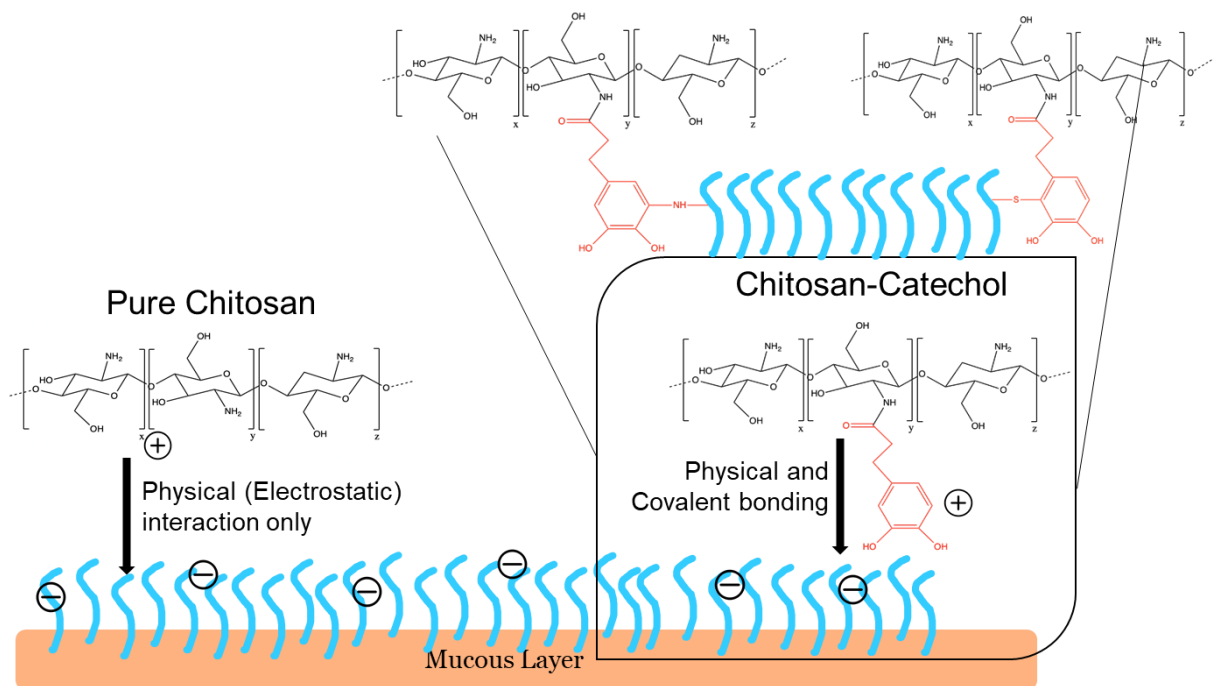
Figure 5-1. Illustration of the interaction of chitosan-catechol with mucus layer

5.2. Materials and methods

5.2.1. Materials

Low M_w chitosan (50k-190k da with 75%-85% deacetylated), EDC (N-(3-dimethylaminopropyl)-N′-ethylcarbodiimide hydrochloride, purum, ≥98.0% (AT)), hydrochloric acid (ACS reagent, 37%), sodium bromide (BioUltra, ≥99.5% (AT)), sodium hypochlorite (10-15 %), 2,2,6,6-tetramethyl-1-piperidinyloxy (TEMPO, 98%) was purchased from Sigma Aldrich (St. Louis, USA.). 3,4-dihydroxy hydrocinnamic acid (hydrocaffeic acid, HCA 98+%) was purchased from Alfa Aesar (Massachusetts, USA.). sodium hydroxide pellets were purchased from Fisher Chemical (Massachusetts, USA). cellulose nanocrystals were supplied by Celluforce (Montreal, Quebec), polydiallyldimethylammonium chloride (pDADMAC, 20 wt% in water), Ethyl 3-aminobenzoate methanesulfonate (MS 222) and (2,3-epoxypropyl)trimethylammonium chloride (GTMAC, technical ≥90%) were purchased from Sigma Aldrich.

5.2.2. Synthesis of CS-cat

CS-cat was synthesized via EDC chemistry as described in Figure 5-2. Briefly, 1 wt. % of CS (0.6 g) was dissolved in a 0.1 M HCl solution under magnetic stirring. The CS solution was adjusted to pH 5.5 with 1 M NaOH. Equimolar HCA (0.29 mg) was added to 5 mL of Milli-Q water. Twice the moles of EDC (0.71 g) were then dissolved in 15 mL of Milli-Q/EtOH (volume ratio 1:1) solution, and the EDC solution was mixed with the HCA solution, and the mixture was quickly added dropwise to the CS solution. The final mixture was vigorously stirred at room temperature for 24 hours with the pH kept at 5.5. The mixture was dialyzed for 3 days with DI water adjusted to pH 5. Maintaining the pH was important to prevent the oxidation of the catechol groups. The CS-cat solution was then freeze-dried over several days and stored for further testing.
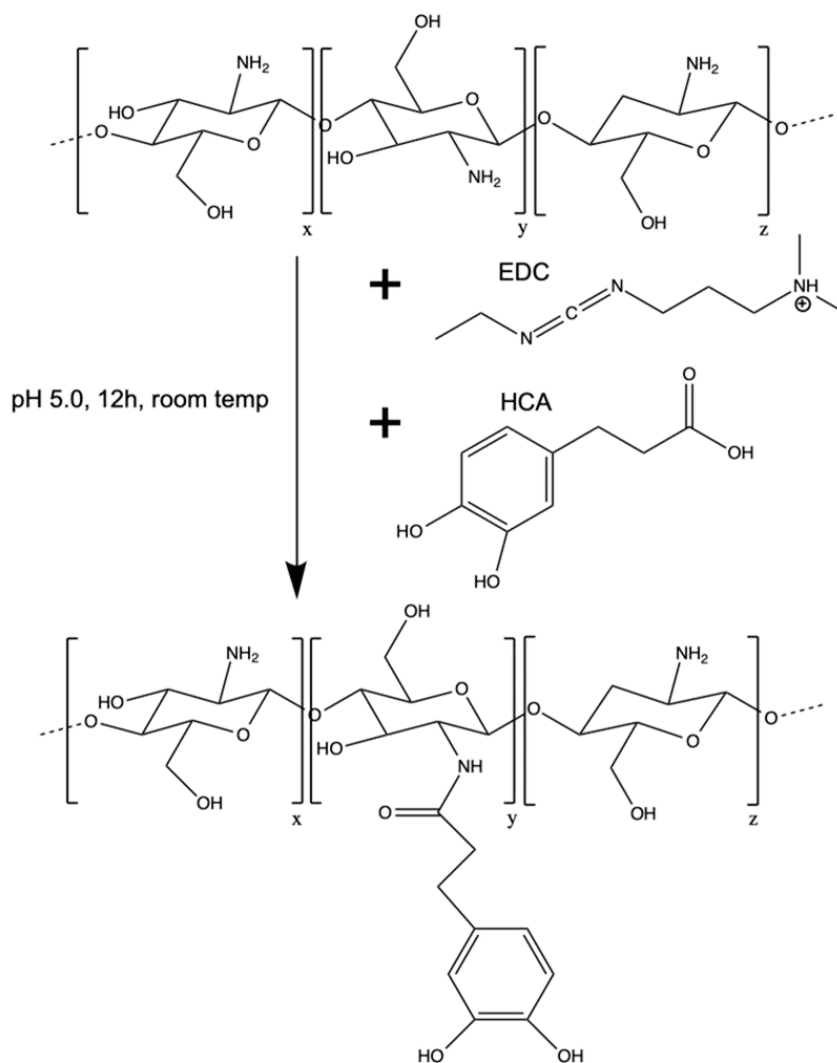
Figure 5-2. Synthesis of chitosan-catechol using EDC chemistry

5.2.3. Synthesis of CNC/CS-cat

CNC/CS-cat nanogels were synthesized through a facile electrostatic gelation technique. Briefly, a 0.5 wt. % CNC solution was prepared by dispersing CNCs in deionized water. Seven CS-cat solutions were prepared using different mass ratios (CS-cat: CNC w/w), and the prepared CS-cat solutions were slowly injected to the CNC solution at 1.5mL/min via a syringe pump under probe sonication.

5.2.4. Synthesis of PDADMAC-CS-cat-CNC

PDADMAC was introduced to the CNC-CS-cat nanoparticle in order to increase the stability of the nanocomplex, and to increase the electrostatic interaction between the nanocomplex and the mucus layer. Briefly, various concentrations of PDADMAC solutions were prepared using different mass ratios (CS-cat: PDADMAC, w/w). Then, the prepared PDADMAC solutions were added to the CS-cat solution. The CS-cat/PDADMAC mixture was slowly injected into the CNC solution at a rate of 1.5mL/min using a syringe pump under probe sonication.

5.2.5. Fluorescence conjugation of CS-CNC, CS-cat-CNC, and CS-Cat-PDADMAC-CNC

CS-CNC, CS-cat-CNC, and CS-Cat-P-CNC were conjugated with Fluorescein isothiocyanate (FITC). Briefly, 1wt. % CS solution was vigorously mixed with FITC (CS: FITC 1:10 w/w) for 4 hours in the dark. The solution was then dialyzed against DI water for two days in the dark and the water was changed twice per day. For CS-cat and CS-cat-PDADMAC, the same procedure was used with a mass ratio of 1:10 (CS:FITC)After dialysis, 0.05% CS-F, CS-cat-CNC-F, and CS-cat-CNC-P-F solutions were added into 0.5% CNC solution in a 1:1 volume ratio and sonicated for 1 minute.

5.2.6. HCA calibration

UV-Vis spectroscopy was used to determine the degree of conjugation of the catechol group as HCA has a distinctive absorbance peak at 280 nm. Briefly, solutions of HCA at various concentrations (10 ppm to 80 ppm) were prepared and their absorbance was measured by UV-vis spectroscopy. HCA calibration curve was plotted based on the absorbance measured at 280 nm.

5.2.7. TEM

The size and morphology of the nanoparticles were analyzed using a Philips CM10 electron microscope at an acceleration voltage of 60 kV. To prepare the sample grid for TEM measurements, the CNC/chitosan-catechol and CNC/chitosan-catechol/PDADMAC nanoparticle suspensions were diluted 10 times with ethanol. Then, a droplet of each diluted sample was placed on a carbon coated copper grid and the excess liquid was carefully removed. The sample was left overnight to dry.

5.2.8. Fourier transform infrared (FTIR) spectroscopy

To confirm the presence of the functional groups, CNC, CS, Gch, CNC/CS-cat, and CNC/PDADMAC/CS-cat nanocomposites were analyzed using a FTIR spectrophotometer (Bruker Tensor 27 FTIR spectrometer, Billerica, MA, USA). Dried samples of each compound were prepared via freeze-drying. The dried samples were ground in a mortar and compressed with potassium bromide to produce homogenous pellets. The FTIR spectrum of each sample was recorded between 4000 cm^{-1} and 400 cm^{-1} at a resolution of 4 cm^{-1} and 32 scans at each wavenumber.

5.2.9. Turbidimetric titration

To evaluate the interaction between the nanoparticle and mucin, turbidity was measured using a UV-vis spectrophotometer based the method proposed by Kim et al.[10] with slight modifications. Briefly, mucin was dissolved in PBS buffer (pH 7.4) at a concentration of 1 mg/mL, and probe sonicated for 5 minutes. CS and CS-cat solutions (10 mg/mL) were dissolved in PBS buffer at pH 2. CS and CS-cat solutions were added to separate mucin solutions. The mixtures were allowed to sit at room temperature for 10 seconds and then the turbidity was measured at a wavelength of 600 nm using a UV-vis spectrophotometer (Cary

100 Bio).

5.2.10. Fluorescence measurement on fish mucus

To assess the mucoadhesive capabilities of the CC-cat nanoparticle, zebra fish was selected as an animal model. The experimental protocol was evaluated and approved by the Animal Care Committee (ACC) at the University of Waterloo. Briefly, a zebra fish was transferred to 200 mL of water and the prepared fluorescence-labelled nanoparticles (50 mg/L) were slowly released into the water. After 30 minutes, the zebra fish was anaesthetized with a buffered 100 mg/L solution of MS222 and washed several times with water to remove any unbound fluorescence-labelled nanoparticles from the mucus surface. As shown in Figure 5-3, the fluorescence on the zebra fish mucus was measured by fluorescence microscopy (Nikon Eclipse 90i fitted with a Nikon D-eclipse C1 scan head using Nikon EZ-C1 software) at 460 nm. The zebra fish was then released back to aquarium after the measurements.
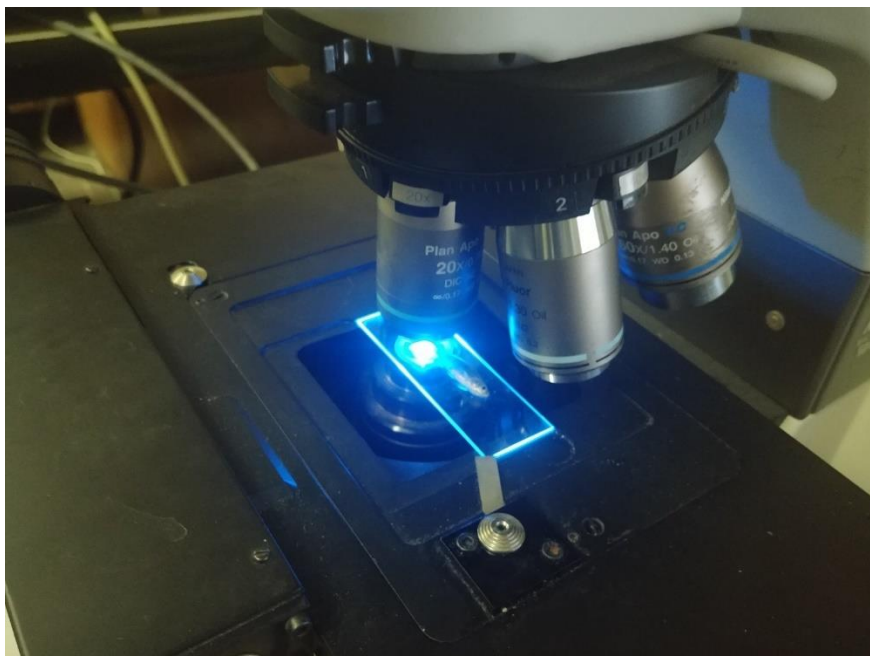
Figure 5-3. Measuring fluorescence on fish mucus by confocal microscopy

5.3. Results and Discussion

5.3.1. Synthesis of CS-cat
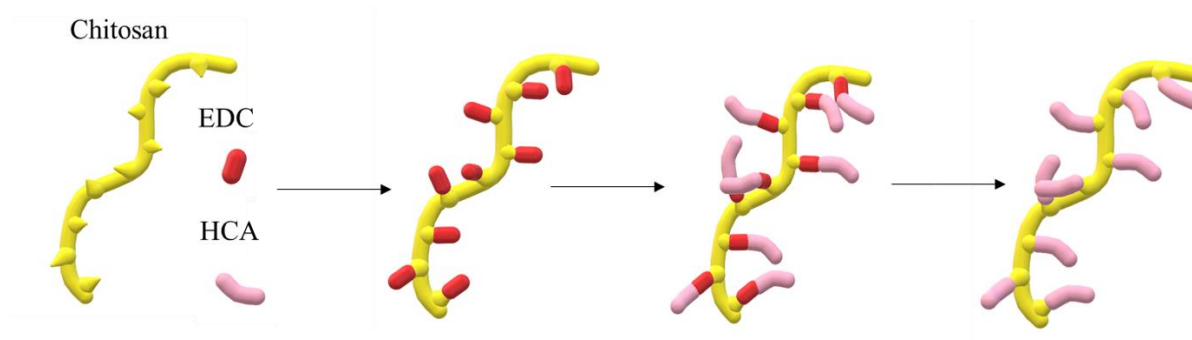
Figure 5-4. A brief synthetic scheme for the preparation of CS-cat (chitosan-catechol group)

HCA was conjugated with the primary amino group of CS via EDC chemistry. EDC is a water-soluble carbodiimide that can be used as a coupling agent between carboxylic acids and primary amines. During the coupling process, the carbonyl group of HCA attacks the carbodiimide group of EDC to form an active O-acylisourea intermediate. The intermediate is substituted by the primary amino group of CS via a nucleophilic substitution reaction. Since the reaction using EDC coupling is most efficient in acidic conditions, CS-cat was prepared at pH 5.5 to enhance the EDC coupling reaction. Furthermore, the redox reaction of the catechol group is highly dependent on pH. In alkaline pH, the catechol group is oxidized to the quinone group and loses its stability, and maintaining a pH of 5.5 is important for the entire process. Figure 5-4 shows the scheme for the synthesis of CS-cat via EDC chemistry. When the EDC solution was added to the HCA solution, the coupling process was initiated between the carbonyl group of HCA and the carbodiimide group from EDC, and the HCA/EDC solution is shown Figure 5-5. The CS solution was quickly added to the HCA/EDC solution and the color changed to light pink as time progressed. The HCA/EDC/CS solution was vigorously stirred for 24 hours, during which the color of the solution changed to dark pink (Fig. 5-5). It was

observed that the pH steadily increased during the first few hours. Since tpH can alter the degree of substitution of the amino group, the pH was brought down to 5.5 and maintained at this condition.

Initial, right after adding HCA/EDC

After 12h mixing
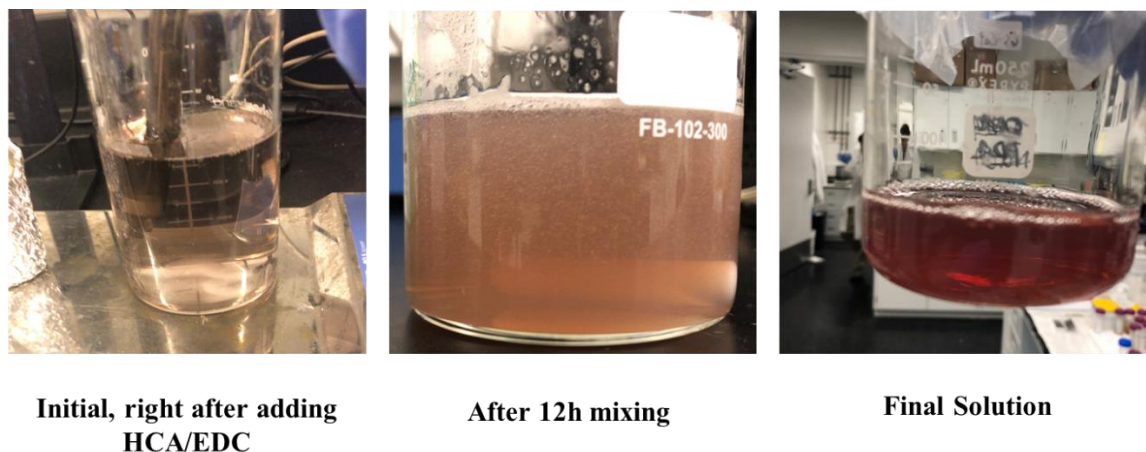
Final Solution

Figure 5-5. OCS-cat solution: initial stage (left), 12 h reaction (middle), and final dialyzed CS-cat (right)

5.3.2. Synthesis of CNC/CS-cat
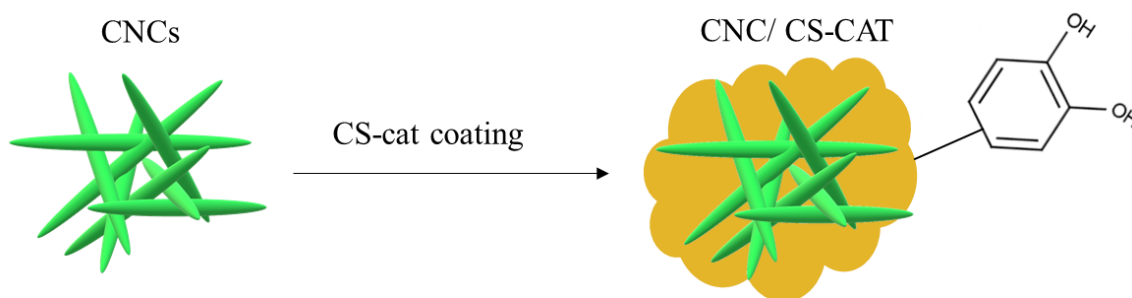
Figure 5-6. Synthesis of CNC-CS-cat

CC-cat (CNC-CS-cat) was synthesized using the same method for the CPEC nanoparticle synthesis described in Chapter 3. CNCs were coated with CS-cat via electrostatic gelation as discussed in Chapter 4. The CS-cat solutions were slowly injected into CNC solution to form a homogenous coating as shown in Figure 5-6. In order to evaluate the physical behavior of CC-cat, seven mass ratios (CS-cat:CNC, w/w) were chosen, and they contained

different amounts of catechol groups. Different concentrations of CC-cat samples were prepared as shown in Figure 5-7. Interestingly, after incorporating the catechol groups on the CNC-CS based nanoparticles, it was observed that the nanoparticles bind to the surface of the glass as shown in the red circle in Fig 33, where the CC-cat nanoparticles bound to the surface of vials that was negatively charged since cationic CC-cat nanoparticles were attracted to the negatively-charged surface.
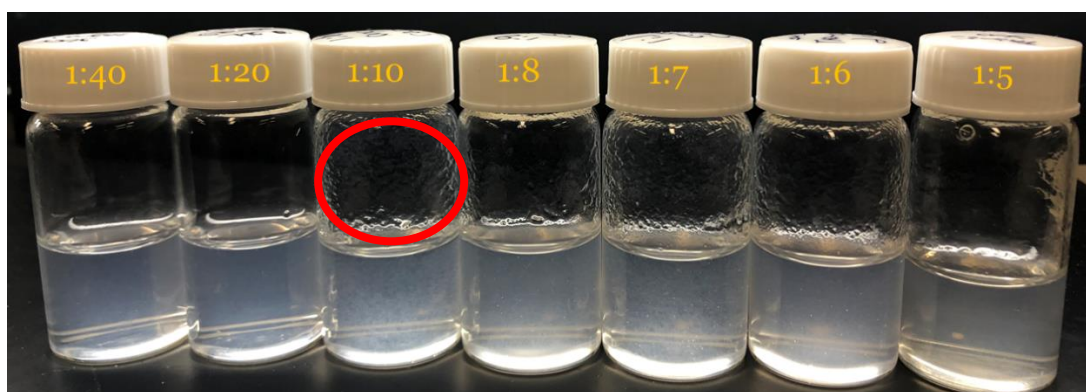
Figure 5-7. Optical image of CC-cat observed at different mass ratios (CS-cat:CNC, w/w)

The particle size and zeta potential (Fig. 5-8) of CC-cat (7 different mass ratios CS-cat:CNC w/w) were determined to evaluate their colloidal behavior. The zeta potential (ZP) was measured across the interface in the two-phase system composed of CC-cat and water, where the ZP of 1:40 (CS-cat: CNC) was -40 mV, indicating that the CS-cat was not fully coated on the surface of the CNCs since pristine CNCs had a ZP of – 50 mV. As more CS-cat was added, the zeta potential gradually increased. Similar to the other CS-CNC based nanoparticles (CPEC and CPCg), CC-cat aggregated at 1:10 to 1:8 (CS-cat: CNC), and the ZP was nearly 0 mV with size of about 2 μm. Beyond 1:7 (CS-cat:CNC), the colloidal system was stable, and the ZP increased to +40 mV at 1:6 (CS-cat:CNC), while the particle size decreased to 200 nm at 1:7 (CS-cat:CNC). The particle size increased again when more CS-cat was added. The polydispersity and the particle sizes are shown in Table 4 below.

Table 6. The PDI (polydispersity) of CC-cat nanoparticle determined from DLS

Mass ratio	1:40	1:20	1:10	1:8	1:7	1:6	1:5
PDI	0.636	0.302	0.718	0.767	0.302	0.636	0.542
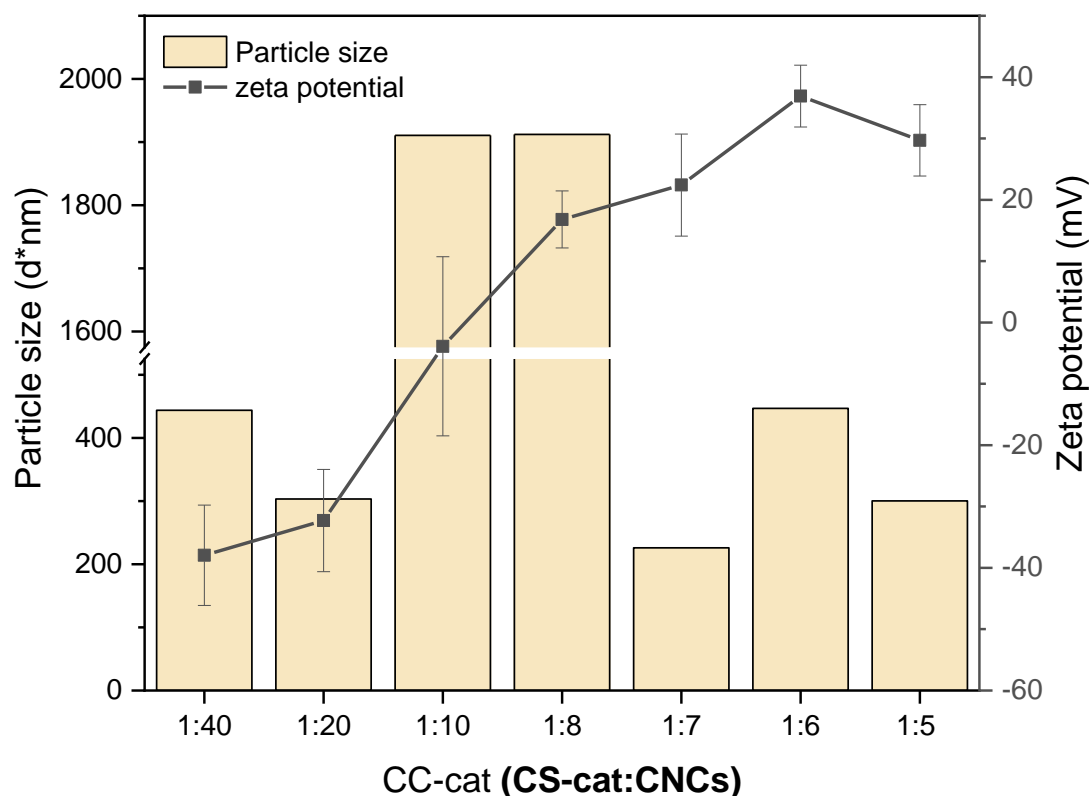
Figure 5-8. Particle size and zeta potential of CC-cat with different mass ratios (CS-cat: CNC)

5.3.3. Characterization of CC-cat

HCA was calibrated using a UV-vis spectrophotometer since the benzene ring of phenolic compounds possessed a UV absorbance peak at 280 nm, hence the concentrations of the CC-cat samples could be determined using the Beer-Lambert law, where the absorbance of HCA at 280 nm is proportional to the concentration of HCA. Based on the UV-vis spectra of HCA at concentrations ranging from 10 to 100 ppm, the calibration curve for HCA was plotted as

shown in Figure 5-9. The slope of the calibration curve corresponded to the absorptivity coefficient, which was determined to be 0.0107. The calibration curve could be used to determine the concentrations of HCA at between 10 and 100 ppm.
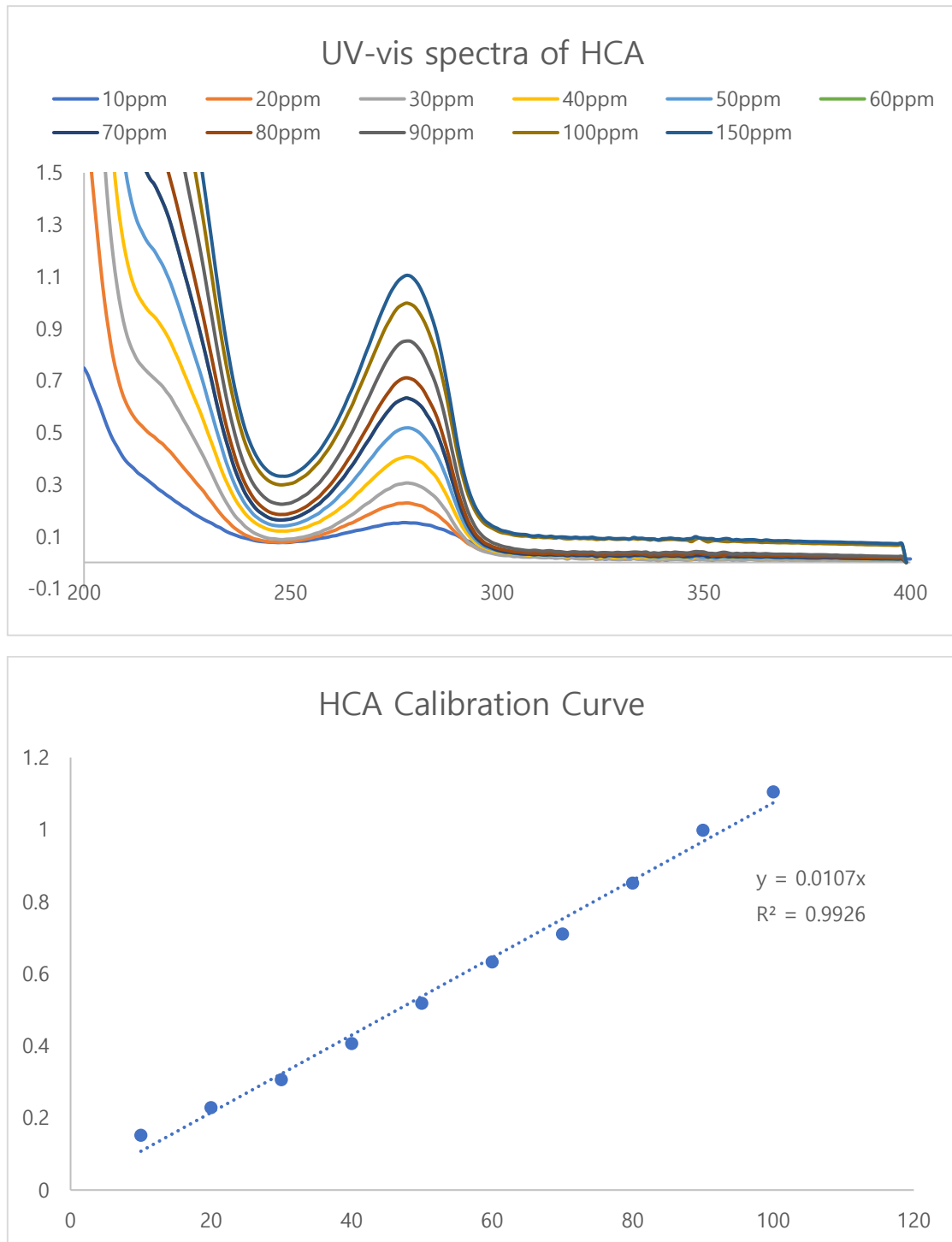
Figure 5-9. A) UV-vis spectra of HCA and B) calibration curve of HCA

The morphology of the CC-cat nanoparticles was confirmed by TEM (Fig. 5-10). Similar to the CNC-CS and CNC-GTMAC-CS nanoparticles, each CNC nanoparticle was coated by CS-cat and a gel comprised of many nanoparticles was formed. The particle size ranged from 200 to 1000 nm. During the drying process, the CC-cat nanoparticles might have aggregated, which could explain the increased particle size compared to the DLS data. The morphology can vary depending on the synthesis conditions, such as reaction time, sonication power, and the mass ratio between CS-cat and CNC.
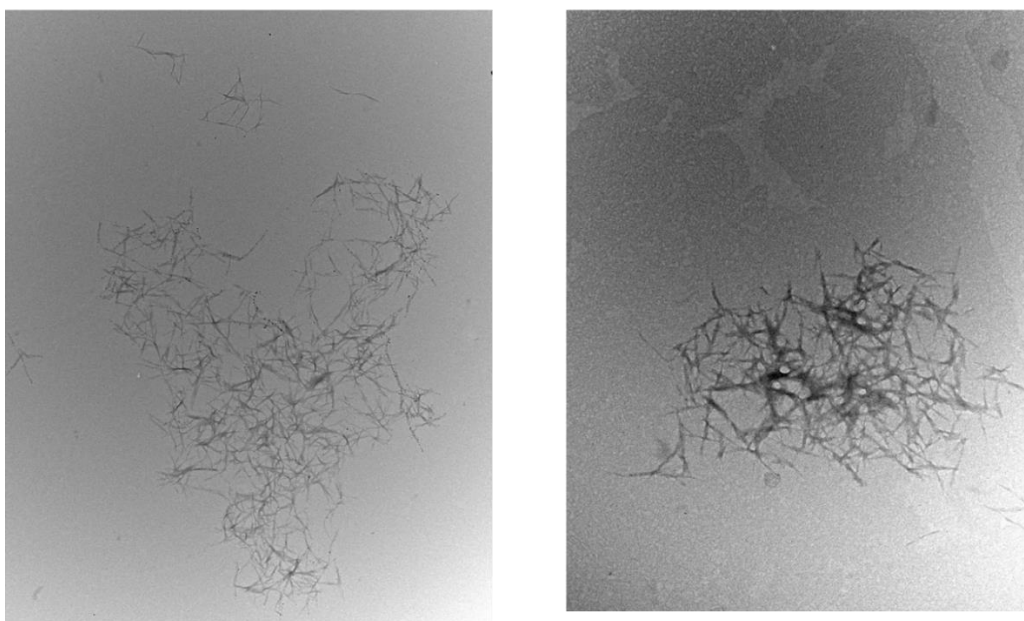
Figure 5-10. TEM image of CC-cat

FTIR spectra (Figure 5-11) of CNC, HCA, and CS were measured to confirm the presence of the functional groups in the prepared nanoparticles. The O-H and the N-H stretching vibration appeared in all the spectra as a broad peak at around 3500 cm^{-1}. The C-H stretching vibration band was observed at 2900 cm^{-1}, while the band observed around 2400 cm^{-1} could be from the carboxyl or carbonated group. Chitosan and chitosan derivatives typically have a peak at around 1600cm^{-1}, which corresponds to the amide linkage and the small peak at

around 1500cm^{-1}, corresponded to NH$_3^+$, and the carbonyl group from hydrocaffeic acid had a peak at 1500 cm^{-1}.
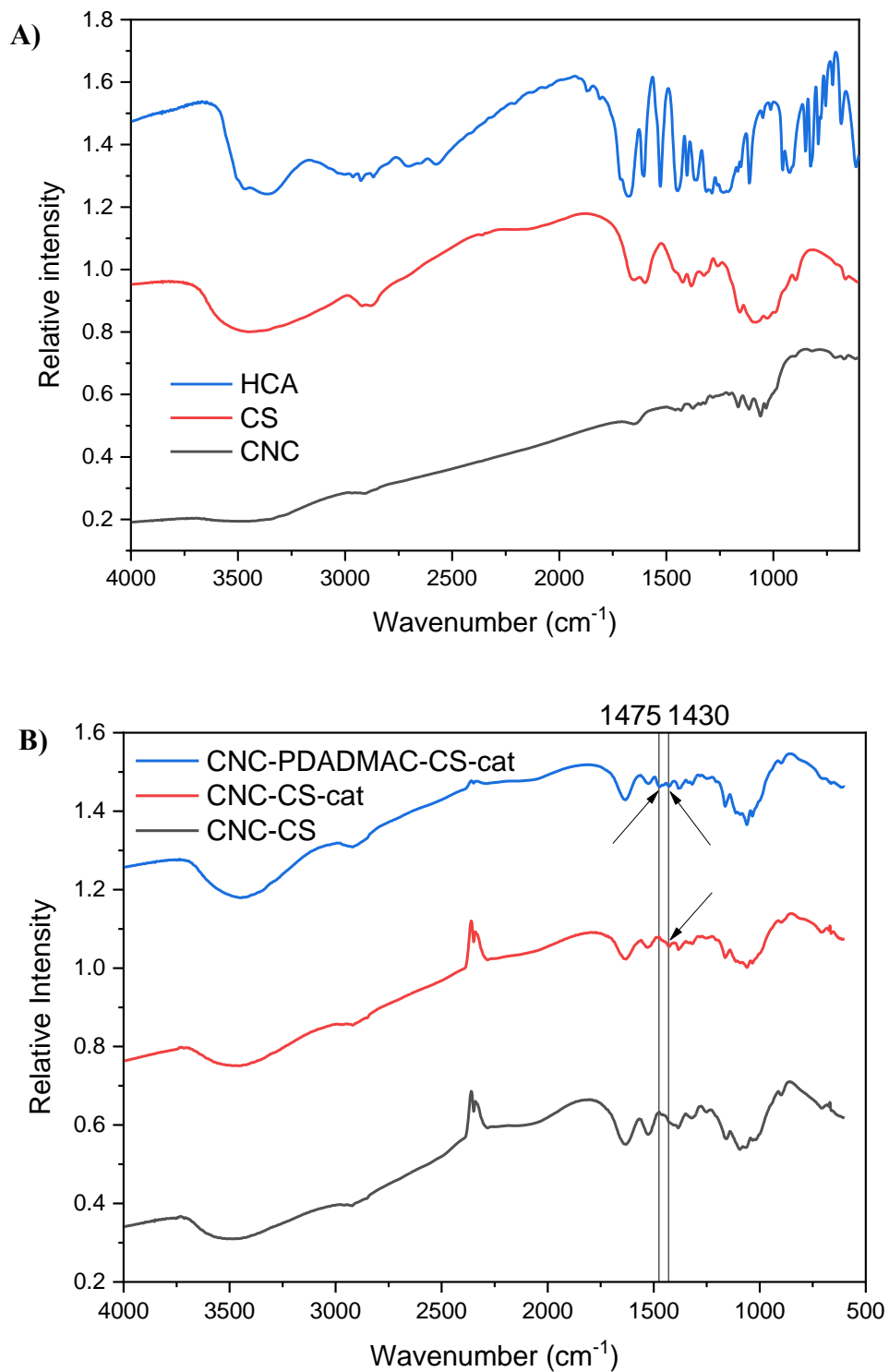
Figure 5-11. FTIR spectra of A) CNC, CS, and HCA, B) CNC-CS, CC-cat, and CPC-cat

5.3.4. Limitations of CC-cat

CC-cat nanoparticles display unstable colloidal behavior beyond the pH of 6.5, which is a big disadvantage. A high degree of catechol conjugation can increase the solubility, but the synthesized CC-cat was only partially soluble and formed aggregates in pH 7 as shown in Figure 5-12D. Kim et al. showed that the maximum degree of conjugation of CS-cat was around 18 %. The poor solubility of CS-cat is due to this low degree of conjugation, which further limits the applications of the CC-cat nanoparticles despite their adhesive properties. In order to increase the degree of substitution of the primary amino group of CS, we tried to conjugate GTMAC on the remaining backbone of CS-cat as shown in Figure 5-12A. It was expected that the primary amino group of CS would be substituted by around 18 % catechol and 60 % GTMAC. However, when CS-cat was synthesized with GTMAC, the color of solution became very dark and the system was highly aggregated (Fig. 5-12C). This is because the catechol group could break down when the temperature of the system is increased up to 60 °C during the synthesis.

In order to protect the catechol groups, CS-GTMAC-cat was synthesized in reverse; CS-GTMAC was synthesized first, followed by conjugation of the catechol groups through the EDC chemistry. This reverse synthesis was successful in conjugating the catechol groups onto the CS-GTMAC. Due to the long chemical reaction time (10 days including reaction and purification), this method of preparation was inefficient. Therefore, we developed a more efficient and facile method to improve the colloidal behavior of CC-cat based nanoparticles, and this will be discussed further in the next section.
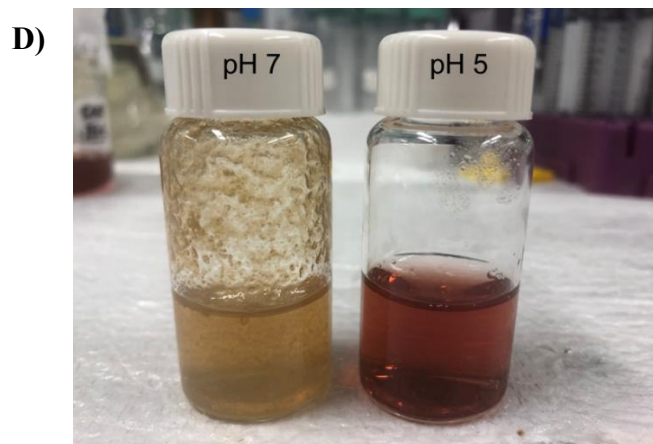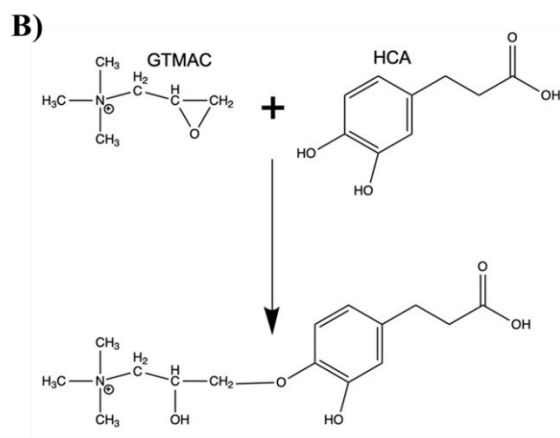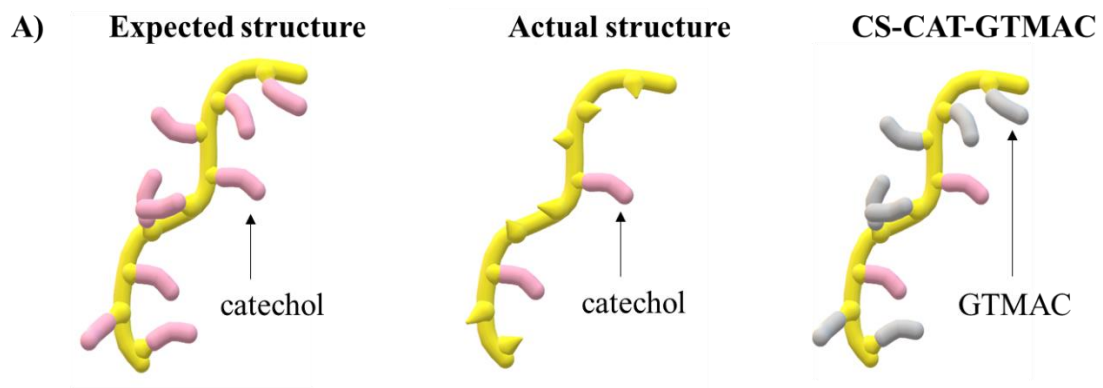
Figure 5-12. A) Chemical structure of the synthesized CS-cat and CS-cat-GTMAC, B)

Possible interaction between HCA and GTMAC, C) Synthesized CS-cat-GTMAC, D) CC-cat

in pH 7 (left), and pH 5 (right)

5.3.5. Synthesis of CNC/CS-cat/PDADMAC

PDADMAC was introduced to improve the colloidal stability and mucoadhesive capabilities of the CC-cat nanoparticles. PDADMAC, a synthetic cationic polymer, has been approved by the Food and Drug Administration and used as an antimicrobial agent in wound dressings.[106] The role of PDADMAC was to increase the positive surface charge of the nanoparticle, leading to improved colloidal stability and mucoadhesive properties. Increased positive charge due to the addition of PDADMAC would induce repulsive intramolecular forces that stabilize the colloidal system. In addition, the increased positive charge would increase the interaction with the negatively charged mucus membrane. In this section, the preparation of CNC-CS-cat-PDADMAC nanoparticles (CPC-cat) using electrostatic interaction is discussed. Optimal synthesis conditions, colloidal behavior, interaction with mucin, and mucoadhesive tests are discussed.

PDADMAC can adhere to the surface of CNCs via strong electrostatic interactions, and Dong et al.[107] prepared CNC-PDADMAC for glucose sensing. The addition of PDADMAC was confirmed by zeta potential, FTIR, and UV-vis spectrophotometry. The synthesized CNC-PDADMAC nanoparticles possessed excellent colloidal stability, where the zeta potential changed from -75 mV to +50 mV. CPC-cat was synthesized via a facile method with slight modifications to the method proposed by Dong et al.[107]. CC-cat was synthesized first and then blended with a 20 wt. % PDADMAC, and the solution was purified by dialysis. The brief synthesis scheme is described in Figure 5-13, and the chemical structure of the synthesized CPC-cat is expected to have both PDADMAC and CS-cat polymer coatings on the CNC surface. The morphology and characterization of the nanoparticles will be discussed.
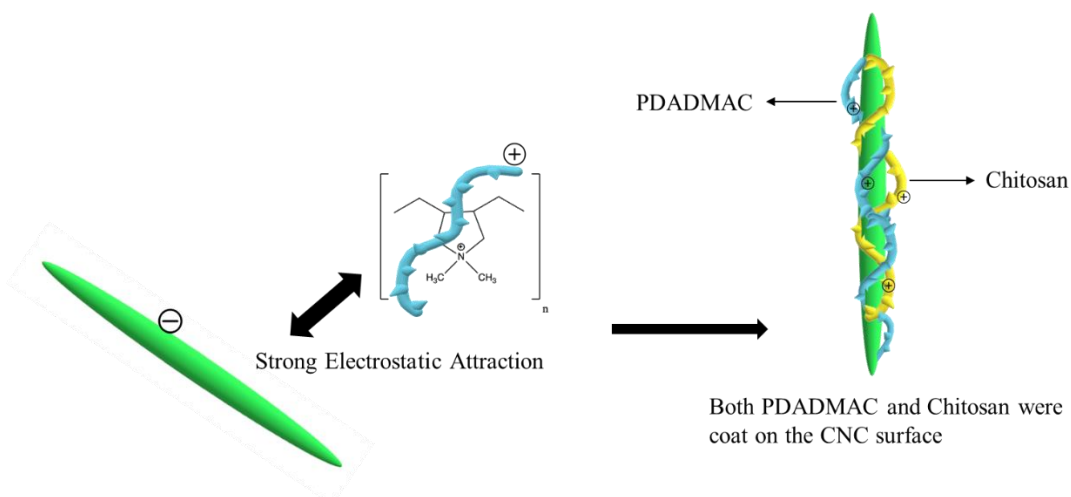
Figure 5-13. Brief synthesis scheme of CNC-cat/PDADMAC (CPC-cat)

5.3.6. Optimal synthetic conditions for CPC-cat

In order to study the colloidal behavior of CPC-cat, the mass ratios between the three major components (CS, CNC, and PDADMAC) were examined as shown in Figure 5-14. In Chapter 3, we determined that a mass ratio of 1: 10 (CS: CNC w/w) was the optimal synthesis condition, where the 1:10 (CS: CNC) formed stable colloidal solutions of CPC-cat nanoparticles.
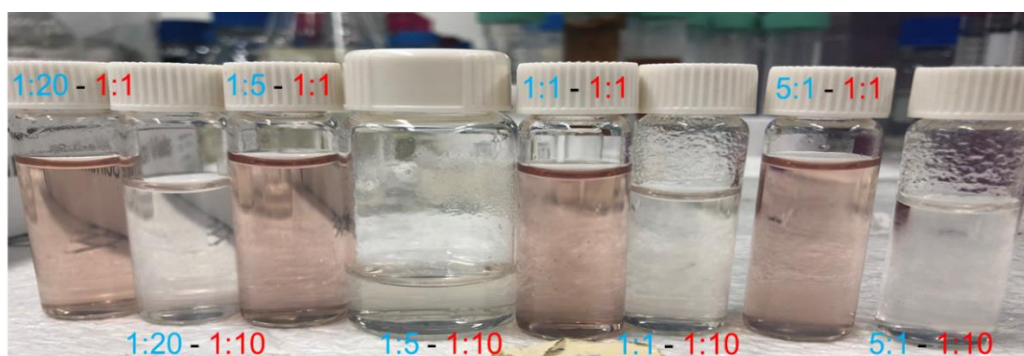
Figure 5-14. CPC-cat with different 1) CS: PDADMAC mass ratio and 2) CS: CNC mass ratio

The particle size and zeta potential of CPC-cat were measured to elucidate the colloidal behavior of the CPC-cat nanoparticles and to determine the optimal CS-cat: PDADMAC mass ratio. The colloidal behavior of CPC-cat at various CS-cat:PDADMAC mass ratios is shown in Figure 5-15. The DLS measurements confirmed that the average particle size of the CPC-cat nanoparticles at 20:1 (CS-cat:PDADMAC) was around 370 nm. However, the particle size decreased as the amount of PDADMAC introduced into the system was increased. Interestingly, the average particle was reduced to 150 nm at 1:5 and 1:6 (CS-cat:PDADMAC, w/w). As the PDADMAC amount was further increased, the particle size increased slightly. This phenomenon of variation in the particle size was also observed for CPEC (Fig. 3-11) and CPECg nanoparticles (Figure 4-6). This implies that modified chitosan has similar colloidal behavior when incorporated with different compounds. The observed colloidal behavior of CPC-cat is due to the electrostatic interactions between CNCs and CS-cat. The zeta potential of the CPC-cat nanoparticle suspension increased as the amount of PDADMAC incorporated into the system was increased from 20:1 to 1:6(CS-cat: PDADMAC, w/w). The zeta potential decreased slightly at 1:8 and 1:10 (CS-cat:PDADMAC), which led to the increased particle size of the CPC-cat nanoparticles. These observations revealed that the optimal mass ratio (CS-cat:PDADMAC) for the synthesis of CPC-cat nanoparticles was between 1:5 to 1:6, where the smallest particle size (~ 150 nm) and the highest zeta potential (~ +51 mV) were observed. Theoretically, at optimal conditions (1:5 to 1:6 mass ratio), the CPC-cat nanoparticles displayed mucoadhesive properties due to the formation of stable colloids with higher zeta potential and reduced particle size.
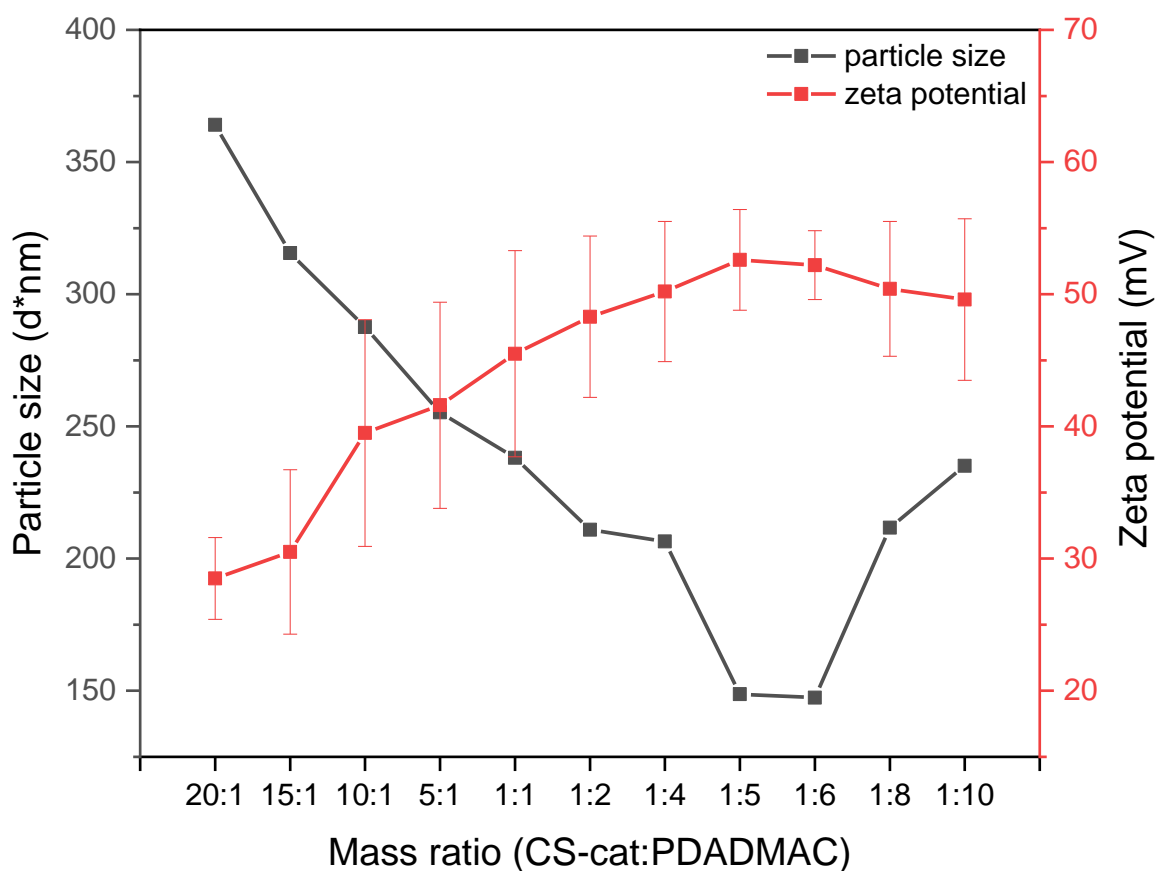
Figure 5-15. Particle size and zeta potential of CPC-cat at different mass ratios (CS-cat:PDADMAC)

In order to determine the effect of pH on the colloidal behavior of CPC-cat nanoparticles, the particle size and zeta potential were measured as shown in the Figure 5-16. Before PDADMAC was incorporated, the CC-cat nanoparticles aggregated after pH 6.5. However, after PDADMAC was incorporated, the system was stable from pH 3 to 9, and the particle sizes of CPC-cat nanoparticles were around 200 nm. At pH 10, the system started to aggregate, and the particle size increased to 1.3 μm at pH 11. The zeta potential of the CPC-cat nanoparticles ranged from + 20 to + 40 mV. The decrease in zeta potential as pH was increased was due to the deprotonation of the primary amino groups at higher pH.
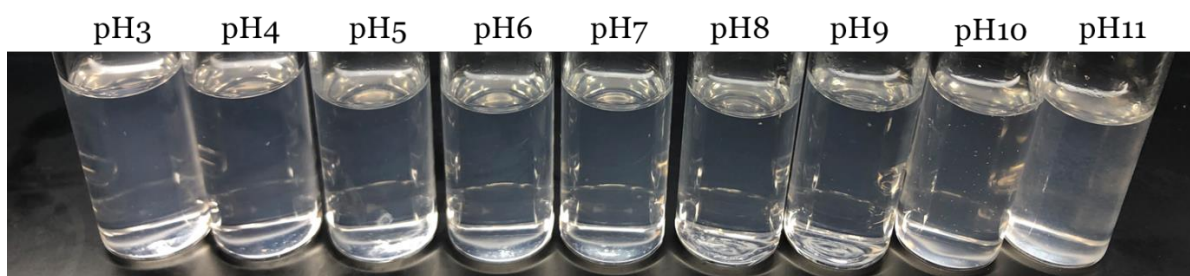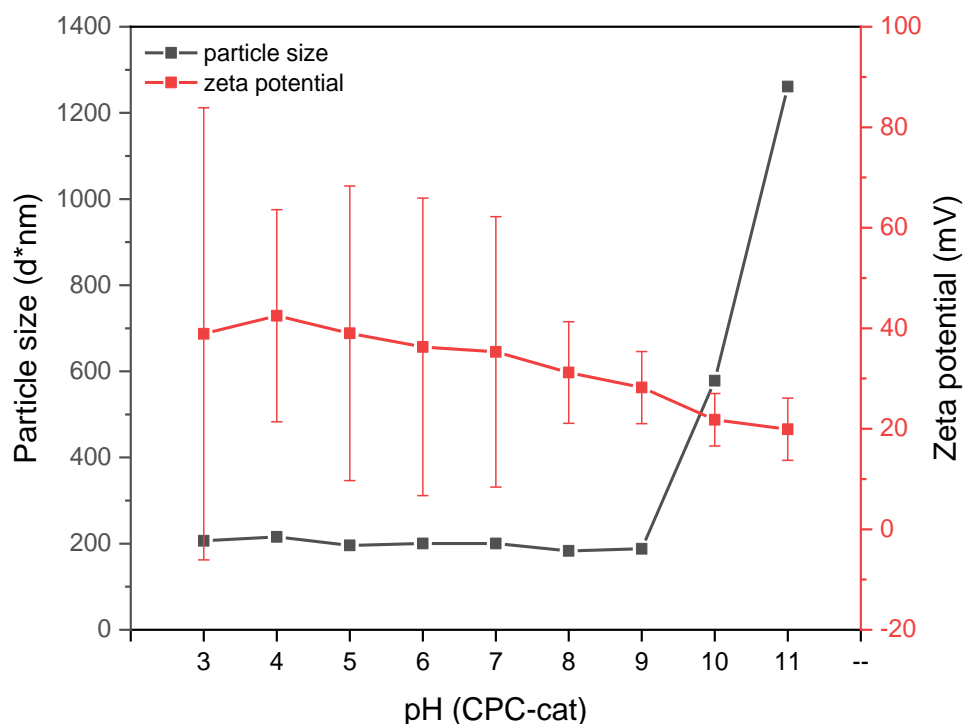
Figure 5-16. A) Particle size and zeta potential of CPC-cat at different pH; B) Synthesized CPC-cat observed in various pH (3 to 11)

The morphology of CPC-cat was confirmed by TEM (Fig. 5-17). The rod-like structure of CNC was roughly 200 nm in length and 20 nm in width. It was observed that several CNCs were coated by chitosan. The CPC-cat nanoparticle exhibited a more uniform shape and size distribution compared to CC-cat nanoparticles (Fig. 5-10). In addition, the particle size and thickness of the CPC-cat nanoparticle were reduced compared to CC-cat. Interestingly, black dots were observed on the CPC-cat nanoparticles, while the CC-cat nanoparticles did not show any black dots on the CNC surface suggesting that the PDADMAC was successfully

incorporated. Similar black dots were observed by Dong et al.[107] on CNC-PDADMAC nanoparticles.
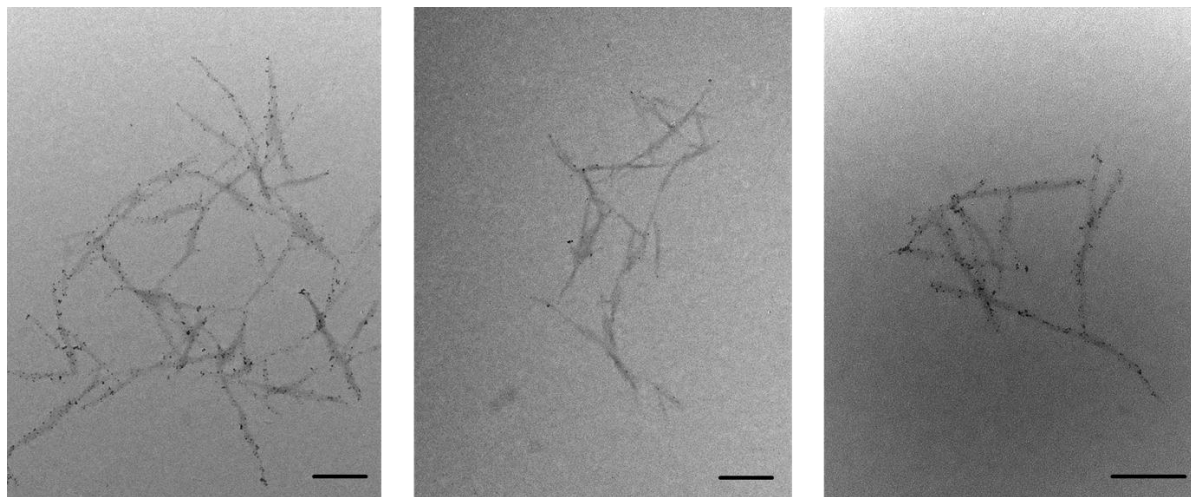
Figure 5-17. TEM image of CPC-cat (scale bar: 200 nm)

5.3.7. Interaction of CS and CS-cat with mucin

In order to confirm the interaction of CS-cat with mucin, the turbidity of a CS-cat and mucin mixture was measured using a UV-vis spectrophotometer. When mucin was mixed with the catechol groups, aggregates were formed, which could be quantitatively analyzed by light scattering at 600 nm. Control of pH of CS-cat and mucin solutions can be used to predict the in vivo results by mimicking the in vivo pH conditions.[10] Both unmodified CS and CS-cat were prepared in pH 2 and mucin was dissolved in PBS buffer (pH 7.4). Low pH in CS and CS-cat solution will generate the electrostatic interaction with mucin polymers, and oxidized catechol in pH 7.4 will form catechol mediated interactions with mucin polymers. As shown in the figure 5-18, the binding interaction between CS-cat and mucin was enhanced compared to pure CS solution. As the concentration of CS-cat was increased, the turbidity of mixture also increased, confirming the improved interactions between CS-cat and mucin.
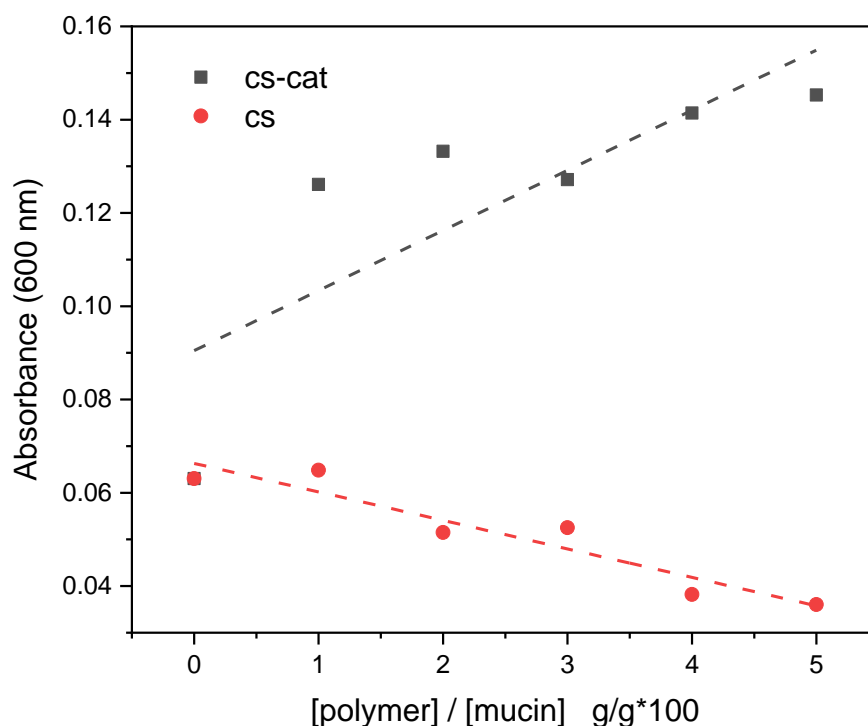
Figure 5-18. The turbidity measurement of the mixture comprised of CS and CS-cat with mucin

5.3.7. Fluorescence spectroscopy on fish mucus

To confirm the mucoadhesive capabilities of the CC-cat nanoparticles, zebra fish was selected as an animal model and it was exposed to fluorescence-labelled CC-cat for 30 minutes. The zebra fish were washed several times to remove unbound CC-cat from the mucus surface. The fluorescence of the bound CC-cat nanoparticles was measured by confocal microscopy as shown in Figure 5-19. Compared to the untreated zebrafish (control), the treated zebrafish displayed stronger fluorescence signals, indicating that CC-cat could bind to zebrafish mucus. The CC-cat nanoparticles were observed over the entire surface of the zebrafish forming distinct florescent patches. This is due to the partial solubility of CC-cat in neutral pH. However, it was interesting that CC-cat particles with a particle size over 100 μm could bind to zebra fish

110

mucus.   All the tested zebrafish survived the exposure to a high concentration of CC-cat (50 mg/L) over 2 hours. When they were returned to the aquarium, no harmful cytotoxic effects were observed for two weeks.

Control (non-treatment)   CNC/CS-cat (30 mins exposure)
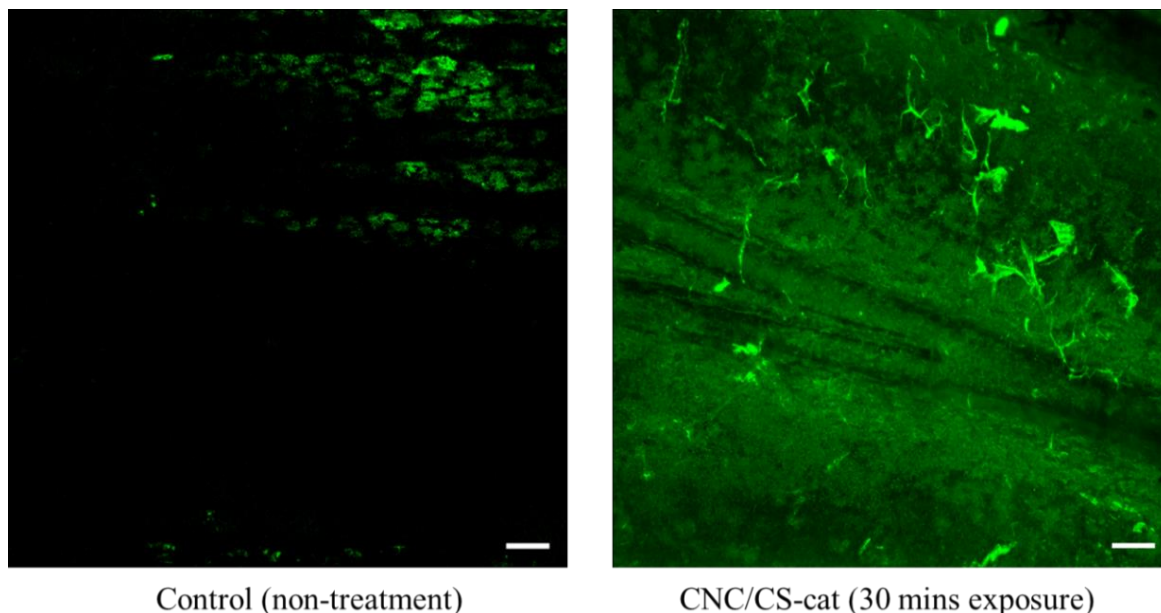
Figure 5-19. CC-cat nanoparticles adhered on zebrafish mucus as observed by confocal fluorescence microscopy:Untreated zebra fish mucus (left) and treated mucus (right) * scale bar: 50 μm

5.4. Conclusions

The mussel-inspired catechol groups were functionalized on CNC-CS based nanoparticles for mucoadhesive applications. The CC-cat nanoparticle was synthesized via electrostatic gelation and the optimized mass ratio between CNC and CS-catechol was found to be 7:1. However, CC-cat exhibited poor solubility above pH 6.5 limiting their application in marine drug delivery. To address this, PDADMAC, a cationic polymer, was incorporated with CC-cat. The synthesized CPC-cat nanoparticles exhibited enhanced colloidal stability (150 nm particle size) and higher zeta potential (up to +50 mV), which improved their mucoadhesive

111

properties. The optimal mass ratio between CS-cat and PDADMAC was found to be between 1:5 to 1:6. The FTIR spectra confirmed the presence of the catechol groups and PDADMAC in the CPC-cat nanoparticles and their morphology was observed by TEM. Turbidity measurements confirmed that the catechol group interacted with the mucin compared to pure chitosan. The mucoadhesive properties of the CC-cat nanoparticles were tested with zebrafish using confocal fluorescence microscopy. The fluorescence images confirmed that the nanoparticles could successfully bind to the zebrafish mucus membrane.

Chapter 6. Future plans

In this thesis, mucoadhesive CNC/CS based nanocomposite and their derivatives were successfully prepared. The optimal condition for synthesis, colloidal behavior, and physical characteristics were examined. However, several aspects are still required to be investigated to prove their mucoadhesive properties and therapeutic effects. The interaction between CNC and CS, CS-cat was evaluated by turbidity measurement. However, turbidity measurement between CNC/CS nanocomposite and mucin protein will elucidate the interaction with mucus membrane. The other possible methods to evaluate mucus interaction with nanocomposite are atomic force microscopy (AFM), surface plasmon resonance (SPR), and rheological assessment. Second, the analysis of antibacterial, antifungal, antiparasitic properties should be examined to demonstrate detailed therapeutic effects of the CNC/CS nanocomposites. Furthermore, there are lots of potentials for CNC/CS based nanocomposite to be applied for agricultural applications such as sea lice treatment, treatment for mucosal infections of livestock such as pig, cow, fish, and etc. The research direction of exploring new agricultural applications using prepared nanocomposite would be included for the future study.

References

1. Charlie-Silva I, de Melo NFS, Gomes JMM, et al. Nanoparticle mucoadhesive system as a new tool for fish immune system modulation. *Fish Shellfish Immunol*. 2018;80:651-654. doi:10.1016/j.fsi.2018.05.057

2. Sajjan AM, Premakshi HG, Kariduraganavar MY. Synthesis and characterization of GTMAC grafted chitosan membranes for the dehydration of low water content isopropanol by pervaporation. *J Ind Eng Chem*. 2015;25:151-161. doi:10.1016/j.jiec.2014.10.027

3. Zhang L, Webster TJ, Zdrojewicz Z, et al. Nanotechnology in therapeutics : a focus on nanoparticles as a drug delivery system R eview. *Carbohydr Polym*. 2016;1(1):71-88. doi:10.1016/j.carbpol.2016.06.026

4. Grishkewich N, Mohammed N, Tang J, Tam KC. Recent advances in the application of cellulose nanocrystals. *Curr Opin Colloid Interface Sci*. 2017;29:32-45. doi:10.1016/j.cocis.2017.01.005

5. Tang J, Sisler J, Grishkewich N, Tam KC. Functionalization of cellulose nanocrystals for advanced applications. *J Colloid Interface Sci*. 2017;494:397-409. doi:10.1016/j.jcis.2017.01.077

6. Mansuri S, Kesharwani P, Jain K, Tekade RK, Jain NK. Mucoadhesion: A promising approach in drug delivery system. *React Funct Polym*. 2016;100:151-172. doi:10.1016/j.reactfunctpolym.2016.01.011

7. Laffleur F. Mucoadhesive therapeutic compositions: A patent review (2011-2014). *Expert Opin Ther Pat*. 2016;26(3):377-388. doi:10.1517/13543776.2016.1145209

8.   Wang G, Wang J, Wu W, Tony To SS, Zhao H, Wang J. Advances in lipid-based drug delivery: Enhancing efficiency for hydrophobic drugs. *Expert Opin Drug Deliv*. 2015;12(9):1475-1499. doi:10.1517/17425247.2015.1021681

9.   Cui PF, Zhuang WR, Hu X, et al. A new strategy for hydrophobic drug delivery using a hydrophilic polymer equipped with stacking units. *Chem Commun*. 2018;54(59):8218-8221. doi:10.1039/c8cc04363a

10. Kim K, Kim K, Ryu JH, Lee H. Chitosan-catechol: A polymer with long-lasting mucoadhesive properties. *Biomaterials*. 2015;52(1):161-170. doi:10.1016/j.biomaterials.2015.02.010

11. Kim D, Islam MS, Tam MKC. *The Use of Nano-Polysaccharides in Biomedical Applications*.; 2019. doi:10.1007/978-981-15-0913-1_5

12. Das D, Pal S. Modified biopolymer-dextrin based crosslinked hydrogels: Application in controlled drug delivery. *RSC Adv*. 2015;5(32):25014-25050. doi:10.1039/c4ra16103c

13. Van Rijt SH, Bein T, Meiners S. Medical nanoparticles for next generation drug delivery to the lungs. *Eur Respir J*. 2014;44(3):765-774. doi:10.1183/09031936.00212813

14. Ahmed A, K.S. Yadav H, V. Lakshmi S, V.N. Namburi B, G. Shivakumar H. Mucoadhesive Nanoparticulate System for Oral Drug Delivery: A Review. *Curr Drug ther*. 2012;7(1):42-55. doi:10.2174/157488512800389137

15. Debele TA, Mekuria SL, Tsai HC. Polysaccharide based nanogels in the drug delivery system: Application as the carrier of pharmaceutical agents. *Mater Sci Eng C*. 2016;68:964-981. doi:10.1016/j.msec.2016.05.121

16. Alhaique F, Matricardi P, Di Meo C, Coviello T, Montanari E. Polysaccharide-based

self-assembling nanohydrogels: An overview on 25-years research on pullulan. *J Drug Deliv Sci Technol*. 2015;30:300-309. doi:10.1016/j.jddst.2015.06.005

17. Swierczewska M, Han HS, Kim K, Park JH, Lee S. Polysaccharide-based nanoparticles for theranostic nanomedicine. *Adv Drug Deliv Rev*. 2016;99:70-84. doi:10.1016/j.addr.2015.11.015

18. Kalepu S, Nekkanti V. Insoluble drug delivery strategies: Review of recent advances and business prospects. *Acta Pharm Sin B*. 2015;5(5):442-453. doi:10.1016/j.apsb.2015.07.003

19. Lombardo D, Kiselev MA, Caccamo MT. Smart Nanoparticles for Drug Delivery Application: Development of Versatile Nanocarrier Platforms in Biotechnology and Nanomedicine. *J Nanomater*. 2019;2019. doi:10.1155/2019/3702518

20. Yang G, Liu Y, Wang H, et al. Bioinspired Core–Shell Nanoparticles for Hydrophobic Drug Delivery. *Angew Chemie - Int Ed*. 2019;58(40):14357-14364. doi:10.1002/anie.201908357

21. Shakeel F, Shafiq S, Haq N, Alanazi FK, Alsarra IA. Nanoemulsions as potential vehicles for transdermal and dermal delivery of hydrophobic compounds: An overview. *Expert Opin Drug Deliv*. 2012;9(8):953-974. doi:10.1517/17425247.2012.696605

22. Shafiq S, Shakeel F, Talegaonkar S, Ahmad FJ, Khar RK, Ali M. Development and bioavailability assessment of ramipril nanoemulsion formulation. *Eur J Pharm Biopharm*. 2007;66(2):227-243. doi:10.1016/j.ejpb.2006.10.014

23. Malam Y, Loizidou M, Seifalian AM. Liposomes and nanoparticles: nanosized vehicles for drug delivery in cancer. *Trends Pharmacol Sci*. 2009;30(11):592-599.

doi:10.1016/j.tips.2009.08.004

24. Gosangari SL, Watkin KL. Effect of preparation techniques on the properties of curcumin liposomes: Characterization of size, release and cytotoxicity on a squamous oral carcinoma cell line. *Pharm Dev Technol*. 2012;17(1):103-109. doi:10.3109/10837450.2010.522583

25. Chen J, Lu WL, Gu W, et al. Drug-in-cyclodextrin-in-liposomes: A promising delivery system for hydrophobic drugs. *Expert Opin Drug Deliv*. 2014;11(4):565-577. doi:10.1517/17425247.2014.884557

26. Li W, Luo T, Yang Y, Tan X, Liu L. Formation of controllable hydrophilic/hydrophobic drug delivery systems by electrospinning of vesicles. *Langmuir*. 2015;31(18):5141-5146. doi:10.1021/la504796v

27. Gu D, O'Connor AJ, G.H. Qiao G, Ladewig K. Hydrogels with smart systems for delivery of hydrophobic drugs. *Expert Opin Drug Deliv*. 2017;14(7):879-895. doi:10.1080/17425247.2017.1245290

28. Hearnden V, Sankar V, Hull K, et al. New developments and opportunities in oral mucosal drug delivery for local and systemic disease. *Adv Drug Deliv Rev*. 2012;64(1):16-28. doi:10.1016/j.addr.2011.02.008

29. Laffleur F. Mucoadhesive polymers for buccal drug delivery. *Drug Dev Ind Pharm*. 2014;40(5):591-598. doi:10.3109/03639045.2014.892959

30. Ahuja A, Khar RK, Ali J. Mucoadhesive drug delivery systems. *Drug Dev Ind Pharm*. 1997;23(5):489-515. doi:10.3109/03639049709148498

31. Woertz C, Preis M, Breitkreutz J, Kleinebudde P. Assessment of test methods evaluating

mucoadhesive polymers and dosage forms: An overview. *Eur J Pharm Biopharm*. 2013;85(3 PART B):843-853. doi:10.1016/j.ejpb.2013.06.023

32. Ameeduzzafar A, Ali J, Fazil M, Qumbar M, Khan N, Ali A. Colloidal drug delivery system: Amplify the ocular delivery. *Drug Deliv*. 2016;23(3):710-726. doi:10.3109/10717544.2014.923065

33. De Araújo Pereira RR, Bruschi ML. Vaginal mucoadhesive drug delivery systems. *Drug Dev Ind Pharm*. 2012;38(6):643-652. doi:10.3109/03639045.2011.623355

34. Ugwoke MI, Verbeke N, Kinget R. The biopharmaceutical aspects of nasal mucoadhesive drug delivery. *J Pharm Pharmacol*. 2001;53(1):3-22. doi:10.1211/0022357011775145

35. Ludwig A. The use of mucoadhesive polymers in ocular drug delivery. *Adv Drug Deliv Rev*. 2005;57(11):1595-1639. doi:10.1016/j.addr.2005.07.005

36. Islam MS, Chen L, Sisler J, Tam KC. Cellulose nanocrystal (CNC)-inorganic hybrid systems: Synthesis, properties and applications. *J Mater Chem B*. 2018;6(6):864-883. doi:10.1039/c7tb03016a

37. Grishkewich N, Akhlaghi SP, Zhaoling Y, Berry R, Tam KC. Cellulose nanocrystal-poly(oligo(ethylene glycol) methacrylate) brushes with tunable LCSTs. *Carbohydr Polym*. 2016;144:215-222. doi:10.1016/j.carbpol.2016.02.044

38. George J, Sabapathi SN. Cellulose nanocrystals: Synthesis, functional properties, and applications. *Nanotechnol Sci Appl*. 2015;8:45-54. doi:10.2147/NSA.S64386

39. Islam MS, Chen L, Sisler J, Tam KC. Cellulose nanocrystal (CNC)–inorganic hybrid systems: synthesis, properties and applications. *J Mater Chem B*. 2018;6(6):864-883.

doi:10.1039/C7TB03016A

40. Habibi Y, Lucia LA, Rojas OJ. Cellulose nanocrystals: Chemistry, self-assembly, and applications. *Chem Rev*. 2010;110(6):3479-3500. doi:10.1021/cr900339w

41. Moon RJ, Martini A, Nairn J, Simonsen J, Youngblood J. *Cellulose Nanomaterials Review: Structure, Properties and Nanocomposites*. Vol 40.; 2011. doi:10.1039/c0cs00108b

42. Favier V, Canova GR, Cavaille JY, Chanzy ' H, Dufresne ' A, Gauthie C. Polymers for Advanced Technologies Nanocomposite Materials from Latex and Cellulose Whiskers. *Polym Adv Technol*. 1995;6:351-355.

43. Natterodt JC, Petri-Fink A, Weder C, Zoppe JO. Cellulose nanocrystals: Surface modification, applications and opportunities at interfaces. *Chimia (Aarau)*. 2017;71(6):376-383. doi:10.2533/chimia.2017.376

44. Shak KPY, Pang YL, Mah SK. Nanocellulose: Recent advances and its prospects in environmental remediation. *Beilstein J Nanotechnol*. 2018;9(1):2479-2498. doi:10.3762/bjnano.9.232

45. Dufresne A. Comparing the mechanical properties of high performances polymer nanocomposites from biological sources. *J Nanosci Nanotechnol*. 2006;6(2):322-330. doi:10.1166/jnn.2006.906

46. Hsu L, Weder C, Rowan SJ. Stimuli-responsive, mechanically-adaptive polymer nanocomposites. *J Mater Chem*. 2011;21(9):2812-2822. doi:10.1039/c0jm02383c

47. Moberg T, Sahlin K, Yao K, et al. Rheological properties of nanocellulose suspensions: effects of fibril/particle dimensions and surface characteristics. *Cellulose*.

2017;24(6):2499-2510. doi:10.1007/s10570-017-1283-0

48. Shafeiei-Sabet S, Hamad WY, Hatzikiriakos SG. Influence of degree of sulfation on the rheology of cellulose nanocrystal suspensions. *Rheol Acta*. 2013;52(8-9):741-751. doi:10.1007/s00397-013-0722-6

49. Markstedt K, Mantas A, Tournier I, Martínez Ávila H, Hägg D, Gatenholm P. 3D bioprinting human chondrocytes with nanocellulose-alginate bioink for cartilage tissue engineering applications. *Biomacromolecules*. 2015;16(5):1489-1496. doi:10.1021/acs.biomac.5b00188

50. Sahlin K, Forsgren L, Moberg T, Bernin D, Rigdahl M, Westman G. Surface treatment of cellulose nanocrystals (CNC): effects on dispersion rheology. *Cellulose*. 2018;25(1):331-345. doi:10.1007/s10570-017-1582-5

51. Wang Y, Wang X, Xie Y, Zhang K. Functional nanomaterials through esterification of cellulose: a review of chemistry and application. *Cellulose*. 2018;25(7):3703-3731. doi:10.1007/s10570-018-1830-3

52. Zhou T, Qi H, Han L, Barbash D, Li CY. Towards controlled polymer brushes via a self-assembly-assisted-grafting-to approach. *Nat Commun*. 2016;7:1-8. doi:10.1038/ncomms11119

53. Zhao B, Brittain WJ. Polymer brushes: Surface-immobilized macromolecules. *Prog Polym Sci*. 2000;25(5):677-710. doi:10.1016/S0079-6700(00)00012-5

54. Zoppe JO, Habibi Y, Rojas OJ, et al. Poly(N -isopropylacrylamide) brushes grafted from cellulose nanocrystals via surface-initiated single-electron transfer living radical polymerization. *Biomacromolecules*. 2010;11(10):2683-2691. doi:10.1021/bm100719d

55. Qian H, Wang X, Yuan K, et al. Delivery of doxorubicin in vitro and in vivo using bio-reductive cellulose nanogels. *Biomater Sci*. 2014;2(2):220-232. doi:10.1039/c3bm60176e

56. Tan J, Kang H, Liu R, et al. Dual-stimuli sensitive nanogels fabricated by self-association of thiolated hydroxypropyl cellulose. *Polym Chem*. 2011;2(3):672-678. doi:10.1039/c0py00348d

57. Mianehrow H, Afshari R, Mazinani S, Sharif F, Abdouss M. Introducing a highly dispersed reduced graphene oxide nano-biohybrid employing chitosan/hydroxyethyl cellulose for controlled drug delivery. *Int J Pharm*. 2016;509(1-2):400-407. doi:10.1016/j.ijpharm.2016.06.015

58. ASTRID M ¨ULLER, ZHIXU NI, NADINE HESSLER, FALKO WESARG, 4 FRANK A. M ¨ULLER, 4 DANA KRALISCH DF. The Biopolymer Bacterial Nanocellulose as Drug Delivery System: Investigation of Drug Loading and Release using the Model Protein Albumin. *J Pharm Sci*. 2012;102:579-592. doi:10.1002/jps

59. Moritz S, Wiegand C, Wesarg F, et al. Active wound dressings based on bacterial nanocellulose as drug delivery system for octenidine. *Int J Pharm*. 2014;471(1-2):45-55. doi:10.1016/j.ijpharm.2014.04.062

60. Müller A, Zink M, Hessler N, et al. Bacterial nanocellulose with a shape-memory effect as potential drug delivery system. *RSC Adv*. 2014;4(100):57173-57184. doi:10.1039/c4ra09898f

61. Ã MR. Chitin and chitosan : Properties and applications. 2006;31:603-632. doi:10.1016/j.progpolymsci.2006.06.001

62. Duarte ARC, Correlo VM, Oliveira JM, Reis RL. Recent Developments on Chitosan Applications in Regenerative Medicine. *Biomater from Nat Adv Devices Ther*. 2016;(Dd):221-243. doi:10.1002/9781119126218.ch14

63. Sashiwa H, Aiba SI. Chemically modified chitin and chitosan as biomaterials. *Prog Polym Sci*. 2004;29(9):887-908. doi:10.1016/j.progpolymsci.2004.04.001

64. Mourya VK, Inamdar NN. Chitosan-modifications and applications: Opportunities galore. *React Funct Polym*. 2008;68(6):1013-1051. doi:10.1016/j.reactfunctpolym.2008.03.002

65. Pillai CKS, Paul W, Sharma CP. Chitin and chitosan polymers: Chemistry, solubility and fiber formation. *Prog Polym Sci*. 2009;34(7):641-678. doi:10.1016/j.progpolymsci.2009.04.001

66. Xing L, Fan YT, Zhou TJ, et al. Chemical modification of Chitosan for efficient vaccine delivery. *Molecules*. 2018;23(2). doi:10.3390/molecules23020229

67. Liu J, Pu H, Liu S, Kan J, Jin C. Synthesis, characterization, bioactivity and potential application of phenolic acid grafted chitosan: A review. *Carbohydr Polym*. 2017;174:999-1017. doi:10.1016/j.carbpol.2017.07.014

68. Alves NM, Mano JF. Chitosan derivatives obtained by chemical modifications for biomedical and environmental applications. *Int J Biol Macromol*. 2008;43(5):401-414. doi:10.1016/j.ijbiomac.2008.09.007

69. Li C, Li J Bin. Preparation of chitosan-ferulic acid conjugate: Structure characterization and in the application of pharmaceuticals. *Int J Biol Macromol*. 2017;105:1539-1543. doi:10.1016/j.ijbiomac.2017.04.103

70. Woranuch S, Yoksan R. Preparation, characterization and antioxidant property of water-soluble ferulic acid grafted chitosan. *Carbohydr Polym*. 2013;96(2):495-502. doi:10.1016/j.carbpol.2013.04.006

71. Woranuch S, Yoksana R, Akashi M. Ferulic acid-coupled chitosan: Thermal stability and utilization as an antioxidant for biodegradable active packaging film. *Carbohydr Polym*. 2015;115:744-751. doi:10.1016/j.carbpol.2014.06.074

72. Lee DS, Woo JY, Ahn CB, Je JY. Chitosan-hydroxycinnamic acid conjugates: Preparation, antioxidant and antimicrobial activity. *Food Chem*. 2014;148:97-104. doi:10.1016/j.foodchem.2013.10.019

73. Cho YS, Kim SK, Ahn CB, Je JY. Preparation, characterization, and antioxidant properties of gallic acid-grafted-chitosans. *Carbohydr Polym*. 2011;83(4):1617-1622. doi:10.1016/j.carbpol.2010.10.019

74. Liu J, Meng C guang, Yan Y hua, Shan Y na, Kan J, Jin C hai. Protocatechuic acid grafted onto chitosan: Characterization and antioxidant activity. *Int J Biol Macromol*. 2016;89:518-526. doi:10.1016/j.ijbiomac.2016.04.089

75. Aytekin AO, Morimura S, Kida K. Synthesis of chitosan-caffeic acid derivatives and evaluation of their antioxidant activities. *J Biosci Bioeng*. 2011;111(2):212-216. doi:10.1016/j.jbiosc.2010.09.018

76. Hofman AH, van Hees IA, Yang J, Kamperman M. Bioinspired Underwater Adhesives by Using the Supramolecular Toolbox. *Adv Mater*. 2018;30(19). doi:10.1002/adma.201704640

77. Lee BP, Messersmith PB, Israelachvili JN, Waite JH. Mussel-Inspired Adhesives and

Coatings. *Annu Rev Mater Res*. 2011;41(1):99-132. doi:10.1146/annurev-matsci-062910-100429

78. Kord Forooshani P, Lee BP. Recent approaches in designing bioadhesive materials inspired by mussel adhesive protein. *J Polym Sci Part A Polym Chem*. 2017;55(1):9-33. doi:10.1002/pola.28368

79. Collier LM, Pinn EH. An assessment of the acute impact of the sea lice treatment ivermectin on a benthic community. *J Exp Mar Bio Ecol*. 1998;230(1):131-147. doi:10.1016/S0022-0981(98)00081-1

80. Crane M, Gross M, Maycock DS, Grant A, Fossum BH. Environmental quality standards for a deltamethrin sea louse treatment in marine finfish aquaculture based on survival time analyses and species sensitivity distributions. *Aquac Res*. 2011;42(SUPPL. 1):68-72. doi:10.1111/j.1365-2109.2010.02665.x

81. Shephard KL. Mucus on the epidermis of fish and its influence on drug delivery. *Adv Drug Deliv Rev*. 1993;11(3):403-417. doi:10.1016/0169-409X(93)90018-Y

82. Benhamed S, Guardiola FA, Mars M, Esteban MÁ. Pathogen bacteria adhesion to skin mucus of fishes. *Vet Microbiol*. 2014;171(1-2):1-12. doi:10.1016/j.vetmic.2014.03.008

83. Costa AC d. S, Brandão HM, da Silva SR, et al. Mucoadhesive nanoparticles: A new perspective for fish drug application. *J Fish Dis*. 2016;39(4):503-506. doi:10.1111/jfd.12373

84. Yang D, Cui B, Wang C, et al. Preparation and Characterization of Emamectin Benzoate Solid Nanodispersion. *J Nanomater*. 2017;2017. doi:10.1155/2017/6560780

85. Shoaib A, Waqas M, Elabasy A, Cheng X, Zhang Q, Shi Z. Preparation and

characterization of emamectin benzoate nanoformulations based on colloidal delivery systems and use in controlling *Plutella xylostella* (L.) (*Lepidoptera* : *Plutellidae*). *RSC Adv*. 2018;8(28):15687-15697. doi:10.1039/C8RA01913D

86. Wang Y, Wang A, Wang C, et al. Synthesis and characterization of emamectin-benzoate slow-release microspheres with different surfactants. *Sci Rep*. 2017;7(1):1-9. doi:10.1038/s41598-017-12724-6

87. Yaroslavov AA, Sybachin A V., Efimova AA. Stabilization of electrostatic polymer-colloid complexes. *Colloids Surfaces A Physicochem Eng Asp*. 2018;558(August):1-7. doi:10.1016/j.colsurfa.2018.08.042

88. Silva M, Calado R, Marto J, Bettencourt A, Almeida A, Gonçalves L. Chitosan Nanoparticles as a Mucoadhesive Drug Delivery System for Ocular Administration. *Mar Drugs*. 2017;15(12):370. doi:10.3390/md15120370

89. Shields PA, Farrah SR. Influence of salts on electrostatic interactions between poliovirus and membrane filters. *Appl Environ Microbiol*. 1983;45(2):526-531. doi:10.1128/aem.45.2.526-531.1983

90. Caly L, Druce JD, Catton MG, Jans DA, Wagstaff KM. The FDA-approved Drug Ivermectin inhibits the replication of SARS-CoV-2 in vitro. *Antiviral Res*. 2020:104787. doi:10.1016/j.antiviral.2020.104787

91. Lu Y, Zhang E, Yang J, Cao Z. Strategies to improve micelle stability for drug delivery. *Nano Res*. 2018;11(10):4985-4998. doi:10.1007/s12274-018-2152-3

92. Ge Y, Zhang Y, He S, Nie F, Teng G, Gu N. Fluorescence modified chitosan-coated magnetic nanoparticles for high-efficient cellular imaging. *Nanoscale Res Lett*.

2009;4(4):287-295. doi:10.1007/s11671-008-9239-9

93. Wu X, Tang J, Duan Y, Yu A, Berry RM, Tam KC. Conductive cellulose nanocrystals with high cycling stability for supercapacitor applications. *J Mater Chem A*. 2014;2(45):19268-19274. doi:10.1039/c4ta04929b

94. M. H, McKelvey CA, Marsac PJ, Carrier RL. Size Selectivity of Intestinal Mucus to Diffusing Particulates is Dependent on Surface Chemistry and Exposure to Lipids. *J Drug Target*. 2015;23:768-774. doi:10.1016/j.physbeh.2017.03.040

95. Napper DH. Steric stabilization. *J Colloid Interface Sci*. 1977;58(2):390-407. doi:10.1016/0021-9797(77)90150-3

96. Berestok T, Guardia P, Ibáñez M, et al. Electrostatic-Driven Gelation of Colloidal Nanocrystals. *Langmuir*. 2018;34(31):9167-9174. doi:10.1021/acs.langmuir.8b01111

97. Shen S, Wu Y, Liu Y, Wu D. High drug-loading nanomedicines : progress , current status , and prospects. *Int J Nanomedicine*. 2017;12:4085-4109.

98. Jiang L, Duan H, Ji X, Wang T, Wang Y, Qiu J. Application of a simple desolvation method to increase the formation yield, physical stability and hydrophobic drug encapsulation capacity of chitosan-based nanoparticles. *Int J Pharm*. 2018;545(1-2):117-127. doi:10.1016/j.ijpharm.2018.03.044

99. Fugelsang KC, Edwards CG. *Wine Microbiology*.; 2007.

100. Kovacs T, Naish V, O'Connor B, et al. An ecotoxicological characterization of nanocrystalline cellulose (NCC). *Nanotoxicology*. 2010;4(3):255-270. doi:10.3109/17435391003628713

101. Sekhavat Pour Z, Makvandi P, Ghaemy M. Performance properties and antibacterial

activity of crosslinked films of quaternary ammonium modified starch and poly(vinyl alcohol). *Int J Biol Macromol*. 2015;80:596-604. doi:10.1016/j.ijbiomac.2015.07.008

102. Baek J, Wahid-Pedro F, Kim K, Kim K, Tam KC. Phosphorylated-CNC/modified-chitosan nanocomplexes for the stabilization of Pickering emulsions. *Carbohydr Polym*. 2019;206(July 2018):520-527. doi:10.1016/j.carbpol.2018.11.006

103. Li H, Du Y, Wu X, Zhan H. Effect of molecular weight and degree of substitution of quaternary chitosan on its adsorption and flocculation properties for potential retention-aids in alkaline papermaking. *Colloids Surfaces A Physicochem Eng Asp*. 2004;242(1-3):1-8. doi:10.1016/j.colsurfa.2004.04.051

104. Sahariah P, Másson M. Antimicrobial Chitosan and Chitosan Derivatives: A Review of the Structure-Activity Relationship. *Biomacromolecules*. 2017;18(11):3846-3868. doi:10.1021/acs.biomac.7b01058

105. Tran PL, Hamood AN, De Souza A, et al. A study on the ability of quaternary ammonium groups attached to a polyurethane foam wound dressing to inhibit bacterial attachment and biofilm formation. *Wound Repair Regen*. 2015;23(1):74-81. doi:10.1111/wrr.12244

106. McNerney T, Thomas A, Senczuk A, et al. PDADMAC flocculation of Chinese hamster ovary cells: Enabling a centrifuge-less harvest process for monoclonal antibodies. *MAbs*. 2015;7(2):413-427. doi:10.1080/19420862.2015.1007824

107. Dong L, Zhang X, Ren S, et al. Poly(diallyldimethylammonium chloride)-cellulose nanocrystals supported Au nanoparticles for nonenzymatic glucose sensing. *RSC Adv*. 2016;6(8):6436-6442. doi:10.1039/c5ra23935d